1999

Development and evaluation of electrochemical sensors for biologically important sulfur-containing compounds

Matthew Edward Johll
Iowa State University

INFORMATION TO USERS

This manuscript has been reproduced from the microfilm master. UMI films the text directly from the original or copy submitted. Thus, some thesis and dissertation copies are in typewriter face, while others may be from any type of computer printer.

The quality of this reproduction is dependent upon the quality of the copy submitted. Broken or indistinct print, colored or poor quality illustrations and photographs, print bleedthrough, substandard margins, and improper alignment can adversely affect reproduction.

In the unlikely event that the author did not send UMI a complete manuscript and there are missing pages, these will be noted. Also, if unauthorized copyright material had to be removed, a note will indicate the deletion.

Oversize materials (e.g., maps, drawings, charts) are reproduced by sectioning the original, beginning at the upper left-hand corner and continuing from left to right in equal sections with small overlaps. Each original is also photographed in one exposure and is included in reduced form at the back of the book.

Photographs included in the original manuscript have been reproduced xerographically in this copy. Higher quality 6" x 9" black and white photographic prints are available for any photographs or illustrations appearing in this copy for an additional charge. Contact UMI directly to order.

UMI®

Bell & Howell Information and Learning
300 North Zeeb Road, Ann Arbor, MI 48106-1346 USA
800-521-0600

Development and evaluation of electrochemical sensors for biologically important sulfur-containing compounds

by

Matthew Edward Johll

A dissertation submitted to the graduate faculty

in partial fulfillment of the requirements for the degree of

DOCTOR OF PHILOSOPHY

Major: Analytical Chemistry

Major Professor: Dennis C. Johnson

Iowa State University

Ames, Iowa

1999

Graduate College
Iowa State University

This is to certify that the Doctoral dissertation of

Matthew Edward Johll

has met the dissertation requirements of Iowa State University

Signature was redacted for privacy.

Committee Member

Signature was redacted for privacy.

Committee Member

Signature was redacted for privacy.

Committee Member

Signature was redacted for privacy.

Committee Member

Signature was redacted for privacy.

Major Professor

Signature was redacted for privacy.

For the Major Program

Signature was redacted for privacy.

For the Graduate College

DEDICATION

I would like to dedicate this thesis to the teachers I have had the privilege to learn from over the last 23 years: Mrs. Carol Manning, 1st grade; Mr. Jerry Sherwin, high school agriculture; Ms. Minda Fortney, high school English; Father William Schwartz, role model; Dr. Harold Fenrick, undergraduate advisor; Dr. Robert Hansen, undergraduate analytical chemistry; Dr. Dennis C. Johnson, Ph.D. advisor and mentor. If I can achieve a fraction of the success these people have had as teachers and educators, I will consider myself blessed.

TABLE OF CONTENTS

ACKNOWLEDGMENTS

The first person I would like to acknowlege is my wife Sally M. Johll, without her understanding, support, encouragement and friendship I would have never made it through. We are about to start a new life together leaving behind our old jobs, friends and home. I have feelings of apprehension, excitement and sadness but most of all I feel confidence because of Sally's love and faith in me.

The next group of people have helped me through the last 5 years of graduate school and have honored me by calling themselves my friends. The "old timers" whose advice was so valuable in the early years and again when I was job hunting: Mark Jensen, Kim Pamplin, John Hoekstra and Steve Johnson. The "comrades" who fought side-by-side with me through our courses and prelim: Natasha B. Popović and Ma'an Amad. You two are family and will always be welcome in my home. You have shown me kindness to the highest degree, even though you kept ruining the grading curve. Natsi, lets have cigars at the Casbah and discuss how K-L plots can give n=37.5. The "guys" who have participated in and been the victim of some of the greatest and dumbest jokes I've ever pulled: Brett Simpson and Tony Layson. You two are the little brothers I never wanted, Bon Temp Roule'! Thanks to the "quiescent organic man" Steve Treimer who had to

listen to me worry and panic during the last year about research, job hunting and home buying. Thanks a million for listening. I need to thank "the wizard" Jianren Feng whose sound advice and experience have been an invaluable resource. I learned more practical electrochemistry during our morning coffee than I could learn in any lecture.

I wanted to end my acknowledgment section with where everything began, my family. My parents, Gregory and Barbara Johll, I owe everything. They gave me more than life and a loving family, they gave me a work ethic, civic patriotism, faith, compassion, confidence, humility and trust. My sisters and brothers; Diane, Deb, Marty and Mike have been role models for my life and I thank you for all the help you have given me since 1972. Especially for wearing down Mom and Dad so the rules weren't as tough when I hit high school! My Grandmothers Marcella Johll and Loretta Hahn, the two most beautiful women in the world who are the definition of strength. My Grandfather George Johll, whose advice and stories are still fresh in my mind, thank you. Finally, I want to acknowledge those who have left this world all too soon and will be remembered lovingly: Thomas Gleason, Edward Johll, and Wilbur Hahn.

CHAPTER 1. GENERAL INTRODUCTION

Introduction

The research described in this dissertation was performed under the direction of Professor Dennis C. Johnson, beginning in August of 1994. The focus of this research has been to increase our knowledge of the fundamental interactions of analyte molecules with the electrode surface and how these interactions affect the rate of heterogenous electrocatalysis. With this knowledge, our goal was to develop and evaluate electrochemical sensors for the detection of biologically important compounds separated by liquid chromatography.

Dissertation Organization

This dissertation consists of four separate papers. The first three papers have been published in peer reviewed journals, with the fourth and final paper to be submitted in the near future. The format of each paper follows that of the journal in which it appears. A general conclusions section, summarizing the significant results of this thesis, is presented in the final chapter. The appendix consists of an original computer program written for this research by the author using the LabVIEW visual programming language.

Literature Review

There has been a renewed interest in the medical community for the detection of aliphatic sulfhydryl and disulfide compounds with the publication of several journal articles that identified elevated total plasma homocysteine (tHCys) levels as an independent risk factor that posses a greater risk for coronary heart disease than that of elevated cholesterol levels (1-3). Homocysteine exists in human plasma in the free thiol state as well as symmetric and unsymmetric disulfides and protein-bound forms. Total homocysteine levels are measured after a reducing reagent, such as dithioerythritol or sodium borohydride, has been added to the sample to release the disulfide and protein bound homocysteine. Medical research on the diseases cystinosis, homocystinuria and cystinuria also requires the measurement of sulfhydryl and disulfide compounds in human plasma(4-6). Thiols serve as powerful antioxidants in human cells and HIV/Aids virus research has shown depleted levels of the thiol glutathione (GSH) in patients (7-9). Currently there is debate in the literature if depleted GSH levels may serve as an indicator for HIV progression in an individual.

The current methods reported in the literature for the detection of sulfhydryl and disulfide compounds include immunoassay, gas chromatography coupled with mass spectrometry, capillary electrophoresis with laser induced fluorescence and liquid chromatography coupled with

UV-Vis, fluorescence, radioisotope, mass spectrometry and electrochemical detection techniques

Immunoassay Detection of Sulfur Compounds: An enzyme labeled immunosorbent assay (ELISA) method developed for homocysteine determination in plasma was based on the conversion of homocysteine to s-adenosyl-L-homocysteine (10). A total of 82 samples were analyzed in 2.5 hours with a relative error of 6% within each assay and 8% between each assay.

Another method for the immunoassay detection of total plasma homocysteine is fluorescence polarization immunoassay (FPIA). Antibody bound antigen, when excited with plane polarized light, will emit light in the same plane as the polarized source. Unbound antigen will rotate during the excitation process thereby decreasing the polarization in the original plane. FPIA has the ability to discriminate between antibody bound antigen and free antigen without physical separation of the two. A recent study compared this method with a liquid chromatography derivitization process and found excellent agreement for results between the two methods (11).

Gas Chromatography-Mass Spectrometry (GC-MS) Detection of Sulfur Compounds: The separation of thiol and disulfide compounds by gas chromatography requires the derivitization of the sulfur species to a volatile product prior to separation and detection by mass spectrometry. A common

derivitization reagent is ethylchloroformate which forms a volatile N(O,S)-ethoxycarbonyl ethyl ester (12, 13), detection limits are in the femtomole levels. A similar derivitization reagent used is *n*-propyl chloroformate to form N(O,S)-propoxycarbonyl propyl ester (14).

Capillary Electrophoresis Detection of Sulfur Compounds: A method for the determination of total plasma homocysteine, cysteine and glutathione based on capillary electrophoresis with laser induced fluorescence reported a detection limit of 50 pmol/L (1.1 attomoles) for homocysteine (15). The determination of oxidized and reduced glutathione by capillary electrophoresis has been reported without a derivitization step. The detection scheme used UV absorption monitored at 214 nm (16). The method proved reproducible and in agreement with the analysis of the samples by liquid chromatography with derivitization by N-(1-pyrenyl)maleimide.

Detection of Sulfur Compounds in Liquid Chromatography: Liquid chromatography is a dominant technique for the analysis of biological samples because complex mixtures can be separated and quantified in a single run. Liquid chromatography is compatible with a variety of detection methods which aids in method development for target analytes.

One of the most common detection methods coupled to liquid chromatography is the absorption of ultraviolet-visible (UV-Vis) radiation.

The detection of biological sulfhydryl and disulfide compounds is complicated by the fact that these compounds lack chromophoric groups that absorb strongly in UV-Vis region of the spectrum. The application of UV-Vis detection for sulfhydryl and disulfide moieties requires derivitization with a chromophoric reagent in either a pre- or post-column reaction.

One of the most common derivatizations used is a reaction of the α-amino group with 2,2-dihydroxy-1,3-indanedione (Ninhydrin). The ninhydrin reaction forms a strongly colored species, monitored at 570 nm. The ninhydrin derivatization reaction has been used to determine cysteine and glutathione bound species at the sub nanomole levels in protein (17). The bound glutathione and cysteine were released from the protein as the sulfonic and sulfinic acids after oxidation with performic acid.

Nanomole levels of glutathione and cysteine mixed disulfides can be detected by derivitization with 1-fluoro-2,4 dinitrobenzene (Sanger's Reagent) to form 2,4-dinitrophenyl derivatives of the compounds monitored at 365 nm (18). The initial step in the derivitization procedure is the formation of S-carboxymethyl derivatives of the free thiols with iodoacetic acid followed by addition of Sanger's Reagent.

Plasma sulfhydryls have been determined by postcolumn addition of 4,4'-dithiodipyridine derivatization reagent with detection at 324 nm (19). The sample preparation involves the reduction of disulfide bonds by the

addition of dithiothreitol and precipitation of the proteins by sulfosalicylic acid. Detection limits reported for homocysteine were less than 50 nM.

There has been one study allowing for the detection of both the thiol and disulfide form of glutathione without a derivitization step (20). The only sample preparation step is the precipitation of protein by sulfosalicylic acid from the plasma sample. Detection limits of nanomole levels for glutathione and glutathione disulfide were achieved with detection at 190 nm, despite the fact that the lower wavelength limit for water is 180 nm.

Another commonly used detection method interfaced with chromatography is fluorescence detection. The biological sulfhydryl and disulfide compounds are commonly derivatized with bimanes and halogenosulfonylbenzofurazans prior to detection. The determination of lower μM concentrations of cysteine, homocysteine and glutathione levels in plasma using monobromobimane (mBrB) has been performed using 380 nm excitation source with detection at 470 nm (21). Caution must be used when mBrB is used because the hydrolysis products of mBrB are fluorescent and may interfere.

The use of 7-fluoro-2,1,3-benzoxadiazole-4 sulfonamide (ABD-F) and ammonium-7-fluorobenzo-2-oxa-1,3-diazole-4-sulfonate (SBD-F) produce derivatives of sulfhydryl compounds that can be excited at 380 nm and monitored at 470 nm (22, 23). The derivitization reaction of SBD-F is

specific for the sulfhydryl moiety but requires 1 hour at 60°C and pH 9.5. The reaction of ABD-F yields a low amount of an amine derivatized side product but the conditions are less extreme at 50°C and pH 8.0-9.5 for 10 minutes (24).

An interesting study on cellular levels of reduced glutathione, cysteine, glutamylcysteine and cysteinylglycine used a combination of N-1(pyrenyl)maleimide (NPM) and ortho-phthalaldehyde (OPA) (25). When the derivatization occurred with just OPA, only the glutathione and glutamylcysteine were detected. In the presence of both OPA and NPM derivatizing agents, all compounds of interest can be detected in the pmole range.

A liquid chromatography method coupled with radioenzymic detection for total homocysteine levels in human plasma and urine was based on the reaction of homocysteine with [^{14}C]adenosine in the presence of S-adenosylhomocysteine hydrolase (26). The radioactive product was detected by a scintillation counter.

Liquid chromatography provides excellent separation power for mixtures but identification of compounds is based on matching retention times of unknowns with the times of standards. Mass spectrometry, however, provides molecular weight and structure specific fragmentation pattern information. Combining the separation power of liquid

chromatography with the identification power of mass spectrometry provides a very powerful tool for the analysis of mixtures.

Liquid chromatography-mass spectrometry has been applied to the analysis of urine for sulfur amino acids and cystathionine metabolites (27). The liquid chromatography system was interfaced to the mass spectrometer by an atmospheric pressure chemical ionization source.

Electrochemical methods provide another alternative for detection methods coupled to liquid chromatography. Electrochemical methods have the advantage that derivitization of the analyte is unnecessary, provided the analyte is electroactive. One common method for the electrochemical detection of thiol compounds employs a Au-Hg amalgam electrode for the oxidation of the thiol moiety. The application of the Au-Hg amalgam electrode for detection of thiol and disulfide mixtures uses a pair of electrodes in series where the first electrode is set at a potential to reduce the disulfide moiety to the corresponding thiol. The downstream electrode oxidizes the thiols and is the working electrode for monitoring the signal (28). This method has been utilized to detect penicillamine, reduced glutathione, homocysteine and their related disulfides (28-31) with typical detection limits in the picomole range. The use of the Au-Hg amalgam electrode raises concerns with Hg exposure, contamination of the waste stream as well as electrode stability issues.

A unique indirect electrochemical method for the detection of the thiol moiety calls for the post-column addition of silver nitrate (32). The silver nitrate will react with the thiol functional group to produce a silver mercaptide. The detection comes from a platinum electrode set at -0.10 V vs. Ag/AgCl which detects a decrease in Ag^+ due to consumption by formation of the electroinactive silver mercaptide.

An alternative electrochemical method for the determination of sulfur compounds is pulsed electrochemical detection (PED). When aliphatic organic compounds are oxidized at noble metal electrodes, the surface is fouled by the polymerization of oxidation products. Pulsed electrochemical detection is based on the application of a pulsed potential-time waveform which regenerates a pristine electrode surface. The waveform consists of three potential steps. The first potential is chosen so that the analyte is oxidized at the electrode and the current for this oxidation is integrated for a period of time, typically 100 msec. The next potential step is to a region where the formation of surface oxide occurs. The surface oxide formation desorbs all fouling species. The final step is a cathodic potential step which reduces the oxide from the electrode surface. PED has been demonstrated to detect thiourea (33-35), methionine, cysteine, cystine and glutathione (36-38). Detection limits were reported in the low picomole level. PED has also been used for the analysis of human plasma for various sulfhydryl

compounds (39, 40).

Electrochemistry of Sulfur Species: Electrochemical studies of sulfur compounds in aqueous solutions have been complicated by the tendency of the compounds to foul solid electrodes (41). An initial study on the oxidation of cysteine at Pt electrode showed the products of oxidation to be cystine and cysteic acid (42). A mechanism was proposed in which the thiol adsorbs as a radical species which then either reacts with another radical to form cystine or is oxidized to cysteic acid by transfer of oxygen from water. A series of studies evaluated the response of biological sulfur compounds at noble metal electrodes in aqueous solution (43-46). Evidence was given for the dissociation of the disulfide bond in cystine to form a chemisorbed species, believed to be the RS• radical, on both Pt and Au (44, 46). Oxidation of cystine occurred concomitantly with oxide formation on the electrode surfaces to produce cysteic acid and an adsorbed product of oxidation that could be reduced from the surface of the electrode at more negative potentials (46). The formation of cysteic acid was proposed to occur through an anodic oxygen-transfer reaction of the adsorbed radical with an adsorbed hydroxyl radical (44). The study further showed that cysteine is adsorbed at both Au and Pt and is oxidized in the identical manner as cystine (43).

The oxidation of biological sulfur compounds has also been studied on

chemically modified electrodes (CME). The adsorption of cobalt phthalocyanine tetrasulfonate (Co-TSP) onto graphite substrates is electrocatalytic for the oxidation of cysteine to cystine and cysteic acid (47).

Mixed-valence ruthenium cyanide (mvRuCN) deposited on glassy-carbon electrodes has proven to be electrocatalytic for the oxidation of cysteine, cystine and methionine (48). Oxidation of cysteine produced the sulfinic and sulfonic acid products with no evidence for the formation of the disulfide cystine. The oxidation product for methionine was the sulfoxide.

Electrochemistry of Alloys: The electrochemistry of alloy electrodes enables one to study the interaction of analytes with the electrode surface as a function of the alloy composition. The properties of the electrode and interactions with analyte molecules can dramatically change with alloy composition.

For example, cathodic reduction of CO_2 at Cu or Ni metal electrodes does not occur; however, a faradaic current for the reduction of CO_2 to form formic acid and methane was observed at Cu-Ni alloy electrodes (49). The faradaic current was optimized at an alloy ratio of 2:1 Cu:Ni. The electrocatalytic mechanism was explained based on hydrogen adsorption at the Ni sites with the adsorption of CO_2 at the Cu sites.

The electrocatalysis for anodic oxidation of aliphatic aldehydes has been demonstrated on Pt-Pd alloy electrodeposited on a glassy carbon

substrate (50). The alloy provides a dramatic improvement for the oxidation of aldehydes compared to the individual components due to improved adsorption of the analyte on the alloy.

The choice of alloying agents can serve the purpose of stabilizing the electrode and preventing dissolution. For example, the Ni oxyhydroxide species catalyzes the oxidation of amino acids, amines, thiols and carbohydrates (51-53) but is a soluble species. In order to stabilize the Ni electrode it has been alloyed with Cu(54), Cr(55, 56), and Ti (57, 58).

The response for the oxidation of aliphatic amines has been compared on Ag-Pb electrodes prepared by either the anodization of Ag-Pb alloys or by the electrodeposition of Ag-Pb onto Pt substrates (59). The anodization of Ag-Pb alloys provided the best electrode in terms of stability. Detection limits in a flow injection system were 6 pmol (20 μL injection).

References

(1) Nygard, O.; Nordrehaug, J. E.; Refsum, H.; Ueland, P. M.; Farstad, M.; Vollset, S. E. *N Engl J Med* **1997,** *337,* 230-6.

(2) Nygard, O.; Vollset, S. E.; Refsum, H.; Stensvold, I.; Tverdal, A.; Nordrehaug, J. E.; Ueland, M.; Kvale, G. *Jama* **1995,** *274,* 1526-33.

(3) Refsum, H.; Ueland, P. M.; Nygard, O.; Vollset, S. E. *Annu Rev Med* **1998,** *49,* 31-62.

(4) Kaniowska, E.; Chwatko, G.; Glowacki, R.; Kubalczyk, P.; Bald, E. *J. Chromatogr., A* **1998,** *798,* 27-35.

(5) Smolin, L. A.; Schneider, J. A. *Anal. Biochem.* **1988,** *168*, 374-9.

(6) Guttormsen, A. B.; Ueland, P. M.; Nesthus, I.; Nygard, O.; Schneede, J.; Vollset, S. E.; Refsum, H. *J Clin Invest* **1996,** *98*, 2174-83.

(7) Walmsley, S. L.; Winn, L. M.; Harrison, M. L.; Uetrecht, J. P.; Wells, P. G. *AIDS (London)* **1997,** *11*, 1689-1697.

(8) Sandstrom, P. A.; Murray, J.; Folks, T. M.; Diamond, A. M. *Free Radic Biol Med* **1998,** *24*, 1485-91.

(9) Bogden, J. D.; Skurnick, J. H.; Kemp, F. W.; Han, S.; Baker, H.; Kloser, P.; Perez, G.; Louria, D. B. *HIV Pathog Treat Conf* **1998.**

(10) Frantzen, F.; Faaren, A. L.; Alfheim, I.; Mordhei, A. K. *Clin. Chem.* **1998,** *44*, 311-316.

(11) Pfeiffer, C. M.; Twite, D.; Shih, J.; Holets-McCormack, S. R.; Gunter, E. W. *Clin. Chem.* **1999,** *45*, 152-153.

(12) Cao, P.; Moini, M. *J. Chromatogr., A* **1995,** *710*, 303-8.

(13) Pietzsch, J.; Julius, U.; Hanefeld, M. Clin. Chem. **1997,** *43*, 2001-2004.

(14) Sass, J. O.; Endres, W. *J. Chromatogr., A* **1997,** *776*, 342-347.

(15) Causse, E.; Siri, N.; Bellet, H.; Champagne, S.; Bayle, C.; Valdiguie, P.; Salvayre, R.; Couderc, F. *Clin. Chem.* **1999,** *45*, 412-414.

(16) Ercal, N.; Le, K.; Treeratphan, P.; Matthews, R. *Biomed. Chromatogr.* **1996,** *10*, 15-18.

(17) Lou, M. F.; McKellar, R.; Chyan, O. *Exp. Eye Res.* **1986,** *42*, 607-16.

(18) Reed, D. J.; Babson, J. R.; Beatty, P. W.; Brodie, A. E.; Ellis, W. W.; Potter, D. W. *Anal. Biochem.* **1980,** *106*, 55-62.

(19) Andersson, A.; Isaksson, A.; Brattstroem, L.; Hultberg, B. *Clin. Chem. (Washington, D. C.)* **1993,** *39*, 1590-7.

(20) Jayatilleke, E.; Shaw, S. *Anal. Biochem.* **1993,** *214*, 452-7.

(21) Bernhard, M.-C.; Junker, E.; Hettinger, A.; Lauterburg, B. H. *J. Hepatol.* **1998,** *28,* 751-755.

(22) Jacob, N.; Guillaume, L.; Garcon, L.; Foglietti, M.-J. *Ann. Biol. Clin.* **1997,** *55,* 583-591.

(23) Fermo, I.; Arcelloni, C.; Mazzola, G.; D'Angelo, A.; Paroni, R. *J. Chromatogr., B: Biomed. Sci. Appl.* **1998,** *719,* 31-36.

(24) Ueland, P. M.; Refsum, H.; Stabler, S. P.; Malinow, M. R.; Andersson, A.; Allen, R. H. *Clin. Chem.* **1993,** *39,* 1764-79.

(25) Parmentier, C.; Leroy, P.; Wellman, M.; Nicolas, A. *J. Chromatogr., B: Biomed. Sci. Appl.* **1998,** *719,* 37-46.

(26) Refsum, H.; Helland, S.; Ueland, P. M. *Clin. Chem.* **1985,** *31,* 624-628.

(27) Watanabe, H.; Fujita, Y.; Sugahara, K.; Kodama, H.; Ohmori, S. *Biol. Mass Spectrom.* **1991,** *20,* 602-8.

(28) Yamashita, G. T.; Rabenstein, D. L. *J. Chromatogr.* **1989,** *491,* 341-54.

(29) Richie, J. P., Jr.; Lang, C. A. *Anal. Biochem.* **1987,** *163,* 9-15.

(30) Rabenstein, D. L.; Yamashita, G. T. *Anal. Biochem.* **1989,** *180,* 259-63.

(31) Dupuy, D.; Szabo, S. *J. Liq. Chromatogr.* **1987,** *10,* 107-19.

(32) Kuninori, T.; Nishiyama, J. *Anal. Biochem.* **1991,** *197,* 19-24.

(33) Polta, T. Z.; Johnson, D. C.; Luecke, G. R. *J. Electroanal. Chem. Interfacial Electrochem.* **1986,** *209,* 171-81.

(34) Polta, T. Z.; Johnson, D. C. *J. Electroanal. Chem. Interfacial Electrochem.* **1986,** *209,* 159-69.

(35) Vandeberg, P. J.; Kowagoe, J. L.; Johnson, D. C. *Anal. Chim. Acta* **1992,** *260,* 1-11.

(36) Owens, G. S.; LaCourse, W. R. *Curr. Sep.* **1996,** *14,* 82-8.

(37) Vandeberg, P. J.; Johnson, D. C. *Anal. Chem.* **1993,** *65*, 2713-18.

(38) Vandeberg, P. J.; Johnson, D. C. *Anal. Chim. Acta* **1994,** *290*, 317-27.

(39) Evrovski, J.; Callaghan, M.; Cole, D. E. C. *Clin. Chem.* **1995,** *41*, 757-758.

(40) Cole, D. E. C.; Lehotay, D. C.; Evrovski, J. *Clin. Chem.* **1998,** *44*, 188-191.

(41) Adams, R. N. *Electrochemistry at Solid Electrodes*; Marcel Dekker: New York, 1969.

(42) Davis, D. G.; Bianco, E. *J. Electroanal. Chem.* **1966,** *12``*, 254-260.

(43) Koryta, J.; Pradac, J. *J. Electroanal. Chem. Interfacial Electrochem.* **1968,** *17*, 185-9.

(44) Koryta, J.; Pradac, J. *J. Electroanal. Chem. Interfacial Electrochem.* **1968,** *17*, 177-83.

(45) Ossendorfova, N.; Pradac, J.; Koryta, J. *J. Electroanal. Chem. Interfacial Electrochem.* **1970,** *28*, 313-18.

(46) Pradac, J.; Koryta, J. *J. Electroanal. Chem. Interfacial Electrochem.* **1968,** *17*, 167-75.

(47) Zagal, J.; Fierro, C.; Rozas, R. *J. Electroanal. Chem. Interfacial Electrochem.* **1981,** *119*, 403-8.

(48) Cox, J. A.; Gray, T. J. *Anal. Chem.* **1990,** *62*, 2742-4.

(49) Watanabe, M.; Shibata, M.; Katoh, A.; Azuma, M.; Sakata, T. *Denki Kagaku oyobi Kogyo Butsuri Kagaku* **1991,** *59*, 508-16.

(50) Wang, J.; Pamidi, P. V. A.; Cepria, G. *Anal. Chim. Acta* **1996,** *330*, 151-158.

(51) Arikawa, Y.; Huber, C. O. *Anal. Chim. Acta* **1990,** *229*, 191-5.

(52) Hui, B. S.; Huber, C. O. *Anal. Chim. Acta* **1982,** *134*, 211-18.

(53) Schick, K. G.; Magearu, V. G.; Huber, C. O. *Clin. Chem.* **1978,** *24,* 448-50.

(54) Marioli, J. M.; Kuwana, T. *Electroanalysis (N. Y.)* **1993,** *5,* 11-15.

(55) Marioli, J. M.; Sereno, L. E. *J. Liq. Chromatogr. Relat. Technol.* **1996,** *19,* 2505-2515.

(56) Marioli, J. M.; Luo, P. F.; Kuwana, T. *Anal. Chim. Acta* **1993,** *282,* 571-80.

(57) Morita, M.; Niwa, O.; Tou, S.; Watanabe, N. *J. Chromatogr., A* **1999,** *837,* 17-24.

(58) Jin, J. Y.; Miwa, T. *Bunseki Kagaku* **1998,** *47,* 665-672.

(59) Ge, J.; Johnson, D. C. *J. Electrochem. Soc.* **1995,** *142,* 1525-31.

CHAPTER 2. ACTIVATED PULSED AMPEROMETRIC DETECTION OF CYSTEINE AT PLATINUM ELECTRODES IN ACIDIC MEDIA

A paper published in *Electroanalysis*

Matthew E. Johll, Douglas G. Williams[1], and Dennis C. Johnson*

Abstract

Anodic voltammetric detection of sulfhydryl compounds, represented here by cysteine, at Pt electrodes in acidic media occurs concomitantly with anodic generation of surface oxide. It is speculated that the adsorbed hydroxyl species (PtOH), proposed to be the intermediate product in formation of the inert oxide (PtO), is the source of O-atoms transferred to the sulfonic acid produced by oxidation of the sulfhydryl moiety. However, as a consequence of this electrocatalytic response mechanism, application of the traditional three-step waveform for pulsed amperometric detection (PAD) of sulfhydryl compounds is accompanied by a large background signal resulting from PtO formation. To diminish the background signal, the traditional three-step PAD waveform has been modified by insertion of a brief (100 ms) anodization step prior to the detection step to activate the Pt surface by generation of PtOH with minimal conversion to PtO. The subsequent negative step from the activation potential (E_{act}) to the detection potential ($E_{det} < E_{act}$) permits the PtOH to be harvested in the detection

mechanism without significant background signal.

Introduction

Pulsed amperometric detection (PAD), based on a three-step potential-time (*E vs. t*) waveform (Fig. 1a), has been applied successfully at Pt and Au electrodes for mixtures of numerous aliphatic organic compounds following their separations by liquid chromatography (LC) [1-13]. Included have been alcohols with detection at Pt electrodes [1]; alditols and saccharides at Pt [2] and Au [3-6]; glycoconjugates at Au [7-10]; alkanolamines at Au [11]; amino acids at Pt [12]; alkyl monoamines and diamines at Au [13]; thiourea at Au [14]; sulfur-containing pesticides at Au [15]; penicillins at Au [16,17]; and other biologically significant thiocompounds at Au, including methionine, cystamine and glutathione [18].

The traditional PAD waveform (Fig. 1a) applies a sequence of three potential steps to achieve anodic detection (E_{det}), oxidative cleaning of the electrode ($E_{oxd} > E_{det}$) and reduction of surface oxide ($E_{red} < E_{det}$). Typically, the frequency of PED waveforms is ca. 1 s^{-1}. Optimal E_{det} values in PAD applied for alditols and carbohydrates are sufficiently low so that a negligible amount of surface oxide is formed. Therefore, background signals are small and detection limits are at low picomolar levels in LC-PAD. Whereas alditols and carbohydrates are detected by PAD at either Pt or Au electrodes, Au

electrodes are most commonly used in LC-PAD. This choice has resulted because O_2(aq) is detected at the optimal E_{det} value for Pt and resulting LC-PAD baselines can be large and exhibit substantial drift.

Anodic detection of organic amines and sulfur compounds using the waveform in Figure 1a requires E_{det} values sufficiently large so that inert surface oxides are formed concomitantly with the detection process. It is believed that adsorbed hydroxyl radicals (PtOH/AuOH) generated as intermediate products in the production of the inert oxides (PtO/AuO) are the source of O-atoms transferred to the oxidation products. Therefore, applications of the traditional PAD waveform for the detection of organic amines and sulfur compounds is characterized by large background signals, due to the concomitant formation of surface oxides, with a resultant increase in detection limits. Furthermore, the calibration plot can exhibit significant deviation from linearity as a consequence of contributions to the total current from oxidative desorption of preadsorbed analytes. In contrast, use of a constant (DC) potential is not acceptable because a persistent response for amines and sulfur compounds is not obtained due to the passivation of electrodes caused by accumulation of the inert oxides (PtO/AuO).

Research in this laboratory continues to focus on examination of alternate waveforms for detection of amines and sulfur compounds at noble

metal electrodes with the goal of minimizing contributions to the total current from the simultaneous anodic formation of surface oxide. For example, Polta and Johnson reversed the sequence for application of the oxidative and reductive pulses in the three-step PAD waveform to decrease the background signal during anodic detection of thiourea at Au electrodes [14]. This strategy now is referred to as 'reversed PAD' (RPAD). Neuburger and Johnson diminished the background signal from oxide formation by the substitution of a rapid triangular potential scan for the constant detection potential of the traditional three-step waveform [19]. This waveform has been applied successfully for detection of underivitized amino acids [20] and several biologically significant thio-compounds [18,21] following their chromatographic separations. More recently, Williams and Johnson described a four-step waveform (Fig. 1b) for detection of $As(OH)_3$ by oxidation to $OAs(OH)_3$ at a Pt electrode in acidic media [22]. This reaction is an example of an anodic O-transfer reaction that requires generation of adsorbed OH-species. This four-step waveform represents a modification of the traditional three-step PAD waveform in which a so-called "activation step" is added prior to the detection step ($E_{act} > E_{det}$). The detection step then is followed by the traditional positive and negative pulses to insure oxidative cleaning and reductive reactivation of the electrode surface. This detection strategy is referred to as 'activated pulsed amperometric detection' (APAD).

The designs of the RPAD and APAD waveforms were inspired by data reported by Gilroy from a study of oxide formation at Pt electrodes in acidic media [23]. Gilroy reported that the anodic charge for oxide growth (q_{ox}) following a positive potential step to a value $E_1 > E_o$, where E_o is the potential for initiation of oxide growth, increases as a linear function of log{t} with a slope proportional to applied overpotential ($\eta = E_1 - E_o$). Gilroy also determined that a subsequent negative step to E_2, where $E_o < E_2 < E_1$, results in a temporary halt in oxide growth [23]. Subsequently, oxide growth resumes at a time consistent with the growth dynamics at E_2. Therefore, the step to E_{ad} in our APAD waveform is believed to generate PtOH that, in turn, can be harvested within the anodic response mechanism following the negative step to E_{det}. Williams and Johnson demonstrated that the background signal for detection of $As(OH)_3$ was substantially smaller for the APAD waveform in comparison to the PAD waveform [22]. More recently, Altunata et al. Compared the S/N for a variety of waveforms, including the RPAD and APAS waveforms, for detection of the thiazolidine ring of penicillin G in a flow-injection system [17]. These workers concluded that the RPAD and APAD do not necessarily present an advantage over the traditional PAD waveform for this compound. However, peak shapes were slightly improved which could be advantageous in LC applications of these detection strategies.

Described here are some results from a reexamination of the APAD waveform applied to cysteine,as a model of sulfhydryl compounds, detected at Pt electrodes in an acidic medium. Anodic oxidation of cysteine has been studied at noble metal electrodes [24-27] as well as multivalent ruthenium oxide electrodes [28]. Davis and Bianco concluded that cysteine adsorbs on Pt electrodes as the thiyl radical (RS_{ads}) and can undergo subsequent oxidization to cystine or cysteic acid, depending on conditions [24]. Pradáč and Koryta also speculated that the thiyl radical is formed during oxidation of cysteine at Pt electrodes [25]. Samec et al. demonstrated that oxidations of both cysteine and cystine leads to formation of adsorbed thiyl radicals (RS_{ads}) at Pt electrodes [26].

Experimental

Chemicals: Sulfuric acid was Certified grade from Fisher Scientific. L(–)cysteine (99% pure) was from Alfa Products. Solutions were prepared with deionized water from a Millipore system.

Instrumentation: Voltammetric measurements were made at a Pt rotated disk electrode (RDE, 0.184 cm^2) with an AFMSRX rotator/controller and a RDE4 potentiostat (Pine Instruments). Electrode potentials were controlled and are reported vs. a saturated calomel electrode (SCE, Fisher Scientific). Data were collected with Labview-4.0 software (National

Instruments) operated on a Pentium 120 personal computer with a AT-MIO-16XE-50 data acquisition board (National Instruments).

Electrospray mass spectrometry (ES-MS) was performed in the positive ion mode on a TSQ700 triple quadrupole mass spectrometer fitted with an ESI interface, both from Finnigan MAT. The flow injection (FI) system consisted of a 7010 injector (Rheodyne) with a 20-μL injection loop, an APM-2 isocratic pump (Dionex), and an ED40 electrochemical detector and flow-through cell (Dionex).

Electrochemical Procedures: The pulsed waveforms were generated digitally within the PC and are described in Table 1. Activated pulsed voltammetry (APV) was performed using the APAD waveform with an increase in E_{det} by 10 mV for each cycle of the waveform throughout the potential region of interest. Current response in APAD and APV waveforms was generated by digital integration of the electrode current at E_{det} over the specified time period (T_{det}) followed by division of the current integral by T_{det} to produce an average amperometric response. Note that there was not a delay period, as found in conventional PAD waveforms, prior to the start of current integration in the detection period. Cyclic voltammetry (CV) was of the conventional design with triangular analog potential-time waveforms generated within the RDE4 potentiostat.

Solutions were deaerated with dispersed N_2(g) (99.99%, Air Products)

before and during studies of CV, APV and APAD response at the Pt RDE.

Results and Discussion

Cyclic Voltammetric Response of Cysteine at Pt RDE: The cyclic voltammetric (CV) response for Pt in 0.10 M H_2SO_4 is shown in Figure 2 by curve a (dotted line). The anodic wave obtained during the positive scan in the region E > ca. 0.6 V corresponds to rapid formation of PtOH with subsequent conversion of PtOH to PtO. Evolution of O_2 becomes prominent for E > 1.3 V (not shown). The cathodic peak observed during the subsequent negative scan in the region ca. 0.5 to 0.2 V corresponds to reduction of surface oxide (PtOH and PtO) to regenerate the pristine Pt surface. The cathodic formation (negative scan) and anodic dissolution (positive scan) of adsorbed H-atoms are observed in the region ca. 0.0 to –0.3 V. Rapid cathodic evolution of H_2 occurs at E < ca. –0.3 V.

The CV response for cysteine as a function of concentration (0.25 mM to 1.0 mM) is shown in Figure 2 by curves b to e (solid lines). The residual response obtained for the absence of cysteine is indicated by the dotted line. The anodic wave for oxidation of cysteine during the positive scan appears to correspond to two unresolved peaks. The anodic signal for the first peak (ca. 0.8 V) is not a linear function of cysteine concentration. Other experiments (data not shown) demonstrated that this peak current also is

not a linear function of the square root of the rotational velocity ($\omega^{1/2}$, rad/s) of the RDE. These observations are consistent with the conclusion that the initial step in cysteine oxidation is under mixed control by concomitant surface-controlled and transport-controlled processes. This is consistent with previous conclusions that oxidation of cysteine (RSH) in this potential region (ca. 0.7 to 0.9 V) corresponds to anodic production of both adsorbed thiyl radicals (RS_{ads}) and soluble cystine (RSSR) [23]. The second anodic peak for cysteine oxidation (Fig. 2, curves b to e) produces a maximum signal at ca. 1.1 V. This peak response is believed to correspond to oxidation of RS_{ads} and RSH to cysteic acid (RSO_3H) [18]. To verify this speculation, a 5.0-mL sample of 0.10 mM cysteine in 0.10 M H_2SO_4 was electrolyzed at a constant potential of 1.0 V at a coiled Pt gauze electrode (ca. 16 cm^2). Following a 16-h electrolysis period, the product solution was analyzed by ES-MS. The product components identified were cystine (RSSR) and cysteic acid (RSO_3H), with the concentration of the later being ca. 40% lower than that of the former. The high level of cystine is evidence that the oxide-covered Pt electrode under DC control is active for oxidation of cysteine to cystine but is not very active in supporting the O-transfer mechanism required to produce cysteic acid.

Upon reversal of the positive scan at 1.4 V (Fig. 2, curves b to e), the anodic current for cysteine is observed to decay quickly. This current decay

is explained on the basis of attenuation of the rate of H_2O discharge to generate the PtOH species needed to support oxidation of cysteine to cysteic acid. However, it is observed that the anodic current does not return to zero, perhaps because of persistent oxidation of cysteine to cystine at the PtO-covered electrode. This small anodic current during the negative scan persists to ca. 0.5 V, i.e., 0.1 V more negative than required for onset of cysteine oxidation during the positive scan. This observation suggests that PtO might be more active than Pt for oxidation of cysteine to cystine. However, increases to the positive scan limit, assumed to produce a more complete layer of PtO, results in a smaller anodic current during the subsequent negative scan (data not shown). It also is apparent in Figure 2 that the small anodic current observed during the negative scan steadily increases throughout the region ca. 1.0 to 0.6 V. A more detailed discussion of this anodic phenomenon will be reserved for a subsequent publication.

APAD Response for Cysteine at Pt RDE: Efforts to determine the optimal values for E_{det} and T_{act} in the APAD waveform were based on APV response obtained by advancing E_{det} in the APAD waveform by 10 mV/cycle throughout the region 0.4 to 1.5 V. The resulting APV curves give an accurate picture of the dependence of the APAD response as a function of E_{det} for the remaining specified values of waveform parameters listed in Table 1. Representative APV data for 1.00 mM cysteine are shown in Figure 3 by

curves a to c for E_{act} = 1.60 V with T_{act} values of 10 ms (a), 100 ms (b) and 300 ms (c). The corresponding background current response is shown in curves a' to c'. The anodic response is independent of the direction of E_{det} scan, as is expected if the applications of E_{oxd} and E_{red} are successful in maintaining a uniform activity for the electrode surface. Whereas the largest cysteine response is obtained in the region E_{det} > 1.0 V for T_{act} = 10 ms (a), the background also is the largest for this value of T_{act}. This anodic background undoubtedly is the result of continued formation of PtOH at E_{det} because T_{act} = 10 ms (E_{act} = 1.60 V) is not sufficient to achieve the equilibrium surface coverage by this species characteristic of the values of E_{det} > 1.0 V. The background signal for T_{act} = 100 (b') and 300 ms (c') is virtually zero over the range E_{det} = 0.7 to1.3V. For E_{det} < ca. 0.7 V, a cathodic background is obtained, undoubtedly because of onset of cathodic reduction of PtOH and PtO. The cysteine response in the region E_{det} = ca. 0.7 to 0.9 V decreases steadily as T_{act} is increased. This is likely to be the consequence of conversion of some PtOH to PtO with corresponding loss of active surface area.

Figure 4 contains detailed results summarizing the dependence of the APAD signal at E_{det} = 1.00 V as a function of T_{act} values in the range 0 to 300 ms (E_{act} = 1.60 V). The background current (curve a) decreases steadily to approximately zero at T_{act} = ca. 100 ms. Whereas the choice of T_{act} > 100 ms

might seem desirable to ensure suppression of the background current, this choice has the disadvantage of an extended waveform period. The total signal for 1.00 mM cysteine as a function of T_{act} is also given in Figure 4 (curve b). This signal decreases significantly as T_{act} is increased to ca. 50 ms with only slight decreases as T_{act} is increased to values > 100 ms. Based on the results given in curves a and b, the value T_{act} = 100 ms was chosen for the remaining studies to produce a significant cysteine signal with minimal background without an excessively long waveform period.

It is appropriate to question whether an APAD waveform with E_{act} = 1.60 V and T_{act} = 100 ms offers a unique advantage over a PAD waveform in which sampling of the anodic signal is delayed for 100 ms following the step to E_{det}. This question can be answered on the basis of chronoamperometric data shown in Figure 5. Curves a and a' were recorded at E_{det} = 1.00 V following the potential step from E_{red} = –0.25 V (T_{red} = 30 s) to E_{det}. The residual response (a') shows a large initial spike, due to rapid anodic formation of surface oxide, with very slow decay for t > 1 s. The total response in the presence of cysteine (a) also exhibits a large initial spike, due to anodic formation of oxide and concomitant oxidative desorption of preadsorbed cysteine, with gradual decay for t > 1 s. Curves b and b' were recorded at E_{det} = 1.00 V following the steps from E_{red} = –0.25 V (T_{red} = 30 s) to E_{act} = 1.60 V (T_{act} = 100 ms) to E_{det}. The residual response (b') exhibits a

small short-lived cathodic spike corresponding to double-layer charging following the step from E_{act} to E_{det}. Thereafter, the background current is virtually zero. The response for 1.00 mM cysteine (b) is devoid of the large initial spike, because preadsorbed cysteine has been oxidatively desorbed at E_{act} and, of course, because there is no contribution to oxide formation in this signal. The fact that the cysteine response in curve b is less than that in curve a is evidence that a portion of the electrode surface has been deactivated by the formation of PtO during the activation pulse. Nevertheless, it is apparent from visual inspection that the signal-to-background ratio (S/B) is superior for the APAD waveform throughout the period represented. To achieve the same S/B by the PAD waveform, an excessive delay time would be required and the resulting waveform frequency would be prohibitory.

The APV response as a function of cysteine concentration is shown in Figure 6 using the APV waveform described in Table 1 with T_{act} = 100 ms. Curves b to e obtained in the presence of cysteine exhibit pseudo plateaus in the region ca. 0.9 to 1.2 V. Based on this fact, and observation that the background current (a) is at a minimum at ca. 1.0 V, the value E_{det} = 1.00 V is chosen for further applications of the APAD waveform for cysteine.

Estimation of n for Cysteine Oxidation: Determination of the number of electrons transferred in the anodic reaction of cysteine is important for

further elucidation of the APAD response mechanism. Levich plots of i *vs.* $\omega^{1/2}$ were constructed for several values of cysteine concentration values based on APAD data obtained using the waveform in Table 1 with T_{det} = 117 ms. These plots (not shown) exhibited negative deviation from linearity at cysteine concentrations > 0.25 mM. Nonlinearity in Levich plots is evidence for mixed transport-kinetic control of the response mechanism. Therefore, Koutecky-Levich plots of $1/i$ vs. $1/\omega^{1/2}$ were constructed and representative plots are shown in Figure 7. In Koutecky-Levich plots, the slope is equal to $1/0.62nFAD^{2/3}\upsilon^{-1/6}C^b$, where n is the number of electrons (eq/mol), F is the faraday constant (C/eq), A is the geometric electrode area (cm^2), D is the diffusion coefficient (cm^2/s), υ is the kinematic viscosity of the solution (cm^2/s) and C^b is the bulk concentration of reactant (mM). Statistical descriptions of all Koutecky-Levich plots constructed are given in Table 2. Using $D = 7.0x10^{-6}$ cm^2/s for cysteine [29], n values were calculated from the slopes of these plots and the values are included in Table 2. The average of the n values is 5.5±0.6 eq/mol.

Stability of APAD Response at Pt RDE: Stability is required for APAD signals if this waveform is to be considered suitable for detection of sulfhydryl compounds in LC systems. To examine the signal stability as a function of cysteine concentration, the Pt RDE was reduced for 30 s at –0.25 V prior to application of the APAD waveform with monitoring of the current

response for a 5-min period. The results are shown in Figure 8. It is apparent for $C^b \leq 0.5$ mM, that the APAD signal is quite stable at low cysteine concentrations. For 0.25 mM cysteine (curve b) the signal at 6 s is within 1% of the signal at 5 min. At higher concentrations, signals at 5 min are 5-10% below that at 6 s.

Flow-injection Detection of Cysteine: It is expected that application of the APAD waveform for sulfhydryl compounds is most likely to be in flow-through thin-layer cells following LC separations of these compounds. Therefore, the APAD response was tested in a flow-through cell as part of a flow-injection (FI) system. Typical FI-APAD data are shown in Figure 9 as a function of cysteine concentration in the range 5 to 50 μM. The average peak signals and standard deviations are: (a) 0.172±0.002 μA, (b) 0.381±0.004 μA, (c) 0.712±0.001 μA, (d) 1.044±0.007 μA, (e) 1.386±0.012 μA and (f) 1.608±0.014 μA. The calibration curve was linear over the concentration range 5 to 40 μM and is described by the following statistics: intercept = 0.0203±0.0225 μA, slope = 0.0342±0.0009 μA/μM and r^2 = 0.9992. Uncertainties in these values correspond to standard deviations. The standard deviation of the background signal (s_{bkd}) was determined for each run and a pooled value of s_{bkd} = 0.0027 μA was calculated. The limit of detection (LOD), corresponding to the amount of cysteine in the 20-μL injection required to produce a signal equal to $3s_{bkd}$, was ca. 2 pmol.

Conclusions

The APAD waveform was demonstrated to produce stable and sensitive anodic response for cysteine at Pt electrodes in 0.10 M H_2SO_4. An average of n=5.5±0.6 eq/mol (Table 2) was calculated from slopes of Koutecky-Levich plots. This value supports the conclusion that the predominant reaction of cysteine under the APAD waveform corresponds to production of cysteic acid (n=6 eq/mol). This reaction is believed to occur by a mechanism that requires the anodic discharge of H_2O to produce adsorbed OH-radicals (PtOH), as indicated by:

$$3(Pt + H_2O \rightarrow PtOH + H^+ + e^-) \quad (1)$$

$$RSH + 3PtOH \rightarrow RSO_3H + 3Pt + 3H^+ + 3e^- \quad (2)$$

$$\text{net: } RSH + 3H_2O \rightarrow RSO_3H + 6H^+ + 6e^- \quad (3)$$

It is apparent that the Pt electrode surface is activated by the brief pulse to E_{act}=1.60 V (T_{act}=100 ms) without excessive deactivation of the electrode by formation of the inert surface oxide (PtO).

The APAD response in a flow-injection system was linear (r^2=0.9992) over the concentration range 5 of 40 μM cysteine with a limit of detection estimated at 2 pmol (20 μL injections). These results are excellent in anticipation of future applications for detection of sulfhydryl compounds following their separations by liquid chromatography.

Acknowledgements

This research was supported by grants CHE-9215963 and CHE-9634544 from National Science Foundation, and a grant from Dionex Corp., Sunnyvale, CA.

References

[1] W.R. LaCourse, D.C. Johnson, M.A. Rey, R.W. Slingsby, *Anal. Chem.* **1991**, *63*, 134.

[2] S. Hughes, D.C. Johnson, *Anal. Chim. Acta* **1981**, *132*, 11.

[3] R.D. Rocklin, C.A. Pohl, *J. Liq. Chromatogr.* **1983**, *6* 1577.

[4] J.D. Olechno, S.R. Carter, W.T. Edwards, D.G. Gillen, *Am. Biotech. Lab.***1987**,*5*, 38.

[5] D.C. Johnson, W.R. LaCourse, *Electroanalysis* **1992**, *4*, 367.

[6] D.C. Johnson, W.R. LaCourse, in *Carbohydrate Analysis: High Performance Liquid Chromatography and Capillary Electrophoresis* (Ed: Z. El Rassi), *Elsevier, Amsterdam* **1995**, ch. 10.

[7] M.R. Hardy, R.R. Townsend, *Proc. Natl. Acad. Sci.* **1988**, *85*, 3289.

[8] M.R. Hardy, R.R. Townsend,Y.C. Lee, *Anal. Biochem.* **1988**, *170*, 54.

[9] J.D. Olechno, S.R. Carter, W.T. Edwards, D.G. Gillen, R.R. Townsend, Y.C. Lee, M.R. Hardy, in *Techniques of Protein Chemistry* (Ed: T.E. Hugli), Academic Press, San Diego **1989**, pp, 364-376.

[10] R.R. Townsend, in *Carbohydrate Analysis: High Performance Liquid Chromatography and Capillary Electrophoresis* (Ed: A. El Rassi), Elsevier, Amsterdam **1995**, ch. 5.

[11] D.A. Dobberpuhl, D.C. Johnson, *J. Chromatogr. A* **1995**, *694*, 391.

[12] J.A. Polta, D.C. Johnson, *J. Liq. Chromatogr.* **1983**, *6*, 1727.

[13] D.A. Dobberpuhl, J.C. Hoekstra, D.C. Johnson, *Anal. Chim. Acta* **1996**, *322*, 55.

[14] T.Z. Polta, D.C. Johnson, *J. Electroanal. Chem.* **1986**, *209*, 159.

[15] A. Ngoviwatchai, D.C. Johnson, *Anal. Chim. Acta* **1989**, *215*, 1.

[16] L. Koprowski, E. Kirchmann, L.E. Welch, *Electroanalysis* **1993**, *5*, 473.

[17] S. Altunata, R.L. Earley, D.M. Mossman, L.E. Welch, *Talanta* **1994**, *42*, 17.

[18] W.R. LaCourse, G.S. Owens, *Anal. Chim. Acta* **1995**, *307*, 301.

[19] G.G. Neuburger, D.C. Johnson, *Anal. Chem.* **1988**, *60*, 2288.

[20] L.E. Welch, W.R. LaCourse, D.A. Mead, Jr., D.C. Johnson, T. Hu, *Anal. Chem.* **1989**, *61*, 555.

[21] P.J. Vandeberg, D.C. Johnson, *Anal. Chim. Acta* **1994**, *290*, 317.

[22] D.G. Williams, D.C. Johnson, *Anal. Chem.* **1992**, *64*, 1785.

[23] D. Gilroy, *J. Electroanal. Chem.*, **71** (1976) 257; **83** (1977) 329.

[24] D. Davis, E. Bianco, *J. Electroanal. Chem.* **1966**, *12*, 254.

[25] J. Pradáč, J. Koryta, *J. Electroanal. Chem.* **1968**, *17*, 185.

[26] Z. Samec, Zh. Malysheva, J. Kortya, J. Pradáč, J. *J. Electroanal. Chem.* **1975**, *65*, 573.

[27] J.A. Reynaud, B. Malfoy, P. Canesson, *J. Electroanal. Chem.* **1980**, *114*, 195.

[28] J. Cox, T. Gray, *Anal. Chem.* **1990**, *62*, 2742.

[29] I.M. Kolthoff, C. Barnum, *J. Amer. Chem. Soc.* **1940**, *62*, 3061; **1941**, *63*, 520.

Table 1. Standard parameters used for the APV and APAD waveforms.

Waveform	E_{det} (V)	T_{det} (ms)	E_{oxd} (V)	T_{oxd} (ms)	E_{red} (V)	T_{red} (ms)	E_{act} (V)	T_{act} (ms)
APV	Stepped	117	1.60	100	–0.25	500	1.60	Varied
APAD	1.00	Varied	1.60	100	–0.25	500	1.60	100

Table 2. Summary of results for Koutecky-Levich plots of cysteine response at the Pt RDE in 0.1 M H_2SO_4.

Concentration (mM)	r^2	Slope ($\mu A^{-1}/(rad/s)^{-1/2}$)	Intercept (μA^{-1})	n (eq/mol)
0.25	0.9989 0.9984	0.1127±0.0023 0.0883±0.0018	0.21±0.36x10^{-3} 2.42±0.24x10^{-3}	4.1 5.2
0.50	0.9992 0.9992	0.0431±0.0014 0.0408±0.0004	1.54±0.22x10^{-3} 2.31±0.07x10^{-3}	5.4 5.6
0.75	0.9981 0.9994	0.0255±0.0004 0.0266±0.0003	2.29±0.06x10^{-3} 1.31±0.04x10^{-3}	6.0 5.8
1.00	0.9974 0.9997	0.0195±0.0022 0.0195±0.0001	2.17±0.34x10^{-3} 1.58±0.02x10^{-3}	5.9 5.9

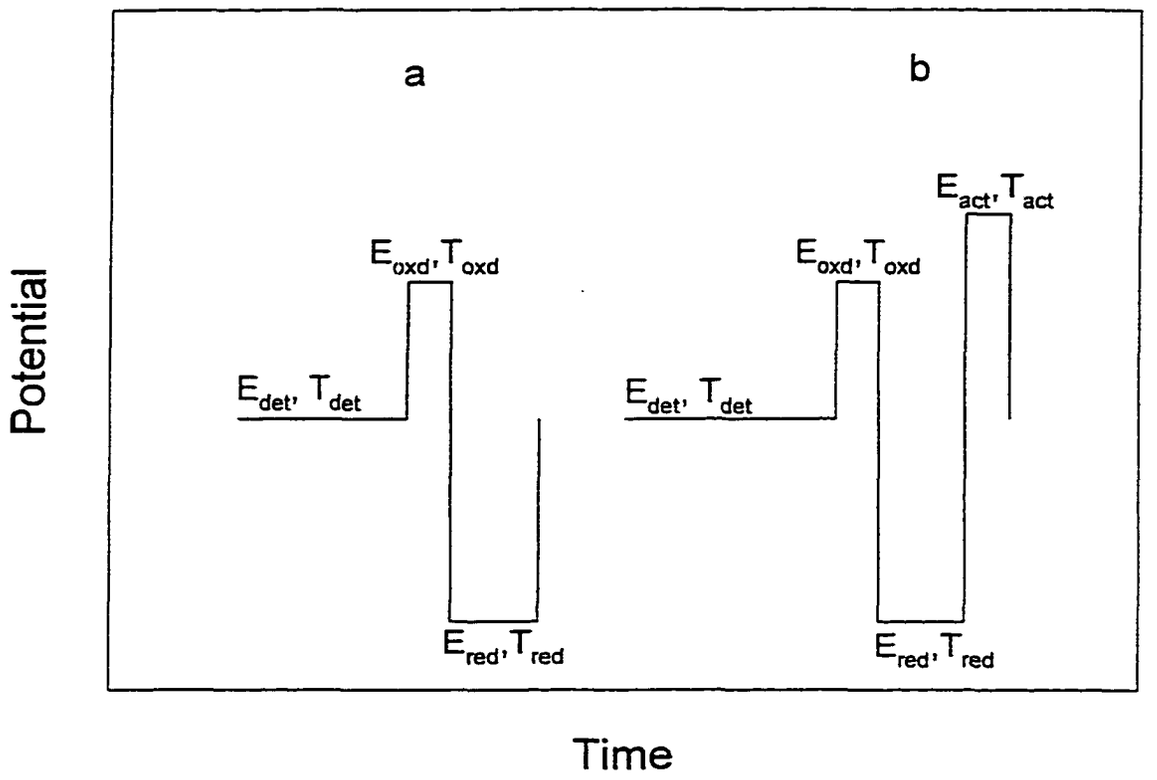

Figure 1. Comparison of (A) three-step PAD and (B) four-step APAD waveforms.

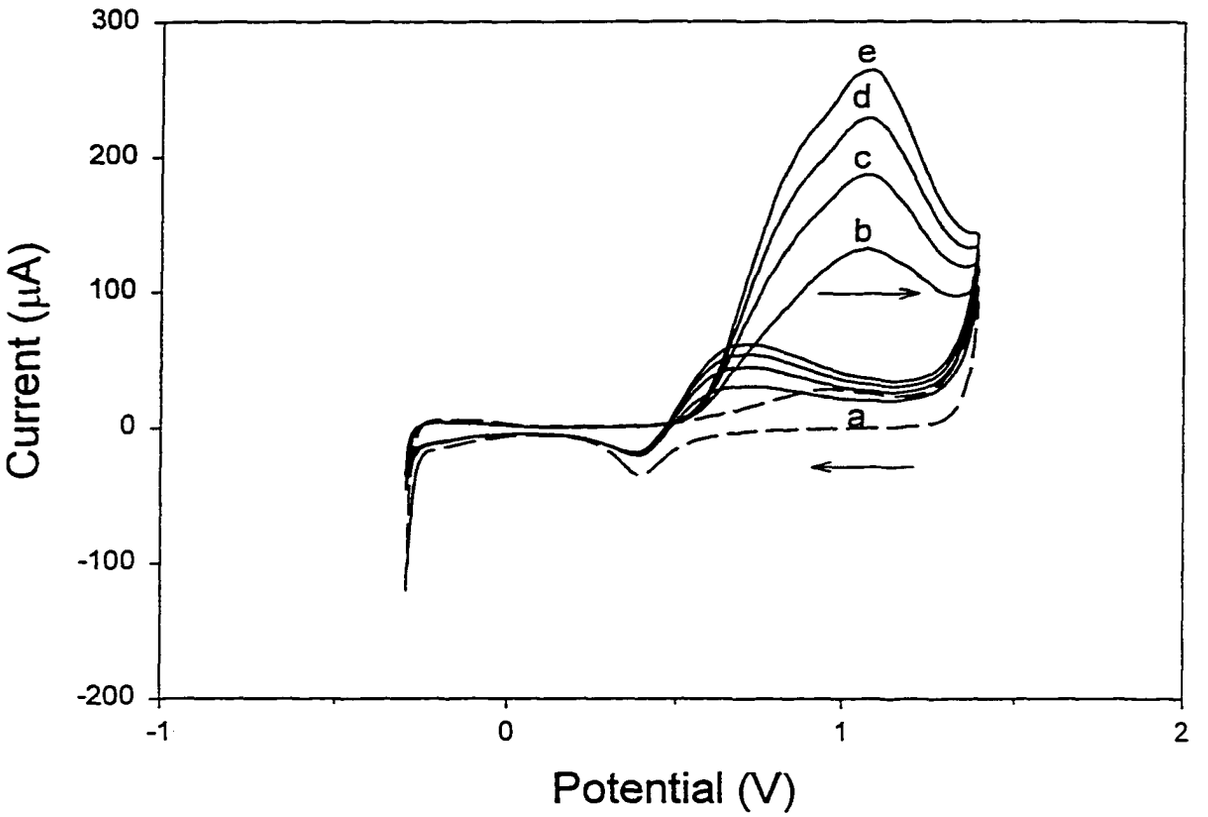

Figure 2. Voltammetric response for cysteine as a function of concentration at a Pt RDE in 0.10 M H_2SO_4. Scan: 50 mV/s. Rotation: 94.2 rad/s. Concentration (mM): (a) 0.00, (b) 0.25, (c) 0.50, (d) 0.75, (e) 1.00.

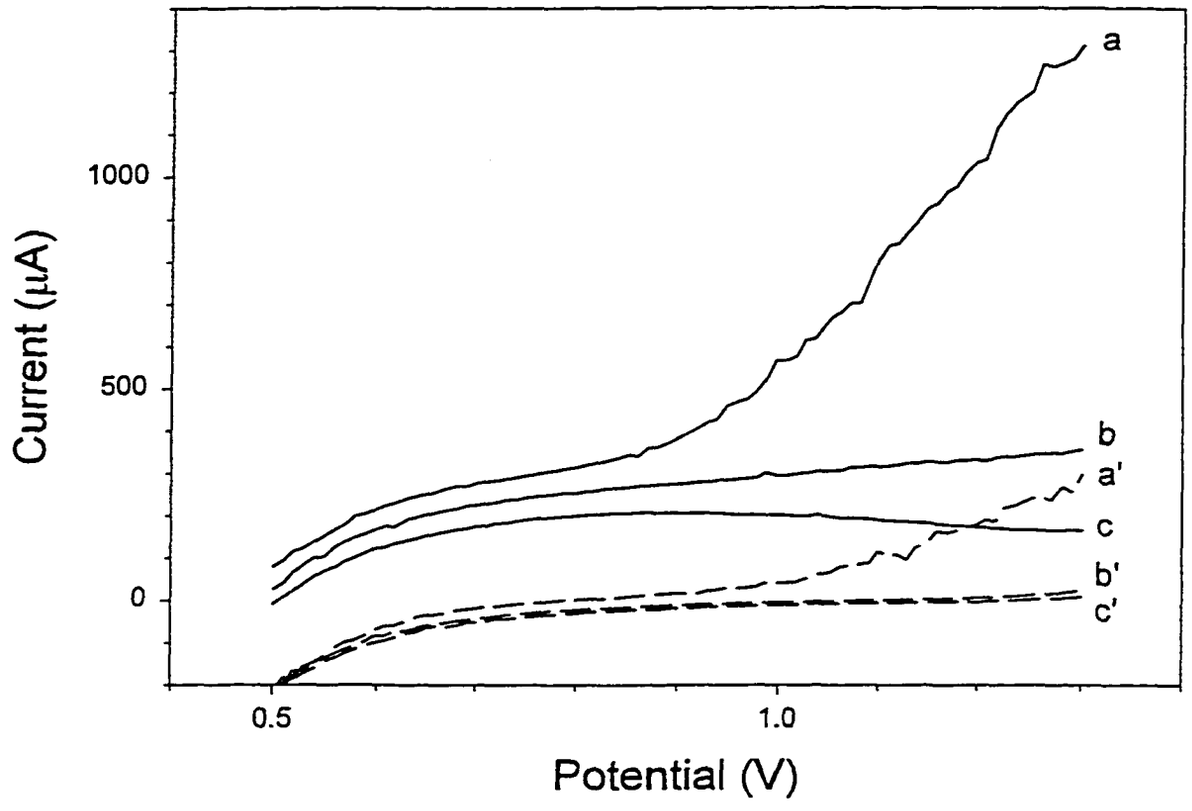

Figure 3. Pulsed voltammetric response for various activation times at the Pt RDE for 1.00 mM cysteine in 0.10 M H_2SO_4. Rotation: 94.2 rad/s. APV waveform: see Table 1. T_{act} (ms): (a) 10, (b) 100, (c) 300.

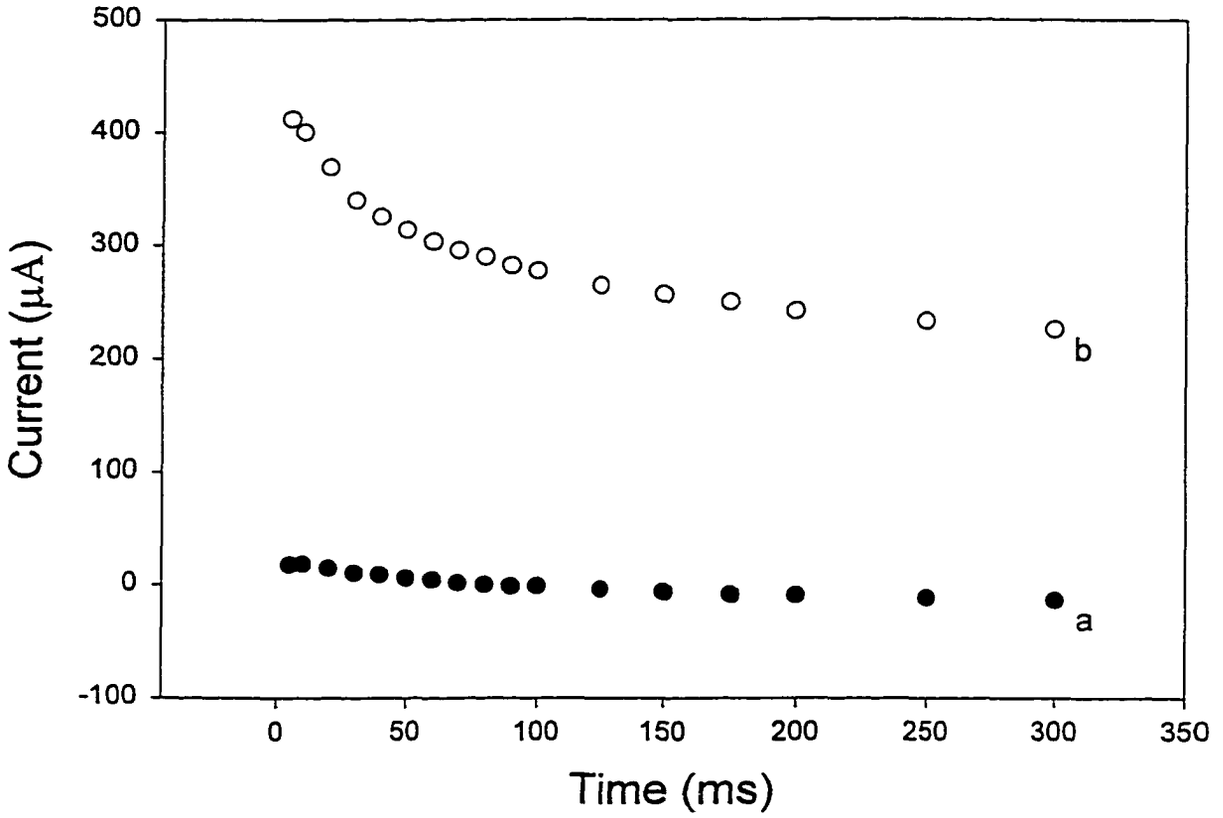

Figure 4. APAD response as a function of activation time at a Pt RDE in 0.10 M H_2SO_4. Rotation: 94.2 rad/s. APAD waveform: see Table 1. T_{det} = 117 ms. Curves: (a) residual, (b) 1.00 mM cysteine.

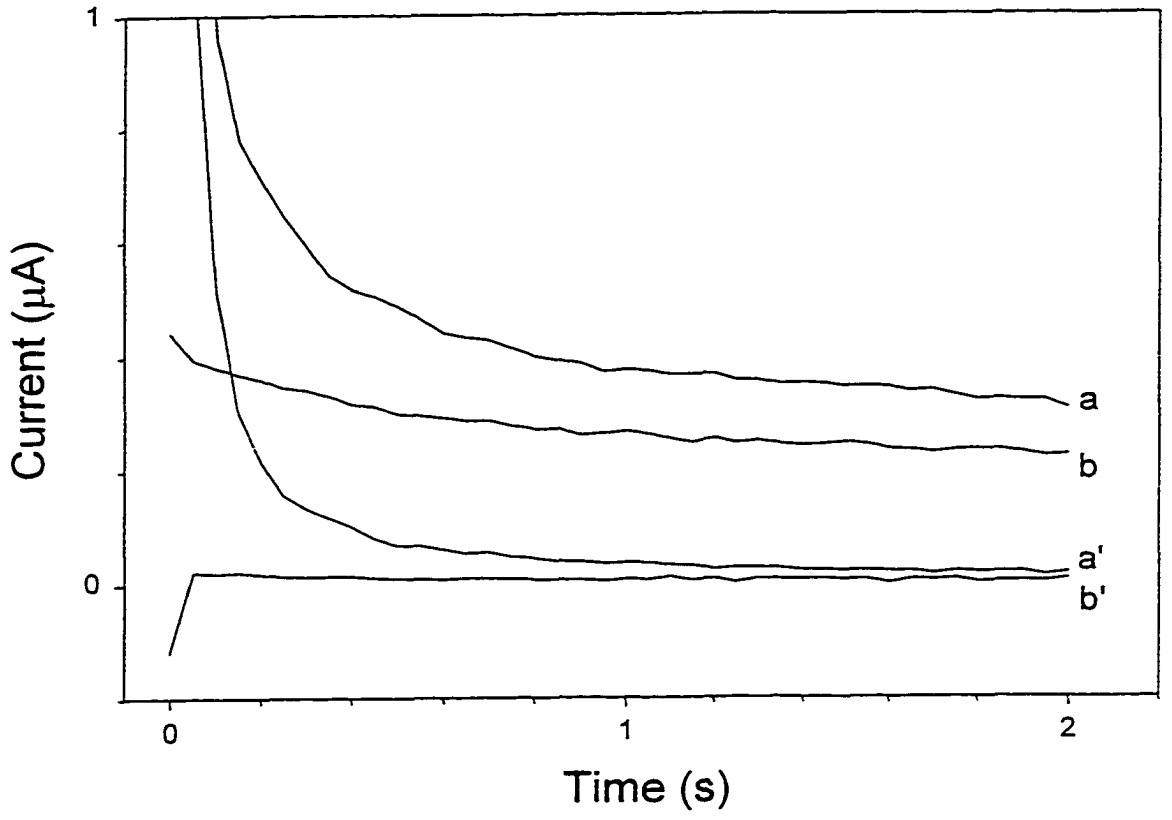

Figure 5. Chronoamperometric data from pulsed waveforms at Pt RDE in 0.10 M H_2SO_4. Curves: (a,a') residual, (b,b') 1.0 mM cysteine. Waveforms: (a,a') E_{red} = –0.25 V (30 s) to E_{det} = 1.00 V; (b,b') E_{red} = –0.25 V (30 s) to E_{act} = 1.60 V (100 ms) to E_{det} = 1.00 V. Current sampling at E_{det}: 20 Hz.

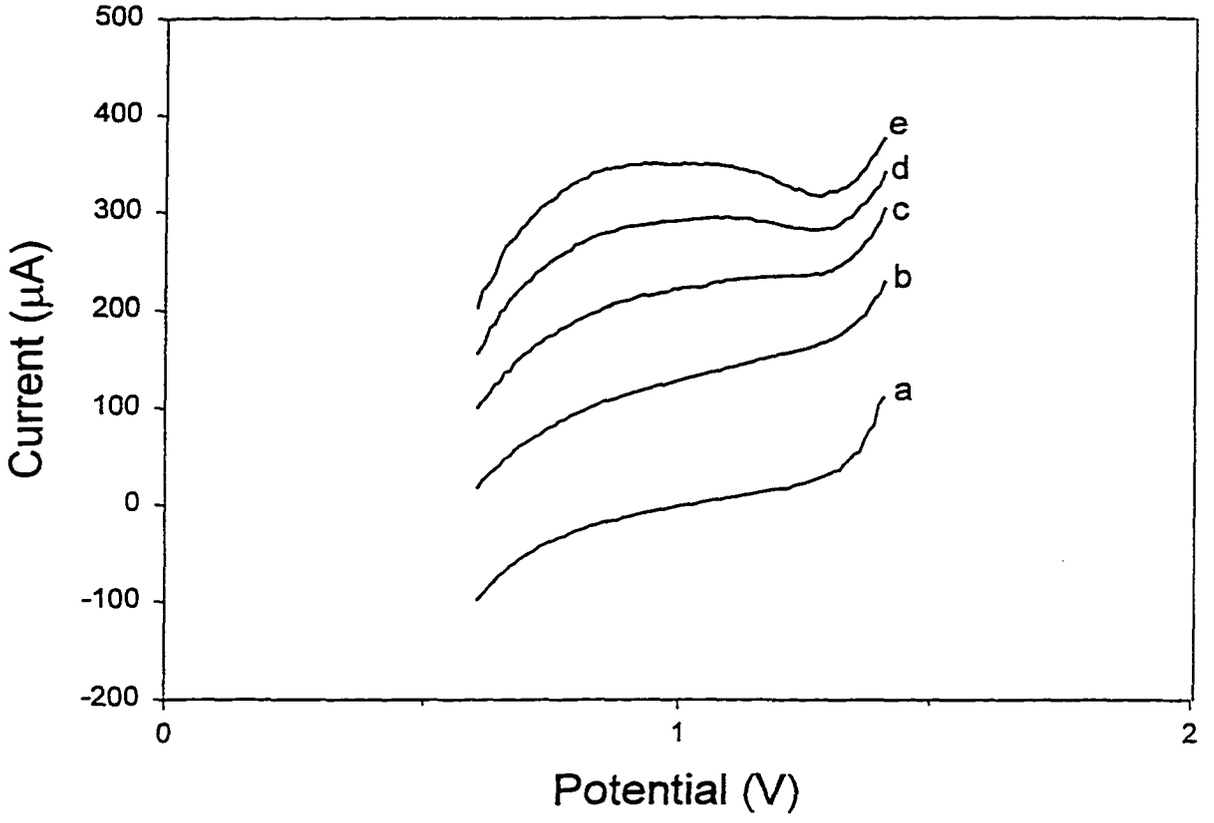

Figure 6. Pulsed voltammetric response for cysteine as a function of concentration at a Pt RDE in 0.10 M H_2SO_4. Rotation: 94.2 rad/s. APV waveform: see Table 1. E_{det} = stepped by 10 mV/cycle, T_{act} = 100 ms. Concentration (mM): (a) 0.00, (b) 0.25, (c) 0.50, (d) 0.75, (e) 1.00.

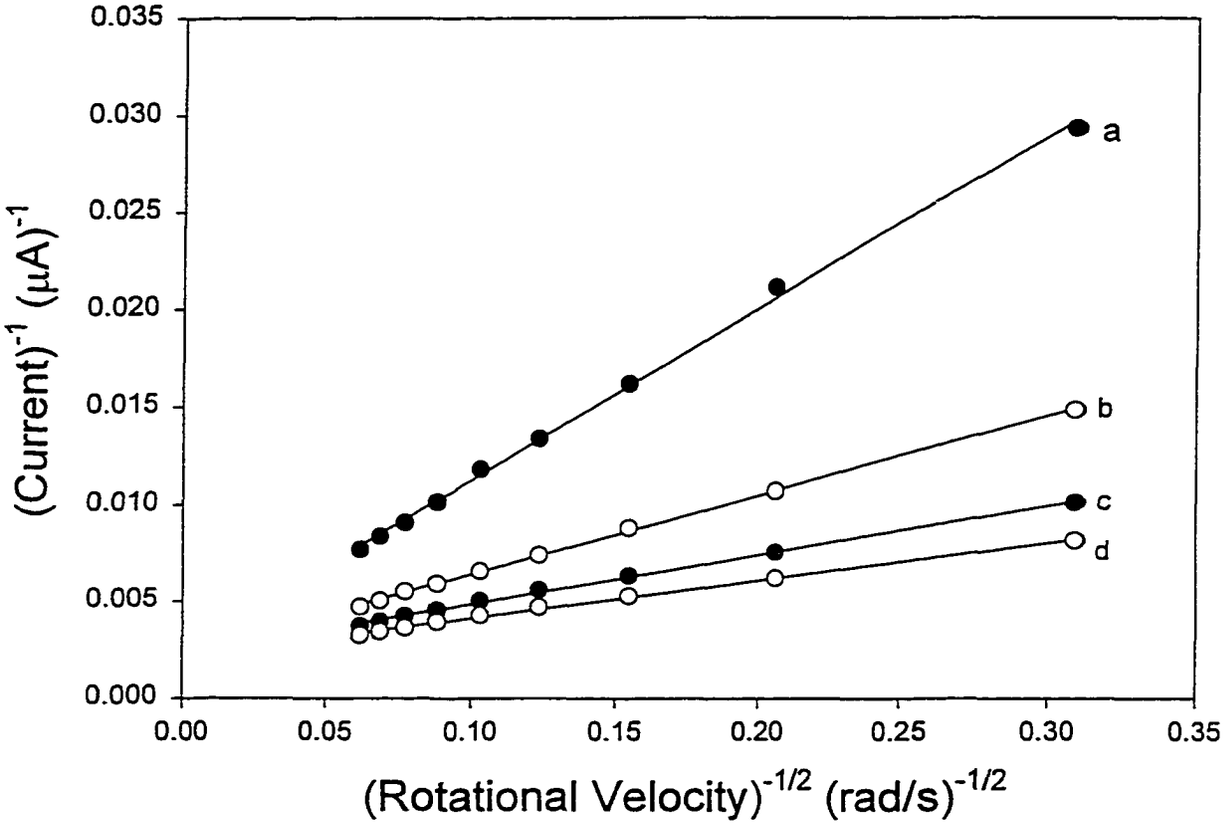

Figure 7. Koutecky-Levich Plots for cysteine at a Pt RDE in 0.10 M H_2SO_4. T_{acq} = 100 ms. Concentration (mM): (a) 0.25, (b), 0.50, (c) 0.75, (d) 1.00.

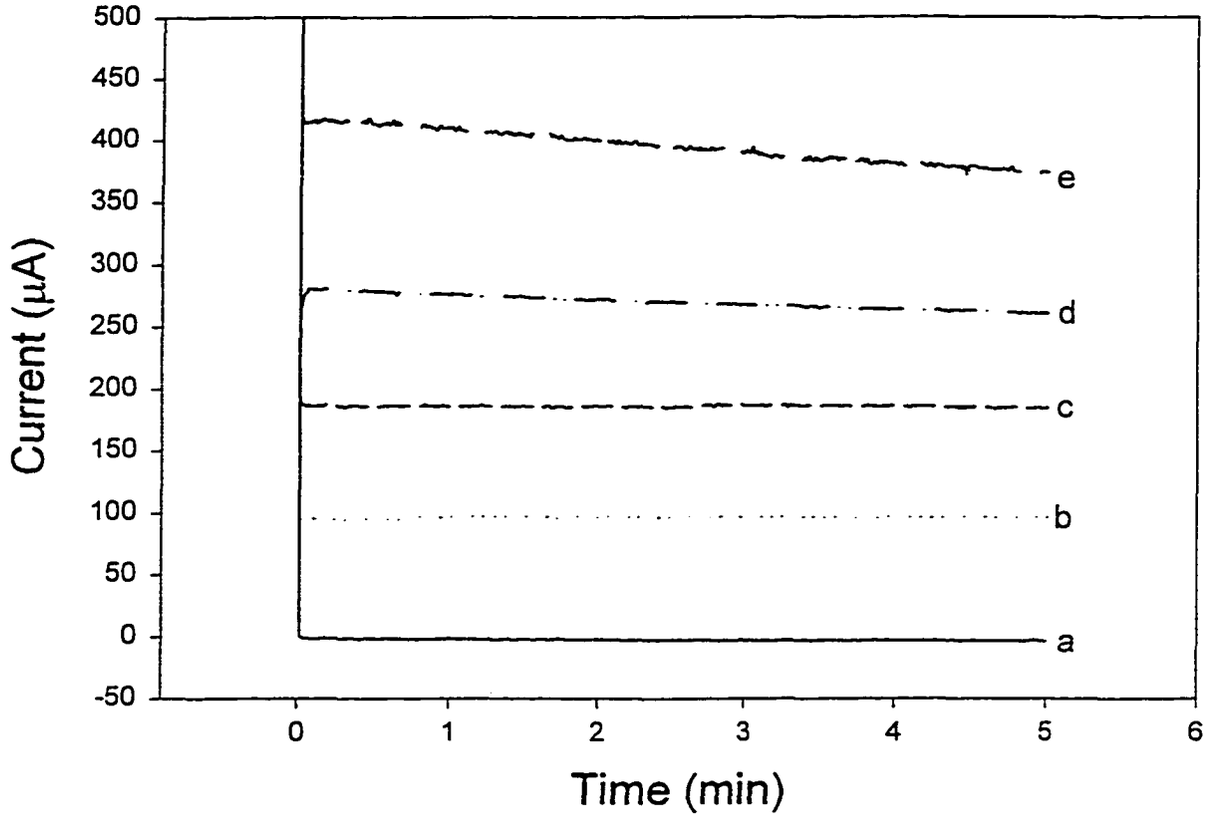

Figure 8. APAD response for cysteine as a function of time at a Pt RDE in 0.10 M H_2SO_4. T_{det} = 110 ms. APAD waveform: see Table 1. Concentration (mM): (a) 0.00, (b) 0.25, (c) 0.50, (d) 1.00, (e) 2.00.

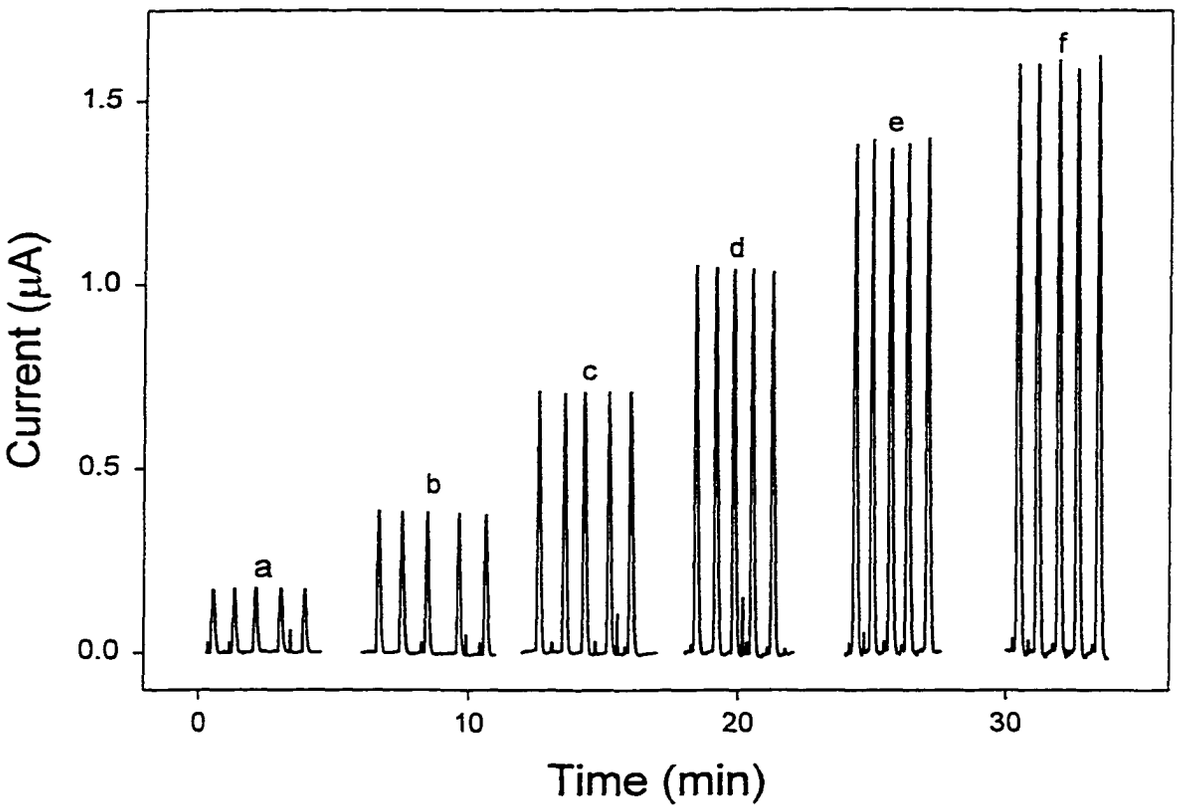

Figure 9. Flow-injection detection of cysteine by APAD at a Pt electrode in 0.10 M H_2SO_4. APAD waveform: see Table 1, T_{del} = 110 ms. Flow Rate: 1.0 mL/min. Concentration (μM): (a) 5, (b) 10, (c) 20, (d) 30, (e) 40, (f) 50.

CHAPTER 3. ANODIC RESPONSE OF CYSTINE AT PREANODIZED Au AND Au-Ag ELECTRODES IN PERCHLORIC ACID MEDIA

A paper published in *Electroanalysis*

Matthew E. Johll and Dennis C. Johnson*

Abstract

This study involves a comparison of the anodic response of the disulfide moiety of cystine at preanodized Au and Au-Ag rotated disk electrodes (RDEs). The goal of the study was the determination of beneficial effects that might result from the introduction of Ag-sites into Au surfaces. An anodic wave is observed for cystine at oxide covered Au and Au-Ag electrodes appearing as a shoulder to the wave for anodic discharge of H_2O with evolution of O_2. Both the half-wave potential for the cystine wave ($E_{1/2}$,RSSR) and the overpotential for anodic evolution of O_2 (O_2) are shifted by 3.6 mV per atomic percent Ag. These negative shifts are attributed to the higher rate of the anodic discharge of H_2O at Ag sites in comparison to Au sites. Values for the apparent number of electrons (n_{app}) transferred during oxidation of 1.0 mM cystine at 1.50 and 1.55 V vs. SCE are approximately 5 eq mol^{-1} for Au and 6 eq mol^{-1} for $Au_{80}Ag_{20}$, as calculated from the slopes of Koutecky-Levich plots. The larger value of n_{app} at the Au-Ag electrode is

attributed to the higher rate for H_2O discharge at the Ag sites. Cysteine sulfonic acid is identified as the product of extensive electrolysis (n = 10 eq mol^{-1}) at a Au electrode. A preanodized Au electrode in a flow-through cell is demonstrated for cystine detection using a flow-injection system. A 6% loss in peak response observed over a 30-min period is attributed to the slow conversion of an active surface oxide, perhaps corresponding to the equivalent of a monolayer, to an inert oxide, probably corresponding to oxide coverage exceeding a monolayer.

Introduction

The design of new electrocatalysts for use as amperometric and/or voltammetric sensors based on anodic oxygen-transfer reactions can benefit from increased knowledge of the interactions of anode surfaces within the desired response mechanisms. The electrocatalytic factors in anodic O-transfer mechanisms that are expected to be sensitive to changes in surface composition include: (i) the overpotential for anodic discharge of H_2O to form adsorbed hydroxyl radicals (OH_{ads}); (ii) the extent of adsorption of reactant species (R_{ads}) to increase their lifetime at the electrode surface; (iii) the rate of anodic transfer of O-atoms from OH_{ads} to R_{ads}; and (iv) the rate at which the OH_{ads} species are converted to O_2, an undesirable competing reaction. Research described here is part of an on-going study directed to the

comparison of the anodic response for peptides containing disulfide moieties at electrodes composed of the pure and mixed metal-oxide films prepared by anodization of pure metals and their alloys.

Numerous anodic electrocatalytic reactions follow electron-transfer mediated mechanisms in which a surface species toggles between two oxidation states to facilitate the electron transfer between the reactant and electrode. The hydrodynamic voltammetric response for electron-transfer mediated oxidations is expected to be peak shaped when the mediator species cannot diffuse out of the applied electric field at the electrode-solution interface. This expectation is based on the premise that, for a large applied overpotential, the mediator species are pinned in their highest oxidation states. This mechanism has been demonstrated for both chemically modified electrodes [1-3] and for metal-oxide electrodes [4-5].

Johnson and coworkers have studied an alternate electrocatalytic mechanism for anodic O-transfer reactions at β-PbO_2 film electrodes that are doped with altervalent metallic cations [6-13]. Popović and Johnson demonstrated for Bi(V)-doped β-PbO_2 films electrodeposited on Au rotated disk electrodes (RDEs) that oxidation of dimethyl sulfoxide (DMSO) to dimethyl sulfone ($DMSO_2$) competes with O_2 evolution for a common precursor [12]. That precursor was concluded to be the OH_{ads} species generated by anodic discharge of H_2O. The voltammetric response for low

DMSO fluxes at these hydrodynamic electrodes is characterized by a current plateau corresponding to the current limited by convective-diffusional transport of DMSO. Furthermore, the plateau current is observed only at sufficiently large potentials for which the flux of the anodically generated OH_{ads} species can be equal to the flux of DMSO arriving at the electrode surface. However, for excessive values of electrode potential, at which the flux of generated OH_{ads} greatly exceeds that of DMSO, the undesired evolution of O_2 is observed to occur. Popović, Cox and Johnson recently described a mathematical model for the voltammetric DMSO response based on the prerequisites of DMSO adsorption at Bi(V) sites with anodic discharge H_2O at Pb(IV) sites [13]. This model was determined to be consistent with observed variations of half-wave potentials ($E_{1/2}$) for the DMSO wave as a function of increasing surface density of Bi(V) sites, as determined by x-ray photoelectron spectroscopy (XPS), and increases in DMSO concentration and rotational velocity of the RDEs.

Alloys have been used as electrode materials for the oxidation of methanol [14-16], formaldehyde [17,18], amines [19] and carbohydrates [20]. The intent of research described here is the comparison of preanodized pure Au and Au-Ag alloy electrodes applied for various anodic O-transfer reactions. Anodic oxidation of the disulfide moiety in cystine at Au electrodes has been studied extensively [21-23] and this is the model

reaction chosen for this study. Cystine (RSSR) is known to adsorb on oxide-free Au surfaces by a dissociative mechanism resulting in formation of adsorbed thiolate radicals (RS_{ads}) [24,25]. Subsequently, the RS_{ads} species can react with the OH_{ads} species generated by discharge of H_2O in the process of forming an oxide layer on the Au surface. It has been concluded that the ultimate product of cystine oxidation can be the corresponding cysteine sulfonic acid ($R\text{-}SO_3H$) [21]. Silver was chosen as the alloying agent in this study because it forms a homogeneous solid solution with Au at any composition level [26]. Furthermore, the overpotential for anodic discharge of H_2O at Ag electrodes is known to be lower than that for Au electrodes [27]. Hence, by addition of Ag into Au electrodes, it is expected that dependence of the voltammetric response of cystine at Au sites will be observed as a function of changes in the net overpotential for H_2O discharge reaction.

The ultimate practical benefit expected from this study is related to the design of electrode materials that are useful for the amperometric detection at constant potential of biologically significant peptides containing the disulfide moiety. Implicit in this statement is the anticipation that the anodic response is not diminished as a consequence of electrode fouling by adsorbed detection products, formation of surface oxide, or as a consequence of changes in electrode composition caused by corrosion. Such an anode material operated at constant potential will have distinct

advantage over the present use of complex potential-time (*E-t*) waveforms applied at Au electrodes in which electrode activity is maintained by alternate anodic formation and subsequent reductive dissolution of surface oxide. The disadvantage of this procedure results from a gradual loss of Au with a corresponding change in electrode dimension and, therefore, decreased response sensitivity in flow-through detector cells [28,29].

Experimental

Electrodes: Samples of pure Au (99.99 %) and Ag (99.985 %), and $Au_{90}Ag_{10}$ and $Au_{80}Ag_{20}$ alloys were prepared and machined into rods (5-mm diameter, 30-mm length) in the Ames Laboratory Metals Preparation Center. The rotated disk electrodes (RDEs) were constructed by sealing each rod in epoxy and Teflon heat-shrink tubing, and mounting into a stainless steel shaft for attachment to a rotator. Electrode surfaces were polished with 0.3 μm alumina on microcloth (Buehler) with H_2O as the lubricant.

Chemicals: Reagent grade concentrated perchloric acid (70%) and certified grade L(-)cystine were obtained from Fisher Scientific. Solutions were prepared with deionized water from a Millipore system. All voltammetric and amperometric measurements were performed in 0.10 M $HClO_4$.

Instrumentation: Voltammetric measurements were made at rotated disk electrodes (RDEs, 0.196 cm^2) using an AFMSRX rotator/controller and a RDE4 potentiostat (Pine Instruments). Electrode potentials were controlled and are reported vs. a miniature saturated calomel electrode (SCE, Fisher Scientific). Data were collected with Labview-4.0 software (National Instruments) operated on a Pentium 120 personal computer with an AT-MIO-16XE-50 data acquisition board (National Instruments).

The flow-injection (FI) system consisted of an APM-2 isocratic solvent pump (Dionex), a 7010 injector (Rheodyne) with a 50 μL injection loop and, where specified, a PCX-500 column (10 cm, Dionex) to separate the cystine peak from the injection artifact. Amperometric detection was achieved with an ED40 electrochemical detection system with a Au electrode (0.79 mm^2) in a flow-through cell (Dionex).

Electrospray mass spectrometry (ES-MS) was performed in the positive ion mode on a TSQ700 triple quadrupole mass spectrometer with an ESI interface (Finnigan MAT).

Procedures: Unless specified to the contrary, Au and Au-Ag electrodes were anodized prior to use by cycling the applied potential (100 mV s^{-1}) between the potentials of 1.00 and 1.70 V vs. SCE until a reproducible residual voltammetric response was obtained. The pure Ag electrode was not preanodized because this electrode material does not form a stable

surface oxide in acidic media. Voltammetric data were obtained in solutions that had been deaerated by dispersion of $N_2(g)$.

Values for the apparent number of electrons transferred (n_{app}, eq mol^{-1}) and the apparent heterogeneous rate constant ($k_{o,app}$, cm s^{-1}) for the anodic reaction were estimated from the slopes and intercepts, respectively, of plots of the reciprocal current ($1/i$, A^{-1}) vs. the reciprocal of the square root of rotational velocity ($1/\omega^{1/2}$, $s^{1/2}$ $rad^{-1/2}$) according to the Koutecky-Levich equation given by [30]:

$$\frac{1}{i} = \frac{1}{n_{app}FAk_{o,app}C^b} + \frac{1}{0.62n_{app}FAD^{2/3}\upsilon^{1/6}C^b}\left(\frac{1}{\omega^{1/2}}\right)$$

In Equation (1), F is the faraday constant (C eq^{-1}), A is the geometric electrode area (cm^2), D is the diffusion coefficient (cm^2 s^{-1}), υ is the kinematic viscosity of the solution (cm^2 s^{-1}), and C^b is the bulk concentration of reactant (mol cm^3). For large $k_{o,app}$, Equation (1) reverts to the Levich equation for the current controlled by the rate of convective-diffusional transport [31].

Values of the overpotential for anodic discharge of H_2O, with concomitant evolution of O_2 (η_{O2}), were determined from current-potential (i-E) curves at a current density of 0.16 mA cm^{-2}. This current density corresponded to the current density at the half-wave potential ($E_{1/2}$) for oxidation of 1.0 mM cystine at the Au RDE for a velocity of 10.5 rad s^{-1}.

Results and Discussion

Au Rotated Disk Electrode: Shown in Figure 1 is the voltammetric response (positive scan) as a function of cystine concentration at a preanodized Au RDE in 0.10M $HClO_4$. In the residual curve (A, dashed line), the rate of anodic discharge of H_2O, with concomitant evolution of O_2, is observed to increase rapidly with increasing potential for E > 1.6 V. In the presence of cystine (B-F, solid lines), the anodic oxidation of cystine is observed to occur for E > ca. 1.3 V as a shoulder to the O_2-evolution wave. The cystine waves are devoid of well-defined current plateaus that normally are expected at hydrodynamic electrodes for faradaic processes occurring at transport-limited rates. However, the general shape of the cystine waves is consistent with that of voltammetric waves obtained for DMSO at Bi(V)-doped β-PbO2 electrodes [13,14]. Those wave shapes have been explained successfully on the basis of an anodic O-transfer mechanism requiring adsorption of the DMSO at Bi(V) sites with anodic discharge of H_2O at Pb(IV) sites. The plot of anodic current at 1.55 V vs. cystine concentration in the range 10 - 100 μM was determined to be linear (r^2 = 0.999). The decreased current response for E < 1.55 V is concluded to result when, at these decreasing potential values, the rate of OH_{ads} generation is not sufficient to support the oxidation of cystine at the rate observed for 1.55 V. For E > 1.6 V, the rapid increase in current with increasing potential is concluded to be

the result of O_2 evolution that occurs as a consequence of the production of OH_{ads} at rates in excess of that needed for the transport-limited oxidation of cystine. This explanation is consistent with that given by Popović, Cox and Johnson for DMSO at Bi(V)-PbO_2 RDEs [14].

The dramatic effect of preanodization of the Au electrode at two widely differing potentials is shown in Figure 2. Curves A' and A correspond to positive voltammetric scans in the absence and presence, respectively, of 1.0 mM cystine following a 5-min anodization at 1.50 V. Curves B' and B correspond to positive voltammetric scans in the absence and presence, respectively, of 1.0 mM cystine following a 2-min anodization at 2.0 V. The absence of cystine response in Curve B is attributed to the conversion of the "active" surface oxide formed at 1.50 V to an "inert" oxide formed at 2.0 V. The increase in anodic current for $E > 1.6$ V indicates that O_2 evolution still occurs at the "inert" surface (Curve B'), albeit at a significantly slower rate than at the "active" surface (Curve A').

To further study the potential dependence for the transition from the active to the inert forms of surface oxide, the preanodization potential for a freshly polished Au RDE electrode was increased from 1.60 to 1.90 V by 20-mV increments. The anodic response for 1.0 mM cystine was measured at 1.55 V during the positive scan of the cyclic voltammetric curve obtained following a 2-s anodization period. These current values are plotted in

Figure 3 as a function of the anodization potential. It is evident that conversion of the active to the inert forms of surface oxide occurs within the approximate potential range 1.70 E 1.80 V. The nature of the so-called "active" and "inert" forms of surface oxide is discussed in a later section.

The chronoamperometric response for 1.0 mM cystine was monitored following a potential step from 1.00 to 1.50 V at the Au RDE that had been preanodization at 1.50 V (5 min). Following an initial current spike, resulting from charging of the double layer and establishment of the diffusion layer, the electrode current remained virtually constant with a decrease of only 1.0 % during a 10-min observation period. This decay is only slightly greater than that predicted (0.5%) to result from depletion of cystine in the bulk solution during this electrolysis period. Therefore, the activity of this electrode is concluded to be virtually constant over this time period without evidence for a significant rate of surface fouling or a rapid conversion of the labile surface oxide to the inert form.

Au-Ag Rotated Disk Electrodes: The Au-Ag alloys were prepared to allow systematic observation of electrocatalytic effects resulting from the introduction of Ag-sites within the Au oxide matrix. Voltammetric data (not shown) indicated that a pure Ag electrode is anodically dissolved very rapidly for E > 0.3 V in 0.10 M $HClO_4$. Gravimetric evidence verified the loss of electrode mass during the anodization at 1.7 V (10-min). Furthermore,

colloidal AgCl(s) was formed when NaCl(aq) was added to the electrolysis solution. However, for the Au-Ag electrodes, there was no gravimetric evidence for dissolution during electrolysis (1.7 V, 10 min) and formation of AgCl(s) was not evident when NaCl(aq) was added to the electrolysis solution. Clearly, the Ag-sites in these Au-Ag alloy electrodes are greatly stabilized by the Au matrix.

Shown in Figure 4 are the residual voltammetric curves obtained at Au (A'), $Au_{90}Ag_{10}$ (B') and $Au_{80}Ag_{20}$ (C') RDEs that had been preanodized at 1.70 V (5 min). Visual comparison of these residual curves support the prediction that the rate of H_2O discharge at Ag-sites is larger than at the Au-sites in these anodized surfaces. Also shown are the voltammetric curves for 1.0 mM cystine obtained at the preanodized Au (A), $Au_{90}Ag_{10}$ (B) and $Au_{80}Ag_{20}$ (C) RDEs. A plot (not shown) of $E_{1/2}$ vs. η_{O2}, measured at 0.16 mA cm^{-2} for the three electrodes was linear (r^2 = 0.997) with a slope of 1.0 and an intercept equal to 0.25 V. This correlation supports the speculation that the O_2 evolution and cystine oxidation mechanisms benefit from generation of the OH_{ads} species that is produced by anodic discharge of H_2O. This speculation is consistent with the suggestion by Vitt and Johnson related to oxidation of I^- to IO_3^- at various noble electrodes in acidic media [32] and, more recently, the conclusion by Popović and Johnson regarding DMSO oxidation at Bi(V)-doped PbO2 electrodes in acidic media [13].

It also is apparent in Figure 4 that a less-well defined plateau region is obtained for cystine at the Au-Ag RDEs in comparison to the Au RDE. Possible explanations for this observation include: (i) a significantly greater potential dependence of the residual current in the presence of cystine, as compared to that observed in the absence of cystine; and (ii) a strong potential dependence of n_{app} and/or $k_{o,app}$ for cystine oxidation at the Au-Ag electrodes. Regardless of its cause, the ill-defined voltammetric curve for cystine at Au-Ag electrodes is considered to be a disadvantage because it places greater constraints on potential control in amperometric applications of these electrodes.

Koutecky-Levich Plots: Figure 5 contains Koutecky-Levich plots ($1/i$ vs. $1/\omega^{1/2}$) for ω = 31.4 - 209 rad s^{-1} according to Equation (1) for current values determined for 1.00 mM cystine at the Au (A) and $Au_{80}Ag_{20}$ (B) RDEs at constant potentials of 1.50 V (•) and 1.55 V (○). Statistical data for this plots are given in Table 1 together with values of n_{app} and $k_{o,app}$ calculated from the slopes and intercepts, respectively, using $D = 5.3 \times 10^{-6}$ cm^2 s^{-1} for cystine [33]. The linearity of these plots ($r^2 \geq 0.998$) indicates that the overall electrode response throughout this extensive range of rotational velocities can be modeled satisfactorily as a single step occurring with transfer of n_{app} electrons and occurring under mixed kinetic-transport control. A larger value for n_{app} is obtained for the Au_{80}-Ag_{20} RDE compared to the Au RDE,

i.e., 5.8±0.2 eq mol^{-1} vs. 5.1±0.1 eq mol^{-1}, respectively, at 1.50 V. This higher value of n_{app} for the $Au_{80}Ag_{20}$ RDE is attributed to the faster rate for H Q discharge at Ag sites in this oxide-covered alloy electrode. Furthermore, for the $Au_{80}Ag_{20}$ RDE, a small but statistically significant increase in n_{app} is observed when the potential is changed from 1.50 (5.8±0.2 eq mol^{-1}) to 1.55 V (6.4±0.1 eq mol^{-1}). This potential dependence of n_{app} at the alloy electrode is concluded to be the primary cause for the ill-shaped plateau region of the cystine wave (see Figure 4, Curve C). It is speculated that this dependence of n_{app} on potential is linked to a potential-dependent surface coverage by OH_{ads} which supports a more extensive oxidation of the cystine at the alloy. The value of $k_{o,app}$ at the Au RDE increases significantly with the change from 1.50 to 1.55 V, i.e., 3.81±0.08 cm s^{-1} vs. 5.31±0.07 cm s^{-1}, respectively. In spite of this increase in $k_{o,app}$, the value of n_{app} remains constant for the indicated increase in potential. In contrast to these results for the Au RDE, only a small increase in $k_{o,app}$ is observed at the $Au_{80}Ag_{20}$ RDE for an increase in potential from 1.50 to 1.55 V, i.e., 3.11±0.07 cm s^{-1} vs. 3.81±0.07 cm s^{-1}, respectively. In spite of this relative constancy of $k_{o,app}$, an increase in n_{app} is observed for the indicated potential change at the $Au_{80}Ag_{20}$ RDE.

Flow-Injection Detection at a Au Electrode: Evidence is presented above that a virtually steady-state response for cystine is obtained at 1.55 V using a preanodized Au RDE. This result led to further tests of a Au electrode

using the method of flow-injection detection in a flow-through cell. Figure 6 contains values of the normalized peak area, i.e., individual peak areas divided by the average of all peak areas, for 30 consecutive injections of 50-μL samples containing 500 pmol cystine. The solid line in Figure 7 corresponds to the normalized peak area of unity that is expected for this method of data presentation and the dashed lines represent ±3% deviation from the expected normalized response. The average standard deviation from unity is 2.3 % for the 30 injections. The net decrease in peak response of approximately 6% over the 30-min period of this experiment is concluded to be the consequent of slow conversion of a small fraction of the labile form of surface oxide to the inert form at this potential.

Next, a calibration curve was obtained using a Dionex PCX-500 column (10-cm) in the flow-injection system to separate the appearance of the cystine peak from the injection artifact apparent when high recording sensitivities were applied for detection of cystine at low concentrations. The calibration curve was linear (r^2 = 0.997) for injections of cystine over the range 5.00 - 2.00x10^2 pmols. The limit of detection (LOD) was estimated by:

$$LOD = 3(s_{baseline})/ slope = 0.5 \text{ pmol}$$

where sbaseline is the standard deviation of baseline variation over a 30-s time period and *slope* is the slope of the calibration plot. The validity of this estimate was demonstrated by the response obtained for injection of 0.5

pmol cystine (data not shown).

Product Identification: A 10-mL solution of 10 mM cystine in 0.10 $HClO_4$ was electrolyzed for an extended period (24 hr) in an undivided cell using a coiled Au-wire anode (ca. 9 cm^2). The product solution was analyzed by electrospray-mass spectrometry (ES-MS). The peaks obtained and their designation are as follows: 241 = 240 + 1 = protonated cystine (R-S-S-R•H^+), 257 = 241 + 16 = protonated thiosulfinic ester (R-SO-S-R•H^+), 275 = 257 + 18 = solvated protonated thiosulfinic ester (R-SO-S-R•H^+•H_2O) and 170 = 169 + 1 = protonated cysteine sulfonic acid (R-SO_3H•H^+). The oxidation of cystine to cysteine sulfonic acid corresponds to n = 10 eq mol^{-1}.

Conclusions

We speculate that the following mechanistic sequence is appropriate for describing the anodic transfer of a single O-atom from H_2O to cystine:

(i) anodic discharge of H_2O to produce an adsorbed hydroxyl radical, as represented by Equation (2);

(ii) anodic adsorption of cystine, as represented by Equation (3);

(iii) transfer of the OH species to the adsorbed cationic cystine followed by rapid deprotonation and desorption, as represented by Equation(4), to complete the overall reaction producing the thiosulfinic ester as represented by Equation (5).

$$H_2O \rightarrow (OH)_{ads} + H^+ + e^- \quad (2)$$

$$R\text{–}S\text{–}S\text{–}R \rightarrow (R\text{–}S^+\text{–}S\text{–}R)_{ads} + e^- \quad (3)$$

$$(R\text{–}S^+\text{–}S\text{–}R)_{ads} + (OH)_{ads} \rightarrow R\text{–}S(O)\text{–}S\text{–}R + H^+ \quad (4)$$

$$\text{net:} \quad R\text{–}S\text{–}S\text{–}R + H_2O \rightarrow R\text{–}S(O)\text{–}S\text{–}R + H^+ + 2e^- \quad (5)$$

Subsequent O-transfer steps can be represented in the manner suggested by Equations (2) - (5).

The linearity ($r^2 \geq 0.99$) of Koutecky-Levich plots over an extended range of rotational velocities (31.4 - 419 rad s^{-1}, see Figure 5 and Table 1) is consistent with a reaction mechanism that can be modeled as a single step occurring with the transfer of n_{app} electrons under mixed transport-kinetic control. The average value n_{app} = 5 eq mol^{-1} for the Au RDE (1.50 and 1.55 V) is consistent with oxidation of cystine to the cationic sulfone, as represented by Equation (6). The approximate value of n_{app} = ca. 6 eq mol^{-1} at the Au_{80}-Ag_{20} RDE (1.50 and 1.55 V) is consistent with the production of the sulfinil sulfone, as represented by Equation (7). The oxidation of cystine to cysteic acid (n = 10 eq mol^{-1}), observed for exhaustive electrolysis of cystine at a Au electrode, is represented by Equation (8).

$$R\text{–}S\text{–}S\text{–}R + 2H_2O \rightarrow (R\text{–}S(O_2)\text{–}S^+\text{–}R)_{ads} + 4H^+ + 5e^- \quad (6)$$

$$R\text{–}S\text{–}S\text{–}R + 3H_2O \rightarrow R\text{–}S(O_2)\text{–}S(O)\text{–}R + 6H^+ + 6e^- \quad (7)$$

$$R\text{–}S\text{–}S\text{–}R + 6H_2O \rightarrow 2R\text{–}S(O_2)\text{–}OH + 10H^+ + 10e^- \quad (8)$$

The observation of a more extensive oxidation at the Au-Ag electrode (n_{app} = ca. 6 eq mol^{-1}), in comparison to the Au electrode (n_{app} = ca. 5 eq mol^{-1}), is attributed to a higher rate of H_2O discharge at Ag-sites in the anodized alloy surface. We speculate that the fact that values of n_{app} do not exceed 6 eq mol^{-1} at these RDEs is a consequence of the steric difficulty of readsorption of the sulfinil sulfone to produce the bis sulfone. The absence of EM-MS peaks for the products of anodic reactions corresponding to $2 < n < 10$ eq mol^{-1} is concluded to be evidence that these intermediate products undergo auto oxidation-reduction reactions to generate, ultimately, cystine sulfonic acid and the thiosulfinic ester.

Adsorption of cystine, as represented by Equation (3), is speculated to occur by a non-dissociative mechanism. This speculation is rationalized on the basis of the large distance expected between oxide-free Au sites in the preanodized surface. Based on reports by Rand and Woods [34], we conclude that anodization of Au at 1.7 V in 0.10 M $HClO_4$ results in formation of the approximate equivalent of a monolayer of surface oxide (AuO). Figure 7 contains schematic diagrams representing cross-sections of the surfaces of an oxide-free Au electrode (A) and a Au electrode covered with a monolayer of surface oxide (B). Figure 7B, based on a model

suggested by Conway et al. [35,36] for a Pt surface covered with the equivalent of a monolayer of oxide (PtO), indicates that a concerted place-exchange reaction has occurred between alternating O-atoms and Au-atoms. Place exchange is considered to be a necessary step in achieving the eventual thermodynamically favored formation of a bulk oxide phase [35-37]. Jusys and Bruckenstein have interpreted data obtained using an electrochemical quartz-crystal microbalance (eqcm), during formation of a monolayer of AuO in acidic media, to be consistent with a place exchange reaction [38]. Based on this model for Au electrodes, approximately 50% of the surface sites are expected to be free of O-atoms when the equivalent of a monolayer of AuO has been formed (Figure 7B). The average Au-Au distance in Au metal is approximately 2.9 Å [39] and, for the surface in Figure 8B, we estimate an average distance of 5.8 Å between nearest oxide-free Au sites. This distance is much greater than the S-S bond length (2.0 Å) for cystine [39]. Therefore, we anticipate that adsorption of cystine at this surface occurs by interaction of a single S-atom of the disulfide moiety with a single oxide-free Au-site. Hence, we speculate that Figure 7B represents our so-called "active" surface oxide formed at 1.7 V for which a well-developed anodic wave is obtained for cystine.

It is known that formation of a higher oxide state occurs at large positive potentials [34-36,40]. Figure 7C is speculated to represent a Au

surface covered with an oxide layer exceeding the equivalent of a monolayer. We propose that Figure 7C, indicating the absence of oxide-free Au sites, corresponds to our so-called "inert" surface oxide formed at E » 1.7 V for which an anodic response for cystine is not observed. Therefore, adsorption of cystine and/or its intermediate oxidation products cannot occur at the inert surface.

The study reported here did not identify a Au-Ag electrode that exceeds the Au electrode in analytical applicability for detection of cystine. Nevertheless, these results do add support to our general persuasion that comparison of pure electrode materials and their alloys can be informative in the study of electrocatalytic phenomena related to anodic O-transfer reactions. In this study, the introduction of Ag-sites into the Au surface lattice, for the purpose of increasing the rate of OH_{ads} production, had the negative impact of causing a potential dependence of n_{app} for cystine oxidation. As a consequence, an analytically suitable current plateau could not be obtained. Based on this evidence, future efforts in this research program will focus on noble alloys in which the minor component functions for reactant adsorption and the major component functions for generation of OH_{ads} by anodic discharge of H_2O.

Research continues in our effort to identify an electrode surface for which the anodic response for disulfide species occurs with n_{app}=10 eq mol^{-1}.

Acknowledgements

The authors acknowledge financial support from National Science Foundation, Grant CHE-9634544. The authors are grateful to L.L. Jones and J.T. Wheelock, Ames Laboratory Materials Preparation Center at Iowa State University, for preparation of electrode materials; and S. Mollah and R.S. Houk, Ames Laboratory, for obtaining ES-MS data. Helpful discussions with W.S. Jenks also are acknowledged.

References

[1] W. Gorkski, J.A Cox, *Anal. Chem.* **1994**, *66*, 2771.

[2] T.J. O'Shea, S.M. Lunte, *Anal. Chem.* **1994**, *66*, 307.

[3] J. Wang, Z. Taha, *Anal. Chem.* **1990**, *62*, 1413.

[4] J.M. Zadeii, J. Mariolim T. Kuwana, *Anal. Chem.* **1991**, *63*, 649.

[5] M.K. Halbert, R.P. Baldwin, *Anal. Chem.* **1990**, *62*, 1413.

[6] I.-H. Yeo, D.C. Johnson, *J. Electrochem. Soc.* **1987**, *134*, 1973.

[7] J. Feng, D.C. Johnson, *J. Electrochem. Soc.* **1990**, *137*, 507.

[8] J. Feng, D.C. Johnson, *J. Electrochem. Soc.* **1991**, *138*, 3328.

[9] C.A.S. Brevett, D.C. Johnson, *J. Electrochem. Soc.* **1992**, *139*, 1314.

[10] K.T. Kawagoe, D.C. Johnson, *J. Electrochem Soc.* **1994**, *141*, 3404.

[11] J. Ge, D.C. Johnson, *J. Electrochem. Soc.* **1995**, *142*, 1525.

[12] N.Đ. Popović and D.C. Johnson, *Anal. Chem.* **1998**, *70*, 468.

[13] N.Đ. Popović, J.A. Cox, D.C. Johnson, *J. Electroanal. Chem.*, **1998**, *455*, 153; **1998**, *456*, 203.

[14] K.L. Ley, R. Liu, P. Cong, *J. Electrochem. Soc.* **1997**, *144*, 1543.

[15] A.B. Anderson, E. Grantscharova, *J. Phys. Chem.* **1995**, *99*, 9149.

[16] S. Swathirajan, Y.M. Mikhail, *J. Electrochem. Soc.* **1991**, *138*, 1321.

[17] K. Nishimura, K. Yamaguti, K. Machida, *J. Applied Electrochem.* **1988**, *18*, 183.

[18] M. Engo, *J. Applied Electrochem.* **1985**, *15*, 907.

[19] J. Ge, D.C. Johnson, *J. Electrochem. Soc.* **1996**, *143*, 2543.

[20] P.F. Luo, T. Kuwana, *Anal. Chem.* **1994**, *66*, 2775.

[21] J. Kortya, J. Prad *J. Electroanal. Chem.* **1968**, *17*, 177.

[22] J.A. Reynaud, B. Malfoy, P. Canesson *J. Electroanal. Chem.* **1980**, *114*, 195.

[23] T.R. Ralph, M.L. Hitchman, J.P. Millington, F.C. Walsh, *J. Electroanal. Chem.* .**1994**, *375*, 1.

[24] C.D. Bain, H.A. Biebuyck and G.M. Whitesides, *Langmuir*, **1989**, *5*, 723.

[25] H.A. Biebuyck, C.D. Bain and G.M. Whitesides, *Langmuir*, **1994**, *10*, 1825.

[26] T.B. Massalski (Ed.) *Binary Alloy Phase Diagrams* 2nd ed., ASM International. **1990**, 13.

[27] S. Trasatti, *J., Electroanal. Chem.* **1980**, *111*, 124.

[28] M.B. Jensen and D.C. Johnson, *Anal. Chem.* **1997**, *69*, 1776.

[29] R.D. Rocklin, A.P. Clarke and M. Weitzhandler, *Anal. Chem.*, **1998**, *70*, 1496.

[30] J. Koutecky and V.G. Levich, *Zh. Fiz. Khim.* **1958**, *32*, 1565.

[31] V.G. Levich, *Acta Physicochim. URSS* **1942**, *17*, 257.

[32] J.E. Vitt and D.C. Johnson, *J. Electrochem. Soc.* **1992**, *139*, 774

[33] I.M. Kolthoff and C. Barnum, *J. Amer. Chem. Soc.* **1941**, *63*, 520.

[34] D.A.J. Rand and R. Woods, *J. Electroanal. Chem.* 1971, *31*, 29; **1973**, *44*, 83.

[35] B.E. Conway, B. Barnett, H. Angerstein-Kozlowska and B.V. Tilak, *J. Chem. Phys.* **1990**, *93*, 8361.

[36] J.O'M. Bockris and S.U.M. Khan, *Surface Electrochemistry: A Molecular Level Approach*, Plenum Press: New York, **1993**, pp. 362-7.

[37] L.D. Burke, in *Electrodes of Conductive Metallic Oxides*, Pt. A, S. Trasatti (Ed.), Elsevier: Amsterdam, **1980**, p. 147-9.

[38] Z. Jusys and S. Bruckenstein, *Electrochem. Solid-State Letters*, **1998**, *1*, 74.

[39] D.R. Lide (Ed.), *CRC Handbook of Chemistry and Physics*, 71st ed., CRC Press,Inc.: Boca Raton, **1990**, p. 9-2.

[40] L.D. Burke, in *Electrodes of Conductive Metallic Oxides*, Pt. A, S. Trasatti (Ed.), Elsevier: Amsterdam, **1980**, p. 170.

Table 1. Description of Koutecky-Levich plots for 1.0 mM cystine response at Au and Au_{80}-Ag_{20} rotated disc electrodes. Uncertainties represent standard deviationsfor indicated parameters.

Electrode	Potential (V vs.SCE)	r^2	Slope ($\mu A^{-1} rad^{-1/2} s^{1/2}$)	Intercept (μA^{-1})	n_{app} (eq mol^{-1})	$k_{o,app}$ (cm s^{-1})
Au	1.500	0.999	$2.57\pm0.03\times10^{-2}$	$2.72\pm0.04\times10^{-3}$	5.1±0.1	$3.81\pm0.08\times10^{-3}$
	1.550	0.999	$2.61\pm0.02\times10^{-2}$	$1.99\pm0.02\times10^{-3}$	5.0±0.1	$5.31\pm0.07\times10^{-3}$
Au_{80}-Ag_{20}	1.500	0.998	$2.24\pm0.04\times10^{-2}$	$2.93\pm0.05\times10^{-3}$	5.8±0.2	$3.11\pm0.07\times10^{-3}$
	1.550	0.999	$2.03\pm0.03\times10^{-2}$	$2.17\pm0.03\times10^{-3}$	6.4±0.1	$3.81\pm0.07\times10^{-3}$

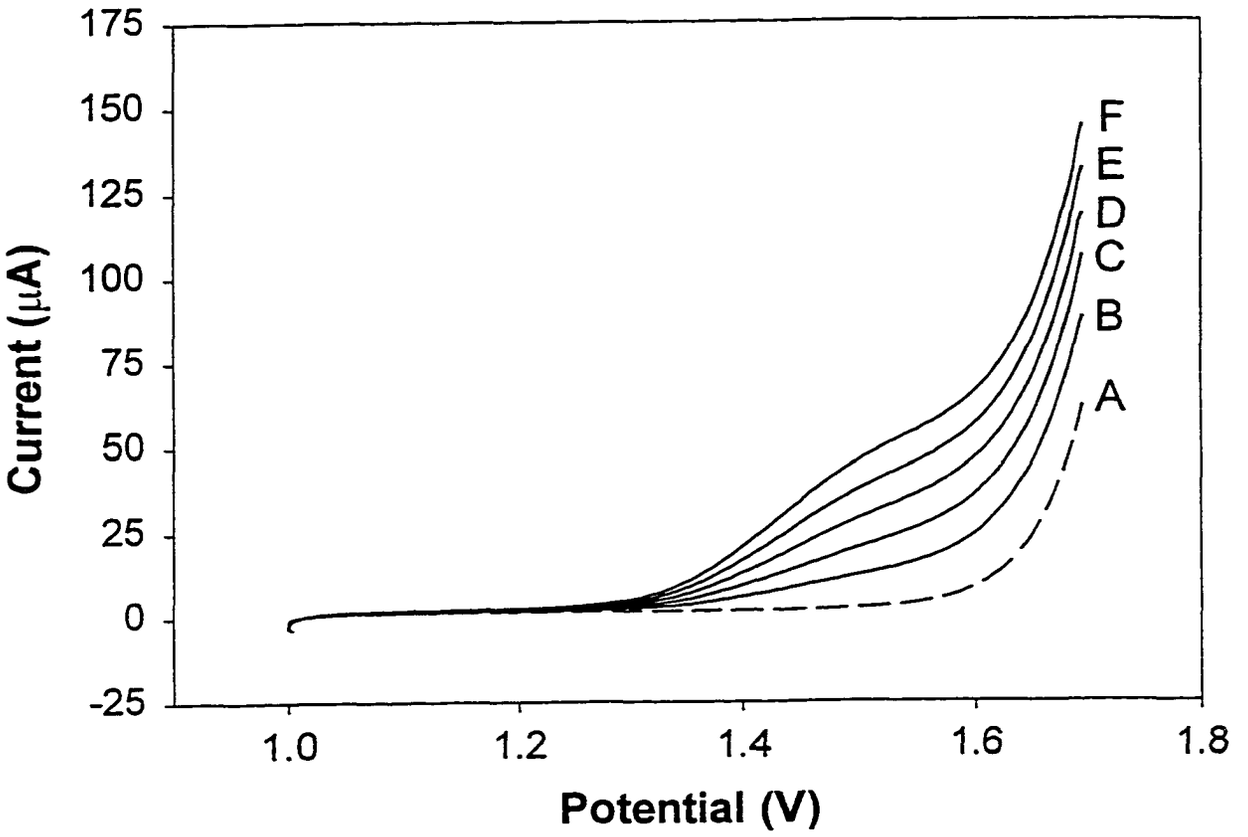

Figure 1. Voltammetric response for cystine as a function of concentration at a preanodized Au RDE in 0.10 M $HClO_4$. Scan: 100 mV s^{-1}. Rotational velocity: 10.5 rad s^{-1}. Cystine concentration (μM): (A) 0, (B) 20, (C) 40, (D) 60, (E) 80, (F) 100.

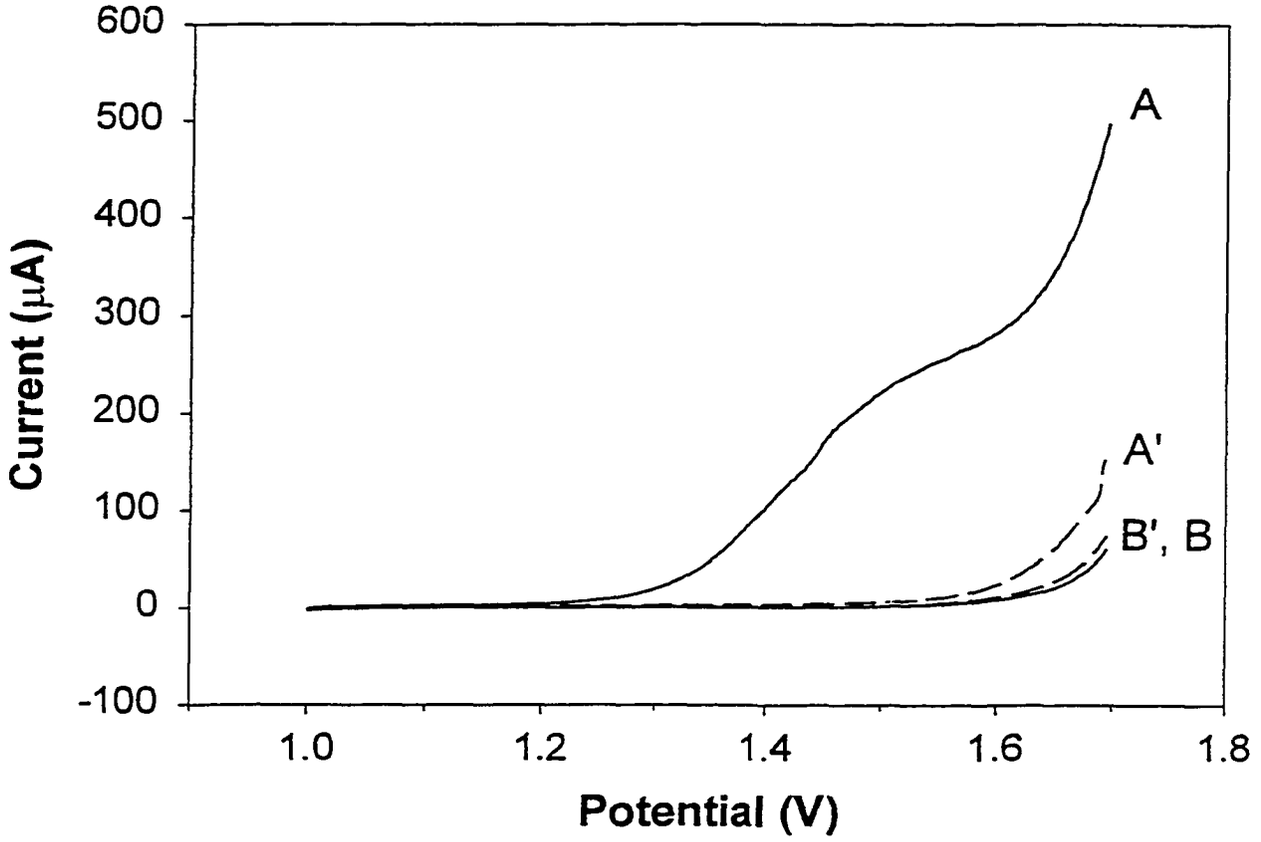

Figure 2. Voltammetric response for cystine at Au oxide electrodes at two different preanodization potentials. Rotation speed: 94.2 rad s^{-1}. Scan rate: 100 mV s^{-1}. Preanodization potential: (A) 1.50 V for 2 min, (B) 2.0 V for 2 min. Cystine concentration (mM): (A',B') 0.0, (A,B) 1.0.

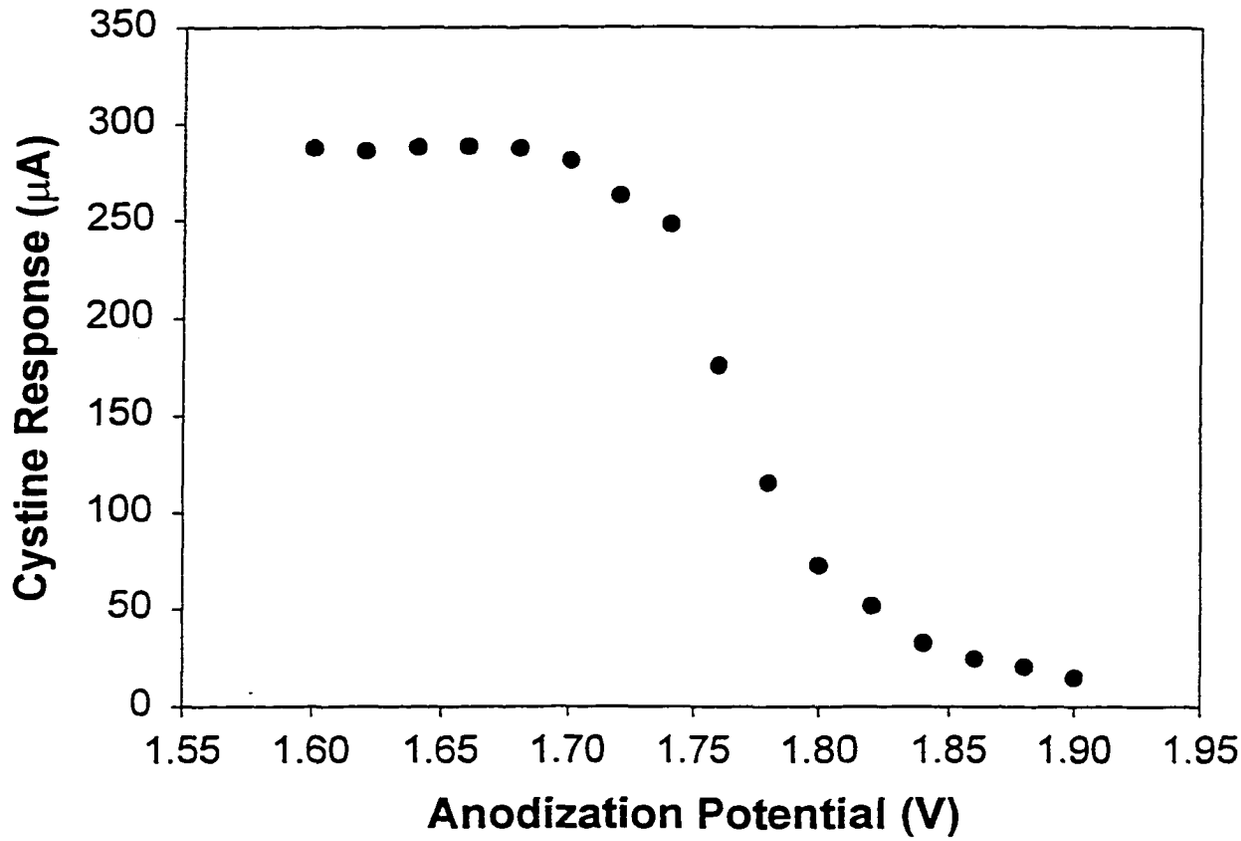

Figure 3. Anodic current at 1.55 V measured during the positive voltammetric scan from 1.60 V following preanodization for a 2-s period at a potential incremented from 1.60 to 1.90 V by 20-mV steps.

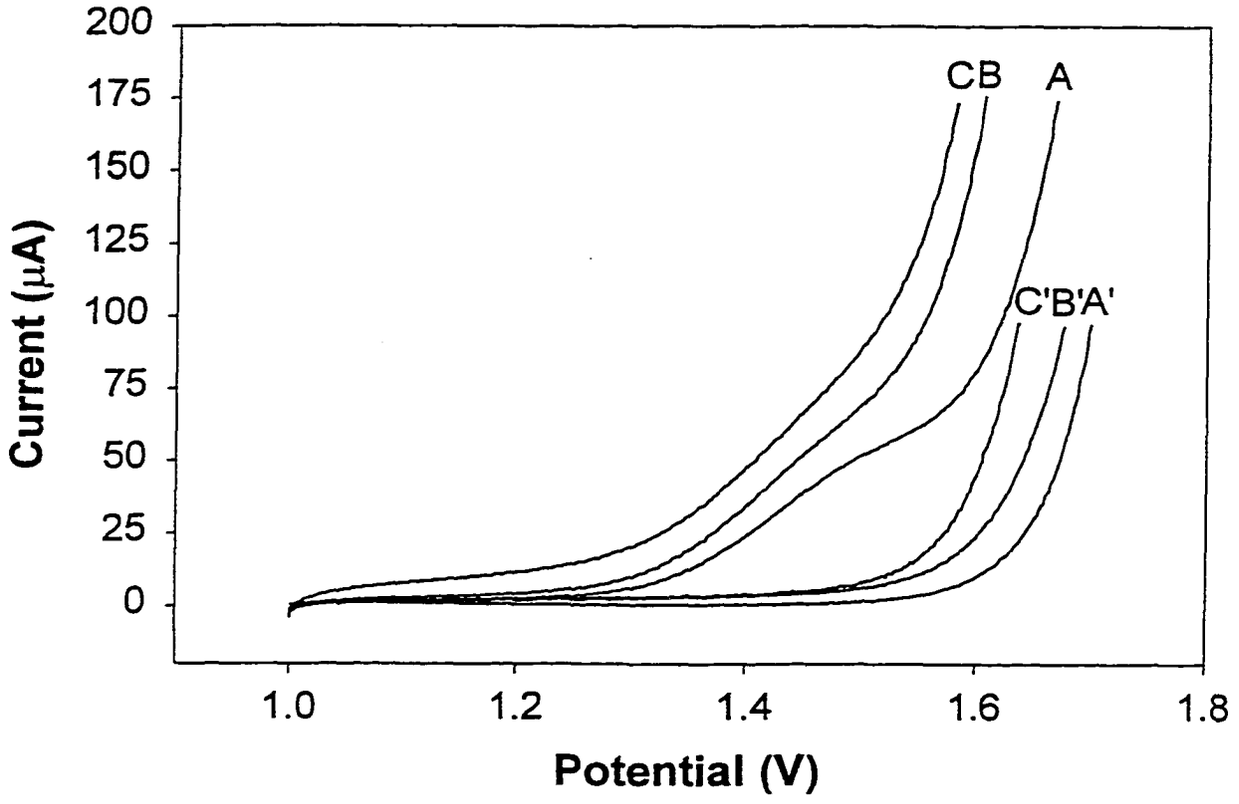

Figure 4. Voltammetric response for cystine at various electrodes in 0.10 M $HClO_4$. Scan rate: 100 mV s^{-1}. Rotational velocity: 10.5 rad s^{-1}. Electrode: (A,A') Au, (B,B') $Au_{90}Ag_{10}$, (C,C') $Au_{80}Ag_{20}$. Cystine concentration: (A',B',C') 0.0, (A,B,C) 1.0 mM.

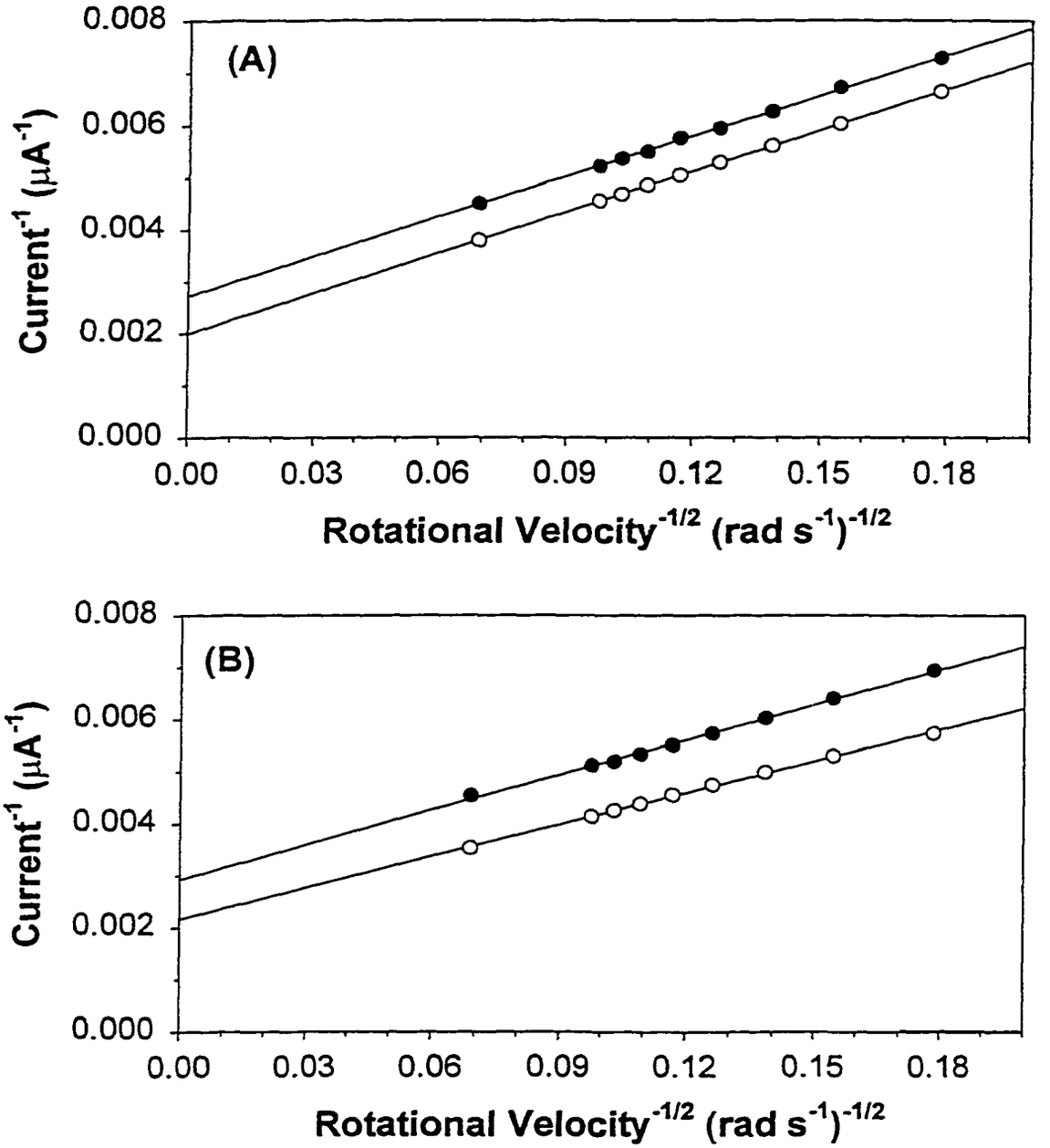

Figure 5. Koutecky-Levich plots of reciprocal current vs. reciprocal square root of rotational velocity for 1.0 mM cystine at preanodized Au (A) and Au_{80}-Ag_{20} (B) rotated disk electrodes in 0.10 M HClO4. Potential (V): (•) 1.50, (○) 1.55.

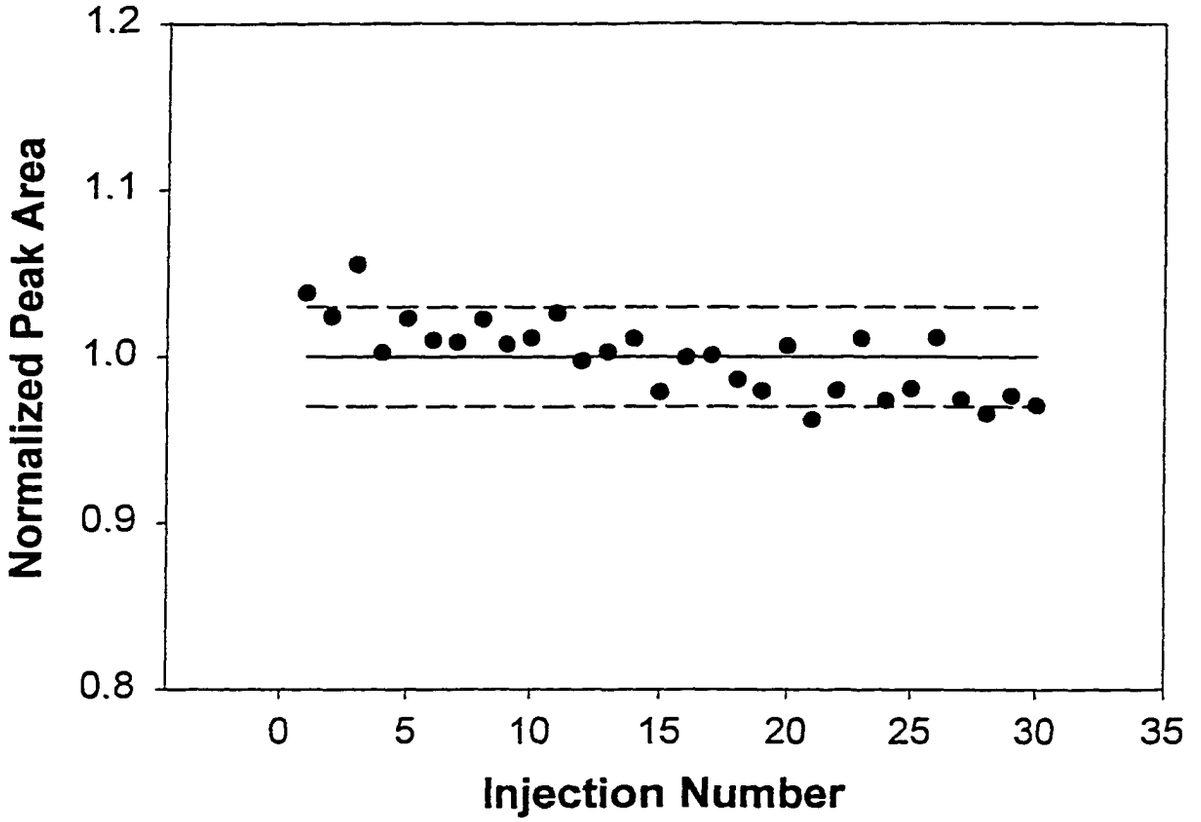

Figure 6. Plot of normalized peak areas for 30 injections of 500 pmol cystine with detection at a preanodized (1.7 V) Au electrode in a flow-through cell. Mobile phase: 0.1M $HClO_4$. Sample loop: 50 μL. Flow rate: 1.0 mL min^{-1}. Potential: 1.55 V. Solid line: average of the normalized peak areas = 1.0. Dashed lines: ±3% deviation from the average of the normalized values.

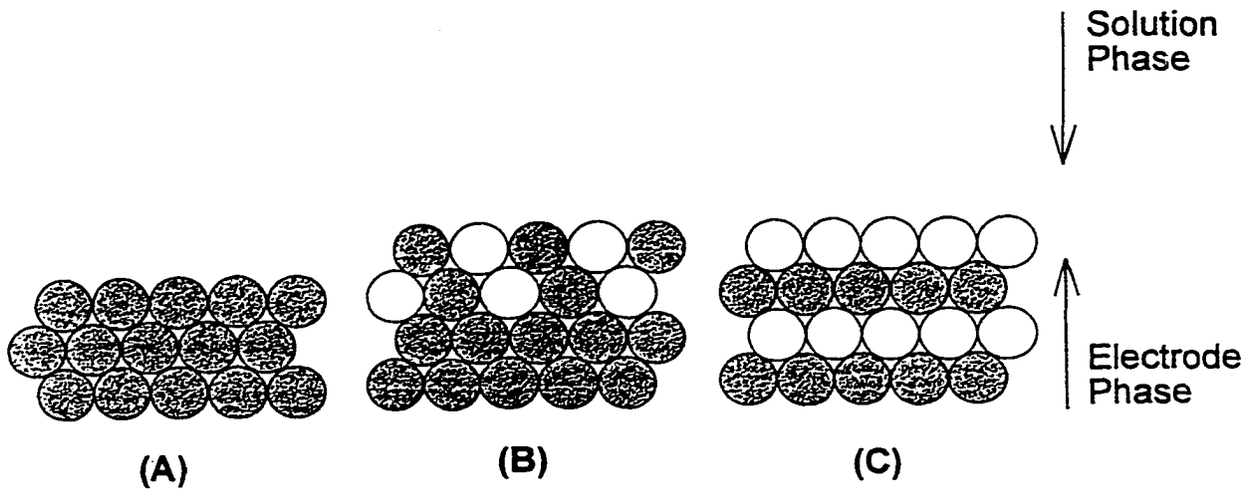

Figure 7. Schematic representations of a Au electrode that is (A) free of surface oxide, (B) covered by the equivalent of a monolayer of O-atoms, and (C) covered by the equivalent of a bilayer of O-atoms.

CHAPTER 4. ANODIC RESPONSE OF CYSTINE AT HIGHLY ROUGHENED GOLD ELECTRODES IN PERCHLORIC ACID MEDIA

A paper published in *Electroanalysis*

Matthew E. Johll, Sze-Shun Wong and Dennis C. Johnson*

Abstract

This manuscript compares the anodic response of the disulfide moiety of cystine at the preanodized surfaces of polished and highly roughened Au rotated disk electrodes (RDEs). The purpose of this study is the determination of the effect that roughening the electrode surface has on the effective number of electrons passed during cystine oxidation. The apparent number of electrons transferred during oxidation of cystine is ca. 10 eq mol^{-1} at the highly roughened Au RDE as compared to ca. 6 eq mol^{-1} at the polished Au RDE. The transfer of 10 eq mol^{-1} corresponds to complete oxidation of the disulfide moiety in cystine to two moles of cysteine sulfonic acid. The specific area of the roughened surface is concluded to be 5 - 7 times larger than that of the polished surface on the basis of comparisons of double-layer charging currents, current for anodic evolution of O_2, and data obtained by atomic force microscopy (AFM). Therefore, the larger value of n_{app} for the roughened electrode is attributed to the electrocatalytic benefit

of an increased specific surface area acting within a response mechanism that is believed to involve co-adsorption of the reactant, cystine, and hydroxyl radicals generated by anodic discharge of H_2O.

Introduction

Goals of research in this laboratory include the exploration of electrocatalytic factors that control the voltammetric response of polar organic compounds at solid electrode materials. Electrodes of interest include preanodized pure metals and bimetallic alloys, and metal oxide films that are heavily doped with altervalent metallic cations. Reactants of interest include small peptides that contain the disulfide moiety, e.g., cystine. The oxidation of cystine at polished noble metal electrodes has been studied extensively [1-4]. The design of electrocatalytic surfaces for the oxidation of sulfur-containing compounds has been pursued using electrodes that were chemically modified by Co-Tsp [5] and mixed valent Ru oxide [6].

The reactions of interest are anodic and involve the transfer of O-atoms from H_2O in the solvent phase to the oxidation products. The prerequisite of this reaction mechanism is believed to be the anodic discharge of H_2O to produce adsorbed hydroxyl radicals (OH_{ads}). The OH_{ads} species also is a precursor in the anodic evolution of O_2 and, therefore,

voltammetric response for these O-transfer reactions appears as a shoulder to the *i-E* wave for O_2 evolution. The anodic evolution of O_2 is pH dependent and, therefore, the formation of OH_{ads} will shift with changes in pH. The actual surface coverage by OH_{ads} is a function of potential at any given pH value. Furthermore, catalytic benefit is believed to come from preadsorption of the reactant at the electrode surface, as demonstrated by Popović et al. at Bi(V)-doped PbO_2-film electrodes [7]. In fact, without the benefit of adsorption, the voltammetric response for cystine is not likely to be resolved from the *i-E* wave for O_2 evolution.

It follows from the co-requisites described above that the apparent values of the number of electrons transferred (n_{app}) and the corresponding heterogeneous rate constant ($k_{o,app}$) for anodic O-transfer reactions might be increased as a beneficial consequence of an increased density of surface sites available for adsorption of the OH and reactant species. This increase can be achieved by increasing the roughness of the electrode surface at the atomic level. Benefit of roughened electrodes is well recognized in industrial applications of electrolysis because an increase in the specific surface area results in a beneficial decrease in the current density of the electrolysis reaction [8]. However, electroanalytical studies directed to the development of new voltammetric/amperometric procedures generally stress the need for reproducible electrode surfaces of the type obtained by polishing to a mirror

finish. An additional benefit of this electrode treatment comes from minimization of double layer charging current to maximize the ratio of signal-to-background currents in voltammetric techniques.

Cystine was chosen as the model reactant because it contains a disulfide moiety that is of biological importance. The amine moiety in cystine can be detected at Au electrodes only under alkaline conditions when this moiety is not protonated and can be adsorbed at the oxide-free Au surface. Experiments described here for cystine were performed in 0.10 M $HClO_4$ wherein there is no contribution from oxidation of amine moiety. The ultimate goal of this research is the development of an amperometric sensor for use in liquid chromatographic separations of complex solutions containing biologically significant sulfur compounds. Separations have been described by Vandeberg and Johnson based on cation-exchange separation from acidic media [9,10].

In a previous study, cystine was determined to produce a well-defined anodic wave appearing as a shoulder on the *i-E* wave for O_2 evolution at a Au RDE that had been polished and preanodized [11]. The cystine response was explained on the basis of the general mechanism given above involving preadsorption of cystine via non-bonded electron pairs on the disulfide moiety with concomitant generation of OH_{ads} species. The potential region of the anodic response corresponds to formation of approximately one

monolayer of gold oxide (AuO) on the electrode surface. Jusys and Bruckenstein have concluded, on the basis of data obtained with a quartz-crystal microbalance, that an atom-atom exchange occurs during formation of the AuO monolayer so that 50% of the surface sites correspond to O-atoms and the remaining 50% correspond to Au-atoms [12]. This conclusion is in agreement with earlier speculation of an atom-atom exchange occurring on Pt electrodes covered by a monolayer of PtO [13,14]. It is well known for oxide-free Au surfaces that cystine is adsorbed by a dissociative mechanism resulting in adsorbed thiolate radicals [15,16]. Therefore, we had anticipated that cystine would be adsorbed at Au-sites in this preanodized surface with the possibility of well-defined voltammetric waves corresponding to anodic O-transfer reactions involving the adsorbed cystine. However, the value of n_{app} for this electrode was determined to be ca. 6 eq mol^{-1} instead of the value 10 eq mol^{-1} anticipated for oxidation to the cysteine sulfonic acid. It was also demonstrated in that study that the response of cystine was eliminated at Au RDEs that had been preanodized at 2.0 V vs. SCE, a potential sufficient to form the equivalent of two monolayers of oxide on the electrode surface [11]. In a study of the anodic response for $Fe(phen)_3^{2+}$, Oesch and Janata determined that this reaction was completely inhibited by the formation of the equivalent of two monolayers of Au oxide [17].

Here, we explore the possible benefit of achieving a substantial increase in the roughness of the preanodized electrode (AuO) to increase the specific surface area of the electrode. Surface roughness can be increased by formation of a multilayer surface oxide using an applied potential of ≥ 1.9 V vs. SCE followed by cathodic reduction at -0.5 V. The topography of Au surfaces roughened in this manner has been studied by Vela et al. who reported the formation of columnar surface microstructures [18,19]. These authors speculated that this structure is created by electroreduction of Au-ions present in a hydrous Au oxide layer. The columnar shape is favored due to a large density of nucleation sites on the Au electrode. During the electroreduction, the available concentration of Au ion is quickly depleted laterally between nucleation sites, in which case the continued growth is from the Au ions found above the nucleation sites resulting in the vertical growth of the deposits.

Experimental

Chemicals: Reagent grade concentrated (70%) perchloric acid (Fisher) was diluted with deionized water (Millipore System) to a final concentration of 0.10 M for use in all experiments. Certified grade L(-) cystine (Fisher) and 99% pure L(-) cysteine (Alfa) were used.

Electrodes: Identical Au rotated disk electrodes (RDE, 0.196 cm^2; Pine Instruments) were utilized in all voltammetric studies reported here. The electrodes were polished to a mirror finish with 0.05-μm alumina on microcloth (Buehler) using deionized water from a Milipore system as the lubricant. After polishing, alumina residue on the electrode surfaces was removed by intermittent rubbing with a wet cotton swab and rinsing with copious amounts of deionized water. Preanodization of Au surfaces was achieved by cycling the applied potential (100 mV s^{-1}) for a 5-min period between the potential limits 1.0 to 1.7 V vs. SCE in 0.10 M $HClO_4$.

The roughened state of Au surfaces was produced by application of a potential of 1.9 V vs. SCE at a polished Au surface for a 30-min period to produce a multi-layer surface coverage by AuO with concomitant surface reconstruction. The potential was then stepped to -0.50 V vs. SCE for a 5-min period to cathodically reduce the oxide layer. Visual evidence for a roughened Au electrode was the appearance of a blackened surface.

Electrodes used to obtain atomic force microscopic data were prepared by hammering the end of a 1.5-mm Au wire to a flattened state followed by polishing to a mirror finish. Procedures for roughening and preanodization of these surfaces were the same as described above.

Instrumentation: A Model RDE4 bipotentiostat equipped with a Model AFMSRX rotator/controller (Pine Instruments) were utilized for all

electrochemical experiments. The reported electrode potentials are all verses a miniature saturated calomel electrode (SCE, Fisher). All current-potential (*i-E*) and current-time (*i-t*) data were acquired using LabView 4.0 software (National Instruments) with an AT-MIO16XE-50 data acquisition board (National Instruments). Scanning force microscopy (SFM) was performed with a Dimension 3000 SFM (Digital Instruments) equipped with a 90-μm tube scanner and operated in the ambient. All SFM topographic images were collected in the contact mode using 200-μm oxide sharpened triangular Si_3N_4 cantilevers (Nanoprobes) with normal bending and torsional force constants of ~0.06 N/m and ~80 N/m, respectively. All images were acquired using a constant-force mode at a normal force of ~30 nN.

Koutecky-Levich plots: Apparent values for the number of electrons transferred (n_{app}) and the associated heterogeneous rate constant ($k_{o,app}$) corresponding to the anodic response of cystine at the Au RDEs were calculated from slopes and intercepts, respectively, of plots of reciprocal current (i^{-1}, μA^{-1}) vs. reciprocal square root of rotational velocity ($\omega^{-1/2}$, $rad^{-1/2}$ $s^{1/2}$) according to the procedure of Koutecky and Levich [20] as applied previously in this laboratory [11].

Results and Discussion

Voltammetry: Figure 1 contains the voltammetric response for cystine (positive scan) obtained in 0.10 M $HClO_4$ using roughened Au (A) and polished Au (B) electrodes that had been preanodized by cycling the applied potential (100 mV s^{-1}, 5 min) between the potential limits 1.0 to 1.7 V. Cathodic reduction of AuO does not occur in 0.10 M $HClO_4$ for $E > 1.0$ V and, therefore, the response shown in Figure 1 corresponds to a uniform coverage of a monolayer of AuO. Curves b - f in Figures 1A and 1B were recorded following standard increases of cystine concentration by 200-μM increments. It is readily apparent from comparison of the *i-E* curves for cystine in these figures that the current response at ca. 1.55 V is substantially larger at the roughened electrode in comparison to the polished electrode. These data are indicative of a larger value for n_{app} at the roughened electrode in comparison to the polished electrode.

The background current for O_2 evolution at 1.65 V at the roughened electrode (Fig. 1A, curve a) is 170 mA as compared to the value 24 mA for the polished electrode (Fig. 1B, curve a). Based on the ratio of these current values, the specific areas of the roughened and polished electrodes is estimated to be ca. 7. The double layer charging currents for the two electrodes used to obtain data in Figures 1A and 1B were measured at ca. 0.40 V, following cathodic reduction of their surface oxides, using a scan

rate of 100 mV s^{-1} in 0.1 M $HClO_4$. The ratio of these charging currents is ca. 5, which is in satisfactory agreement with the ratio based on the O_2-evolution currents.

Figure 2 contains *i-E* curves for 1.0 mM cystine as a function of rotational velocity at the roughened (A) and polished (B) electrodes. Whereas the current response at 1.5 V for the roughened electrode (Fig. 2A) exhibits a nearly uniform increase with each incremental increase in rotational velocity, the response is substantially smaller at 1.5 V for the polished electrode. This is evidence for a mass-transport controlled response at the roughened electrode and mixed transport-kinetic controlled response at the polished electrode.

Koutecky-Levich plots: Values of n_{app} and $k_{o,app}$ were calculated from the slope and intercept, respectively, of Koutecky-Levich plots constructed from the current response at 1.55 V shown in Figures 2A and 2B as a function of rotational velocity. For these calculations, the value 5.3×10^{-6} cm^2 s^{-1} was used for the diffusion coefficient of cystine [21]. The statistics of these plots are summarized in Table 1 where the uncertainties represent standard deviations. For the polished electrode, n_{app} = 5.6±0.1 eq mol^{-1} and $k_{o,app}$ = 6.8±0.1$\times 10^{-3}$ cm s^{-1}. This value of n_{app} is in fair agreement with the value 5.1±0.1 eq mol^{-1} obtained in the previous study using a polished Au RDE [11]. The value n_{app} = 5 eq mol^{-1} is consistent with anodic formation of

a cationic sulfone and n_{app} = 6 eq mol^{-1} is consistent with formation of the sulfinil sulfone [11]. For the roughened electrode, n_{app} = 9.9±0.3 eq mol^{-1} and $k_{o,app}$ = 7.9±0.3x10^{-3} cm s^{-}. This value of n_{app} is in excellent agreement with the value n_{app} = 10 eq mol^{-1} expected for complete oxidation of cystine to two moles of cysteine sulfonic acid, as indicated by:

$$R\text{-}S\text{-}S\text{-}R + 6H_2O \rightarrow 2R\text{-}SO_3H + 10H^+ + 10e^- \quad (1)$$

The value of $k_{o,app}$ for the roughened electrode is only 16% larger than that for the polished electrode. Therefore, it is apparent that the increase in specific surface area can have a significant impact on n_{app} without a large increase in $k_{o,app}$. Previous work has shown that the product of exhaustive electrolysis of cystine at preanodized Au electrodes in acidic media is the cysteine sulfonic acid [11].

Chronoamperometry: Figure 3A contains chronoamperometric data (*i-t*) obtained at the roughened and preanodized Au RDE following addition of 1.0 mM cystine at applied potentials of 1.50 V (curve a) and 1.00 V (curve b). Following thorough mixing of the solution by the RDE (t = 100 s), the anodic response in curve a is very stable with a decrease of only 0.8 % at t = 600 s. This is slightly larger than the 0.3 % depletion of cystine estimated for this time interval. The absence of current response for cystine at 1.00 V (curve b) is consistent with the voltammetric response shown in Figures 1A and 2A.

Figure 3B contains chronoamperometric data obtained for the

roughened and preanodized Au RDE following addition of 1.0 mM cysteine. At 1.50 V (curve a), the anodic signal reaches a fairly stable response at t = 100 s with a subsequent decay of approximately 1.5 % at t = 600 s. However, curve b obtained at 1.00 V shows only a very small initial current (t < 20 s) followed by a rapid increase in current (50 < t < 200 s) to a nearly stable value of 380 mA (t > 250 s). This response at E = 1.00 V for cysteine, a sulfhydryl (Fig. 3B, curve b), is in sharp contrast to that of cystine, a disulfide (Fig. 3A, curve b). It is known that cysteine is adsorbed at oxide-free Au surfaces by an anodic mechanism to produce the adsorbed thiolate species [16]. Furthermore, at 1.00 V, the monolayer of oxide is thermodynamically unstable albeit kinetically stable. Therefore, we speculate that a major portion of the AuO on the preanodized surface is chemically reduced by cysteine during the period t < 200 s to produce a surface that is nearly free of oxide. As a result, the anodic response observed for t > 200 s (Fig. 3B, curve b) corresponds to oxidation of cysteine at Au. This anodic response was confirmed by measurement of the anodic signal for cysteine at 1.00 V following complete reduction of the oxide at -0.5 V.

The conclusion above is supported by the appearance of a substantial anodic wave for the first positive scan of potential at the electrode following the recording of curve b in Figure 3B (see Fig. 4, curve a). This anodic wave

corresponds to formation of the surface oxide with concomitant oxidative desorption of adsorbed thiolate species. In contrast, the second consecutive cyclic scan exhibits very little anodic signal (see Fig. 4, curve b) because the time was not sufficient to allow for a significant reduction of surface oxide formed on the preceding scan to 1.7 V.

Scanning force microscopy (SFM): Figure 5 contains 10-μm x 10-μm topographic images and their cross-sectional profiles of polished (A) and roughened (B) Au electrodes as obtained by SFM. The columnar surface projections observed for the roughened surface (Fig. 5B) are similar to those reported by Arvia et al. for Au electrodes roughened by a similar procedure [18,19]. Based on the cross-sectional profiles in Figure 5, we estimate the specific area for the roughened electrode to be ca. 5 times greater than that for the polished electrode. The maximum depth of surface pits is approximately 100 nm. This value corresponds to only 10% of the diffusion-layer thickness (δ) estimated to be 5.7×10^3 nm on the basis of the equation below using the values 5.3×10^{-6} cm^2 s^{-1} for D, the diffusion coefficient of cystine; 8.9×10^{-3} cm^2 s^{-1} for υ, the kinematic viscosity of the solution; and 513 rad s^{-1} for ω, the maximum rotational velocity of rotation in this study.

$$\delta = 1.61 D^{1/3} \upsilon^{1/6} \omega^{-1/2}$$

Conclusions

The preanodized roughened Au electrode exhibits a significantly higher electrocatalytic activity with n_{app} = ca. 10 eq mol^{-1} for oxidation of cystine, as compared to n_{app} = ca. 6 eq mol^{-1} for the preanodized polished Au electrode. This increase in activity is concluded to be the result of the higher specific surface area at the roughened electrode. The increased electrocatalytic activity coming as a result of increased specific surface area is concluded to be indicative of a response mechanism that involves adsorption of the hydroxyl radicals and cystine prior to the O-transfer step.

It is significant that values of $k_{o,app}$ are nearly the same at the roughened and polished electrodes in spite of the larger value of n_{app} obtained for cystine at the roughened electrode. We conclude that the larger n_{app} value at the roughened electrode is the result of a higher flux density (mol s^{-1} cm^{-2}) for the generation of OH_{ads}, as calculated on the basis of the geometric electrode area. The conclusion of a higher flux density for OH_{ads} is consistent with the observation of a current for O_2 evolution that is ca. 7X larger at the roughened electrode in comparison to the polished electrode. In contrast, the flux density for cystine is independent of electrode roughness whenever the dimension of surface roughness is significantly less than the thickness of the diffusion layer adjacent to the electrode surface.

Future work will examine the use of roughened Au electrodes as

amperometric sensors for other biologically important compounds that contain sulfur moieties, e.g., homocysteine, methionine and cysteine. Roughened and preanodized Au electrodes operated at constant potential show promise as anodic amperometric sensors for application of liquid chromatography. However, based on observation of a slight decay in response in Figure 3A (<0.8% in 10 min at 1.50 V vs. SCE), it might be necessary to periodically restore the electrode activity by application of a pulsed potential-time waveform to cathodically reduce and anodically rebuild the surface oxide film.

Acknowledgment

The authors acknowledge financial support from National Science Foundation, Grant CHE-9634544.

References:

[1] Samec, Zh. Malysheva, J. Kortya and J. Pradáć, *J. Electroanal. Chem.*, **1975**, *65*, 573.

[2] J. Pradáć and J. Kortya, *J. Electroanal. Chem.*, **1968**, *17*, 167, 177, 185.

[3] D.G. Davis and E. Bianco, *J. Electroanal. Chem.*, **1966**, *121*, 254.

[4] J.A. Reynaud, B. Malfoy, and P. Canesson, *J. Electroanal. Chem.*, **1980**, *114*, 195.

[5] J. Zagal, C. Fierro and R. Rozas, *J. Electroanal. Chem.*, **1981**, *119*, 403.

[6] J.A. Cox and T.J. Gray, *Anal. Chem.*, **1990**, *62*, 2742.

[7] N.Đ. Popović, J.A. Cox and D.C. Johnson, *J. Electroanal. Chem.*, **1998**, *455*, 153; **1998**, *456*, 203.

[8] D. Pletcher and F. Walsh, *Industrial Electrochemistry*, 2nd ed., Balckie Academic and Professional Publishing: London, **1993**, p. 47.

[9] P.J. Vandeberg and D.C. Johnson, *Anal. Chem.*, **1993**, *65*, 2713.

[10] P.J. Vandeberg and D.C. Johnson, *Anal. Chim. Acta*, **1994**, *290*, 317.

[11] M.E. Johll and D.C. Johnson, *Electroanalysis*, in review.

[12] Z. Jusys and S. Bruckenstein, *Electrochem. Solid-State Letters*, **1998**, *1*, 74.

[13] E. Conway, B. Barnett, H. Angerstein-Kozlowska and B.V. Tilak, *J. Chem. Phys.*, **1990**, *93*, 8361.

[14] J.O'M. Bockris and S.U.M. Khan, *Surface Electrochemistry: A Molecular Level Approach*, Plenum Press: New York, **1993**, pp. 362-7.

[15] C.D. Bain, H.A. Biebuyck and G.M. Whitesides, *Langmuir*, **1989**, *5*, 723.

[16] H.A. Biebuyck, C.D. Bain and G.M. Whitesides, *Langmuir*, **1994**, *10*, 1825.

[17] U. Oesch and J. Janata, *Electrochim. Acta*, **1983**, *28*, 1247.

[18] M.E. Vela, R.C. Salvarezza and A.J. Arvia, *Electrochim. Acta*, **1990**, *35*, 117.

[19] M.E. Vela, S.L. Marchiano, R.C. Salvarezza and A.J. Arvia, *J. Electroanal. Chem.*, **1995**, *388*, 133.

[20] J. Koutecky and V.G. Levich, *Zh. Fiz. Khim.* **1958**, *32*, 1565.

[21] I.M. Kolthoff and C. Barnum, *J. Amer. Chem. Soc.* **1941**, *63*, 520.

Table 1. Description of Koutecky-Levich plots for anodic detection of 1.0 mM cystine at the preanodized polished and roughened Au RDEs in 0.10M $HClO_4$.

Electrode Surface	r^2	Slope ($\mu A^{-1}s^{1/2}$)	n_{app} (eq mol^{-1})	Intercept (μA^{-1})	$k_{o,app}$ (cm s^{-1})
Polished	0.999	$2.28\pm0.03\times10^{-2}$	5.6±0.1	$1.4\pm0.1\times10^{-3}$	$6.8\pm0.1\times10^{-3}$
Roughened	0.997	$1.29\pm0.03\times10^{-2}$	9.9±0.3	$6.7\pm0.2\times10^{-4}$	$7.9\pm0.3\times10^{-3}$

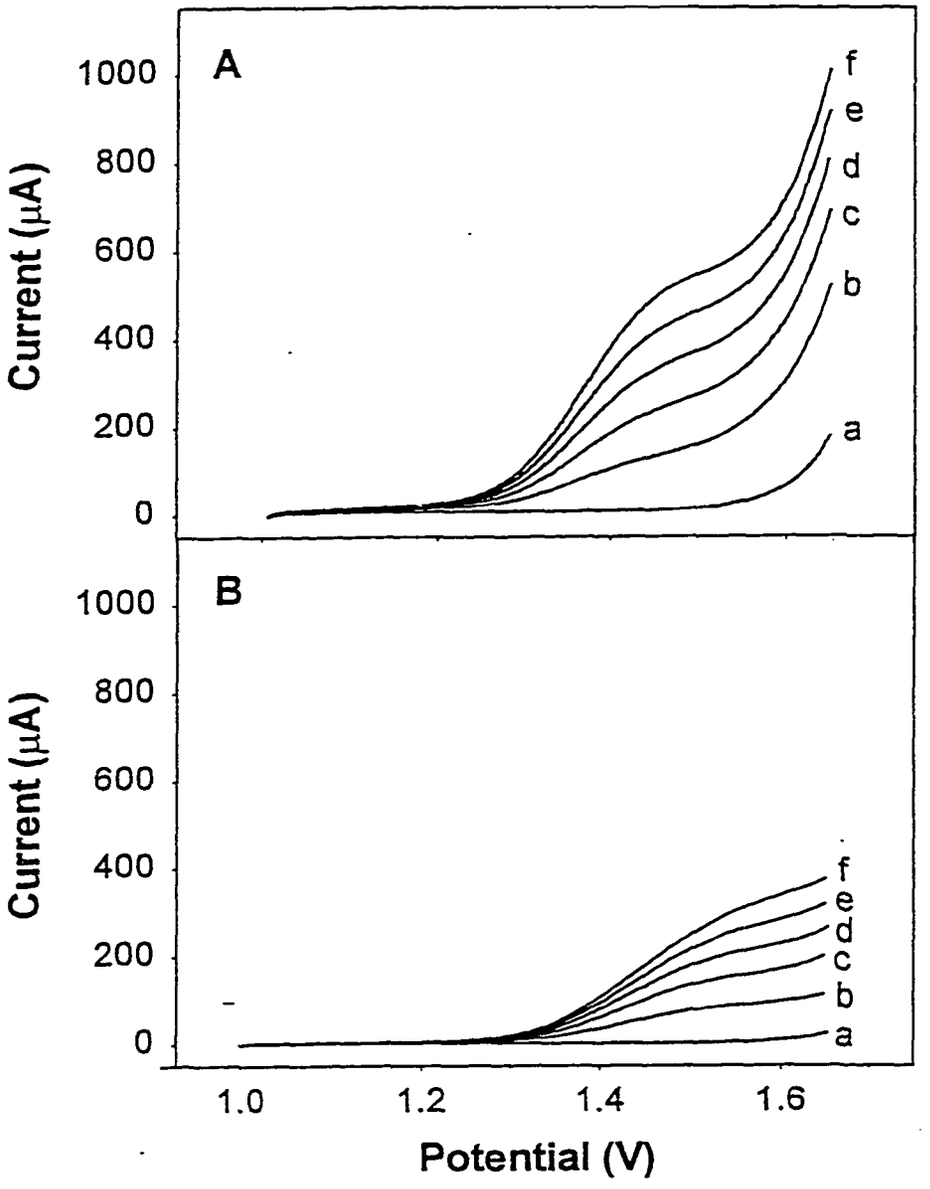

Figure 1. Voltammetric response (positive scan) for cystine as a function of concentration in 0.10M $HClO_4$ at a preanodized roughened (A) and polished (B) Au rotated disk electrode. Scan rate: 100 mV s^{-1}. Rotational velocity: 104.7 rad s^{-1}. Cystine concentration (mM): (a) 0, (b) 0.20, (c) 0.40, (d) 0.60, (e) 0.80, (f) 1.00.

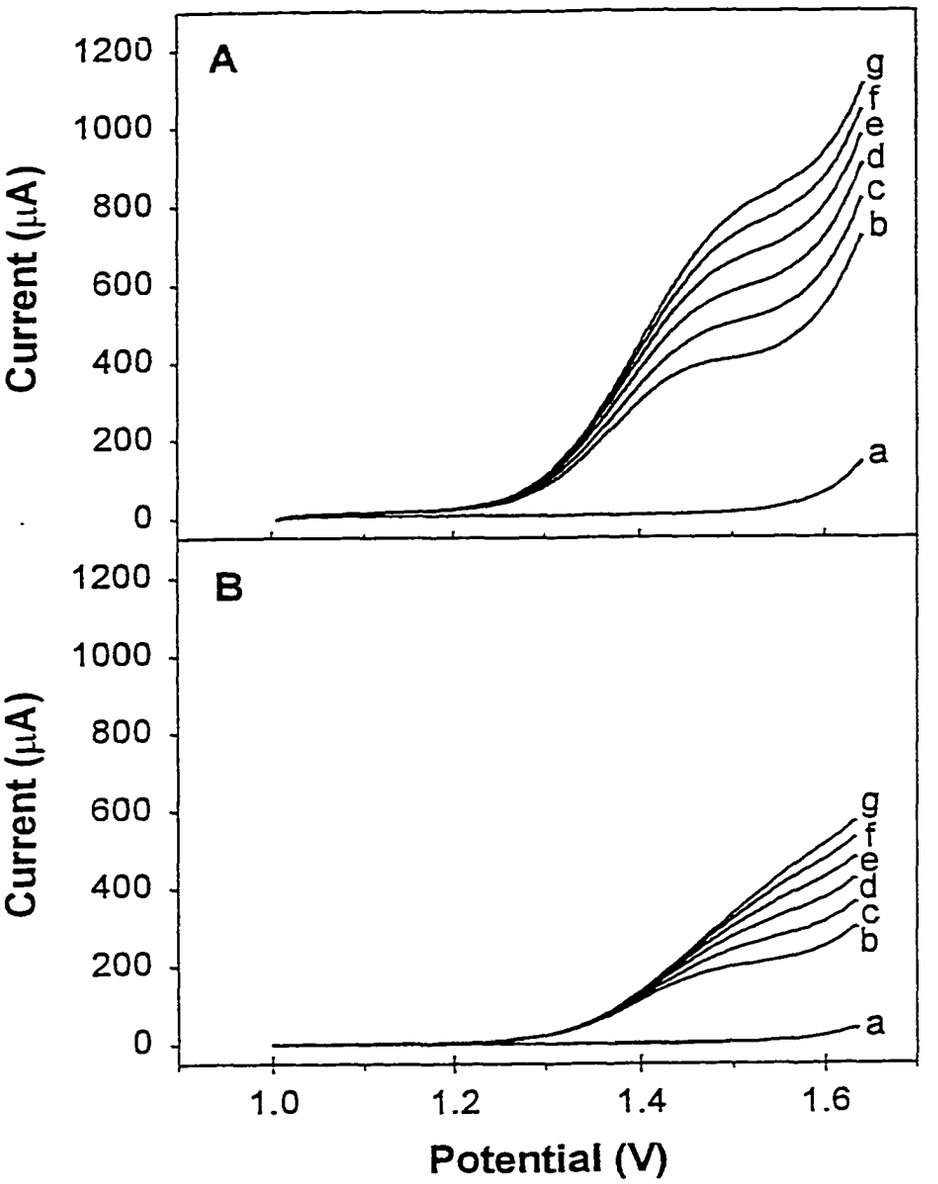

Figure 2. Voltammetric response (positive scan) for cystine as a function of rotational velocity in 0.10 M $HClO_4$ at a preanodized roughened (A) and polished (B) Au rotated disk electrode. Cystine concentration (mM): (a) 0, (b-g) 1.0. Scan rate: 100 mV s^{-1}. Rotational velocity: (rad s^{-1}): (a,b) 41.9, (c) 94.2, (d) 167.5, (e) 261.8, (f) 376.9, (g) 513.0.

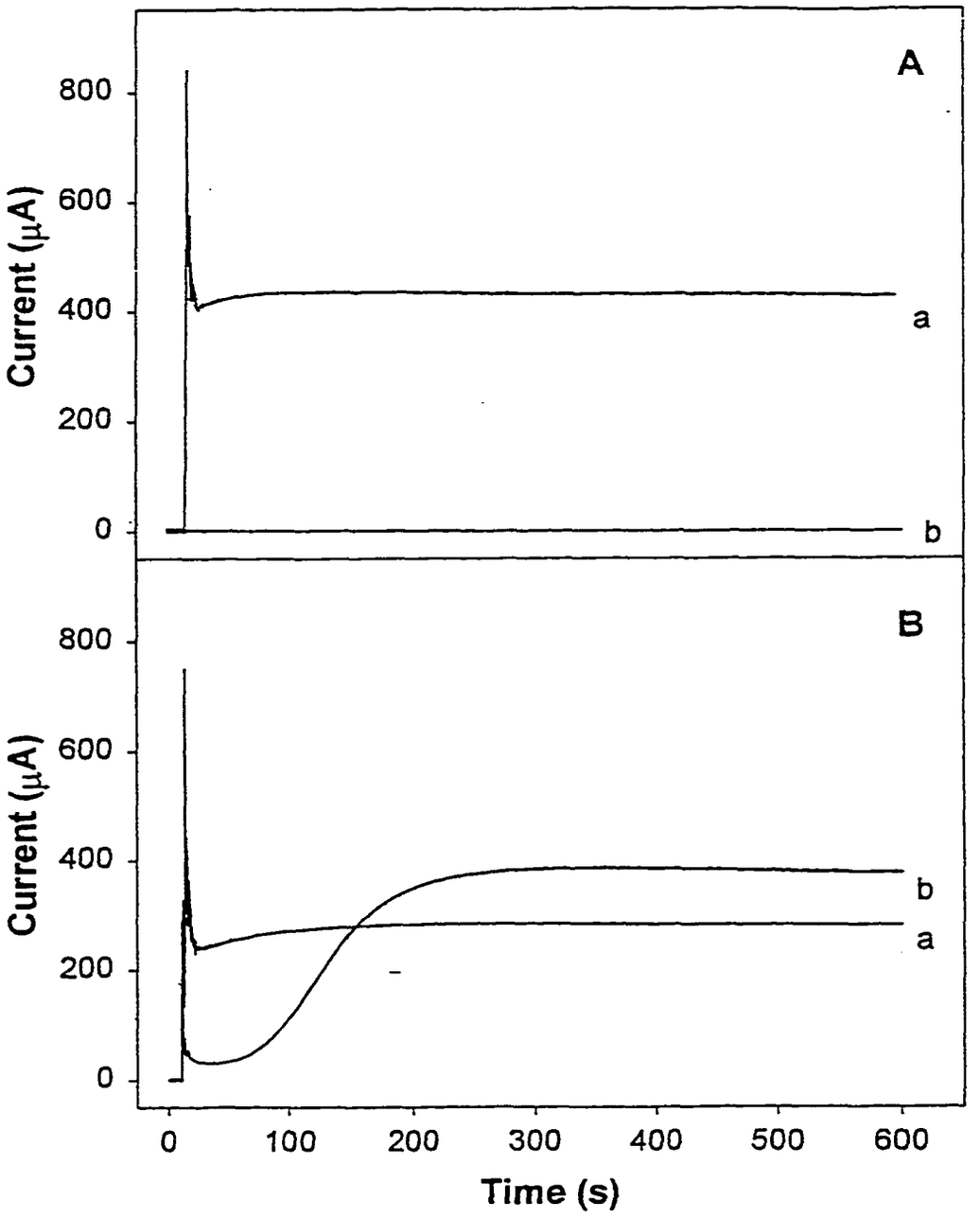

Figure 3. Hydrodynamic amperometric response for 1.0 mM cystine (A) and 1.0 mM cysteine (B) in 0.10 M $HClO_4$ as a function of potential for a preanodized roughened Au rotated disk electrode. Rotational velocity: 104.7 rad s^{-1}. Potential (V): (a) 1.50, (b) 1.00.

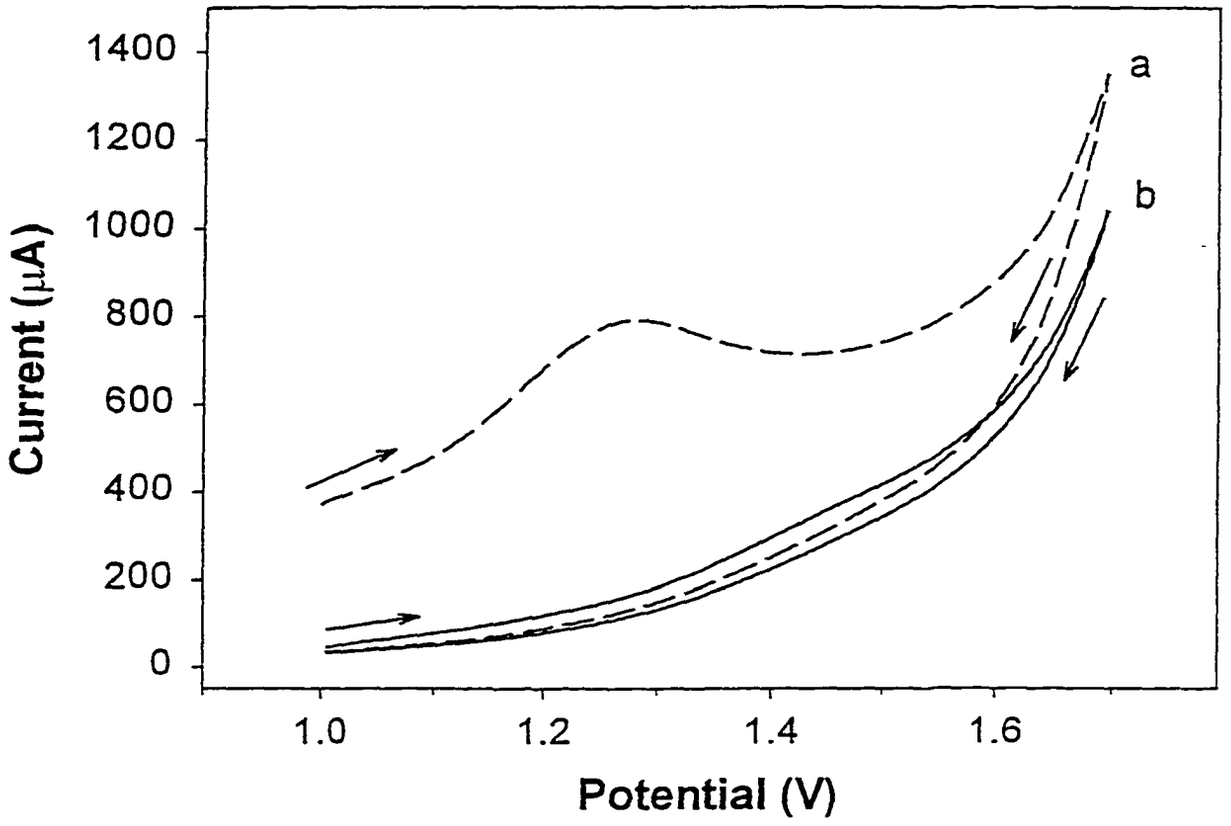

Figure 4. Voltammetric response for 1.0 mM cysteine in 0.10 M $HClO_4$ at a preanodized roughened Au rotated disk electrode following a 10-min period at 1.00V. Scan rate: 100 mV s-1. Rotational velocity: 104.7 rad s^{-1}. Scan number: (a) 1st, (b) 2nd.

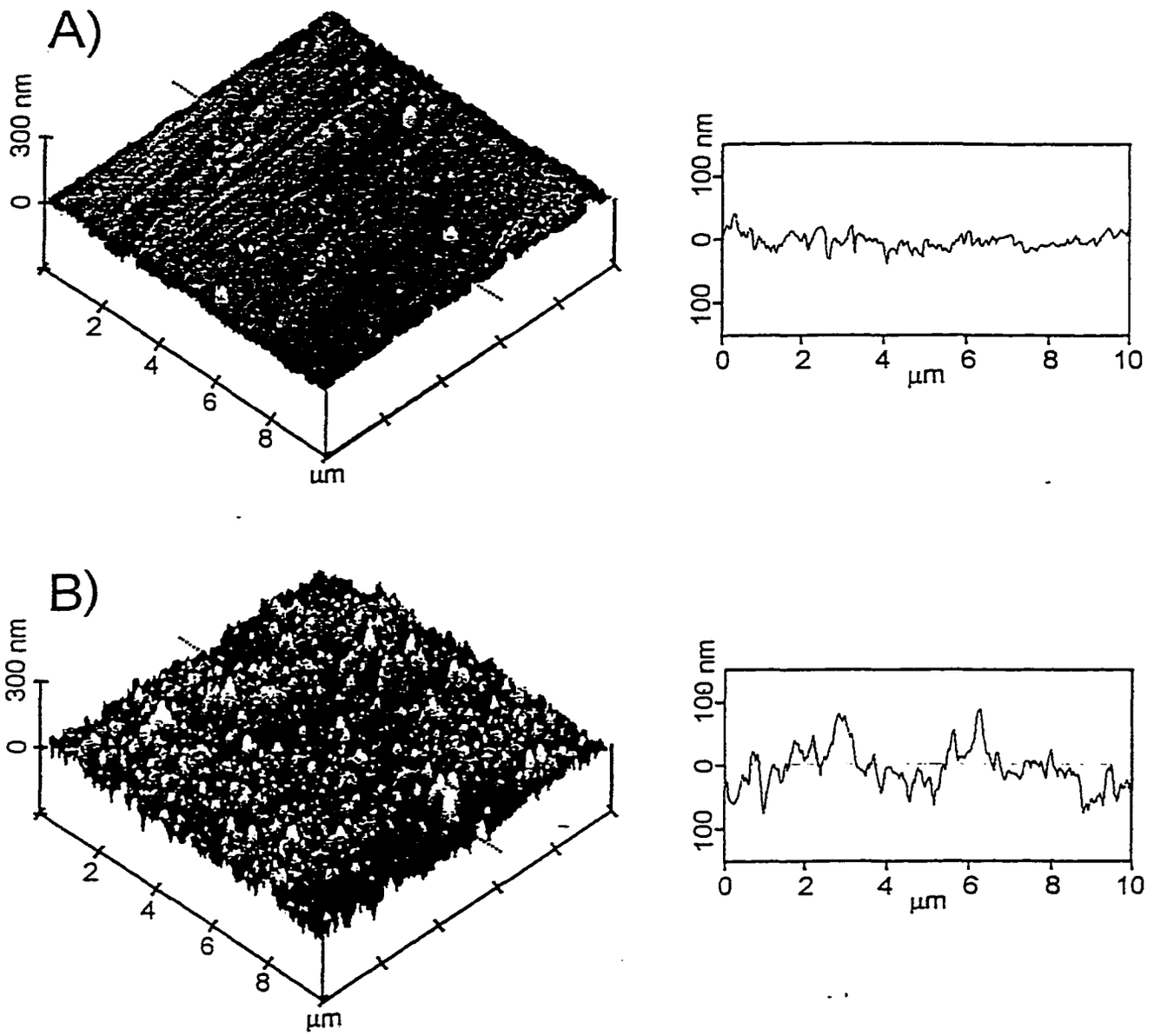

Figure 5. Scanning force microscopy topographic images with their cross sectional profiles of polished Au (A) and roughened Au (B). Dashed lines on 3-D image represent region used for plotting cross sections.

CHAPTER 5. A VOLTAMMETRIC INVESTIGATION OF ETHYLAMINE OXIDATION AT Au, Ag AND Au-Ag ELECTRODES IN ALKALINE MEDIA

A paper submitted for publication in *Electroanalysis*

Matthew E. Johll, Kathryn S. Asala, Melissa Swarts,

James W. Anderegg and Dennis C. Johnson

Abstract

A voltammetric comparison is presented for the anodic response of ethylamine at Ag, Au and $Au_{80}Ag_{20}$ rotated disk electrodes (RDEs) in carbonate buffer (pH 11.2). This study is part of a systematic search for unique anodic response mechanisms at binary alloy electrodes that are not existent at electrodes made from the pure component metals. The primary anodic response for ethylamine at the Au RDE corresponds to oxidative desorption of reactant concomitantly with formation of surface oxide (AuO) during the positive potential scan. For the Ag RDE, ethylamine enhances the anodic wave corresponding to formation of surface oxide (Ag_2O) during the positive scan; however, the majority of this current enhancement is attributed to chemical stripping of Ag_2O by the amine with formation of additional surface oxide. Evidence for this anodic stripping mechanism includes rapid roughening of the electrode surface. The response for ethylamine obtained at the $Au_{80}Ag_{20}$ RDE is concluded to correspond to the

superposition of voltammetric response characteristic of Au electrodes with a response at the Ag sites that is dramatically different from the response observed at the Ag RDE. Data obtained by x-ray photoelectron spectroscopy (XPS) indicate that the surface composition of the $Au_{80}Ag_{20}$ electrode does not change as a result of exposure to ethylamine. Therefore, it is apparent that the Au matrix stabilizes the Ag atoms thereby preventing their dissolution from the $Au_{80}Ag_{20}$ electrode. The voltammetric response for ethylamine at the Ag sites observed during the positive scan is independent of rotational velocity; however, for the negative scan, an inverse Levich behavior is observed. Consideration is given to possible mechanisms to explain the ethylamine response at the Ag sites in the alloy electrode.

Introduction

Research in this laboratory has centered on voltammetric and amperometric studies of the response of polar aliphatic compounds at novel electrode materials in aqueous media. The reactions of greatest interest are anodic and they occur with transfer of oxygen atoms from H_2O in the solvent phase to the oxidation products. Experimental observations have led to conclusions that the fundamental O-transfer step in these anodic reactions does not occur by hydrolysis. Therefore, the goal of this research is the diagnosis of those catalytic properties of electrode surfaces that can

uniquely support anodic O-transfer reactions at rates that are necessary for their electroanalytical applications. Of particular interest is the discovery of new and novel electrode materials that support the anodic O-transfer reactions without loss of response when operated at constant applied potentials. Electrode materials tested in these studies have included preanodized binary alloys [1-3] as well as thin films of metal oxides that are doped with altervalent metallic species [4-7].

Oxidation of primary amines at Au electrodes has been shown to occur concomitantly with the formation of surface oxide (AuO) [8-10]. The anodic signal for these amines is comprised of a primary contribution from oxidative desorption of the preadsorbed reactant with a secondary contribution from oxidation of reactant that is transported to the electrode surface concomitantly with the oxide-formation process. Whereas AuO formation catalyzes amine oxidation, the oxide-covered Au surface is virtually inert for continued amine oxidation. Pulsed potential-time waveforms have been demonstrated to enable use of Au electrodes for detection of alkyl amines following their separation by liquid chromatography [11]. These waveforms, applied at frequencies of ca. 1 Hz, manage the alternate processes of AuO formation with concomitant amine detection followed by cathodic regeneration of the oxide-free Au surface with subsequent adsorption of the amine species, prior to application of the next cycle of the waveform.

Oxidation of amine compounds on Ag electrodes in 1.0 M NaOH has been studied by Hampson et al. [12]. These authors reported that the initial step is the reaction sequence corresponds to oxidation of the amine to the corresponding imine, as indicated by reaction (1). This imine can undergo hydrolysis to form acetaldehyde and ammonia, as indicated by reaction (2), or it can undergo further oxidation to form acetonitrile, as indicated by reaction (3). The ratio of aldehyde to nitrile was determined to be dependent on potential, hydroxide ion concentration, and amine concentration.

$$(CH_3\text{-}CH_2\text{-}NH_2)_{ads} \rightarrow CH_3\text{-}CH{=}NH + 2H^+ + 2e^- \quad (1)$$

$$CH_3\text{-}CH\text{-}NH + H_2O \rightarrow CH_3\text{-}CHO + NH_3 \quad (2)$$

$$CH_3\text{-}CH\text{-}NH \rightarrow CH_3\text{-}C{\equiv}N + 2H^+ + 2e^- \quad (3)$$

Hampson et al. report that the Ag_2O film at their Ag electrode was dissolved in the presence of the amines and this dissolution was attributed to the formation of stable coordination compounds of Ag^+ with the amines [12]. Clearly, Ag electrodes cannot be utilized satisfactorily for anodic detection of amine compounds unless some means is discovered for stabilization of this active metal.

One approach to achieve stabilization of active metals involves their incorporation with inert metals into binary alloys. For example, preanodized Ni electrodes show promise for amperometric detection of carbohydrates in alkaline media [13]. However, the slight solubility of NiO in alkaline media

complicates long-term electroanalytical applications of this electrode. The problem of NiO can be substantially diminished by stabilization of the Ni with Cr [14] and Ti [15, 16] in their binary alloys. In another example, it was determined that there is no anodic dissolution of Ag during anodization of Au-Ag alloys in acidic media [3]. In comparison, pure Ag electrodes are quickly dissolved in acidic media.

Goals of electrocatalytic research in this laboratory include the discovery of alloy electrodes that are applicable for the voltammetric and amperometric detection of a variety of polar aliphatic compounds, including alkyl amines and amino acids. Reported here are results obtained in a voltammetric study of the anodic response of ethylamine at a $Au_{80}Ag_{20}$ electrode in 0.10 M Na_2CO_3.

Experimental

Chemicals: Ethylamine (70 wt %) was obtained from Aldrich and anhydrous sodium carbonate (Certified A.C.S.) was obtained from Fisher Chemical Co. Solutions were prepared with water that was deionized in a Millipore system. All experiments were performed in 0.10 M Na_2CO_3 (pH 11.2) that was deaerated using N_2 (99.99%, Air Products).

Instrumentation: Electrodes were rotated in a AFMSRX rotator-controller (Pine Instrument). Potentiostatic control was achieved using the

K1-circuit of a RDE4 bipotentiostat (Pine Instrument). Electrode potentials were controlled and are reported versus a miniature saturated calomel electrode (SCE, Fisher). All current-potential (*i-E*) and current-time (*i-t*) data were acquired by a personal computer (Apex) using LabVIEW 4.0 software with an AT-MIO16XE-50 data acquisition board (National Instruments). XPS data was acquired using a Model 5500 Multitechnique Chamber with PHI-ACCESS software (Perkin-Elmer). The base pressure of the chamber was $3x10^{-10}$ Torr or lower. The x-ray source provided monochromatic Al *K* radiation at a power of 250 W.

*Electrodes:*All electrodes were configured as rotated disk electrodes (RDEs) having an area of 0.20 cm^2. Rods (5.0-mm diameter, 30-mm length) of pure Au (99.99%) and Ag (99.985%), and $Au_{80}Ag_{20}$ alloy were prepared on this campus by the Metals Preparation Center of Ames Laboratory. Each rod was coated with a thin film of epoxy and sealed in Teflon heat-shrink tubing. Then end surface of each rod was ground perpendicular to its axis using 1200-grit sandpaper (Buehler). After thorough cleaning, these end surfaces were polished with 0.3-μm and 0.05-μm alumina on a polishing wheel covered with microcloth (Buehler) using deionized H_2O as the lubricant. The rods then were mounted into stainless steel shafts for operation in the rotator.

Where specified, electrode surfaces were pretreated by application of a

triangular waveform (100 mV s^{-1}) within the potential limits -1.4 and 1.1 V vs. SCE in 0.10 M Na_2CO_3. This pretreatment procedure was halted after several minutes when successive *i-E* curves were observed to be identical.

Results and Discussion

Ethylamine response at the Ag electrode: Figure 1 contains representative *i-E* curves obtained by cyclic voltammetry at the Ag RDE in 0.10 M Na_2CO_3 (pH 11.2). In the absence of ethylamine (curve a), a broad anodic current peak (E_{peak} = ca. 1.2 V) is observed during the positive scan. Inspection of the electrode surface following termination of the scan at 2.0 V revealed a uniformly light gray appearance. The anodic process occurring during the positive scan is concluded to correspond to formation of a thin film of oxide, probably Ag_2O, on the Ag surface in this alkaline medium. Addition of ethylamine (curve b) results in an enhancement of the anodic peak speculated to correspond to formation of Ag_2O. Inspection of the electrode surface following several applications of the triangular waveform in the presence of ethylamine revealed a highly roughened and blackened surface. Furthermore, dark particles, presumably Ag_2O, occasionally were observed to become detached from the electrode surface under these conditions. Therefore, the enhancement of the anodic peak resulting from the presence of ethylamine, as well as the surface roughening, are concluded

to be caused by chemical stripping of Ag_2O to form a stable Ag(I) coordination compound with the ethylamine. This speculation is in agreement with the conclusion of Hampson et al. reported for 1.0 M NaOH [12].

The broad cathodic peak (E_{peak} = -1.0 V) shown in Figure 1 for the negative scan undoubtedly corresponds to reduction of the Ag_2O film. The enhancement of this peak in the presence of ethylamine probably occurs as a consequence of the increased quantity of Ag_2O formed on the roughened surface. Based on this evidence for the instability of the Ag electrode, we conclude that this electrode has no practical electroanalytical utility for anodic detection of alkyl amines in alkaline media.

Ethylamine response at the Au electrode: Figure 2 contains representative *i-E* curves obtained by cyclic voltammetry at the Au RDE in 0.10 M Na_2CO_3. The residual response (curve a) observed at E > ca. 0.2 V during the positive scan is indicative of the anodic formation of a thin oxide film (AuO). Following scan reversal at 1.1 V, anodic formation of AuO ceases and cathodic reduction of the AuO film occurs in the region 0.2 > E > -0.2 V. Curves b - f, recorded following incremental additions of ethylamine, demonstrate that anodic response for ethylamine is obtained concomitantly with formation of AuO during the positive scan (E > 0.2 V). Following scan reversal at 1.1 V, the anodic signal for ethylamine is quickly attenuated as

further growth of the AuO film ceases. Whereas a large peak in the anodic signal is obtained at ca. 0.4 V (positive scan) for 2 mM ethylamine (curve b), only slight increases in this peak signal are obtained for further increases in ethylamine concentration (curves c - f). This behavior is in agreement with the response mechanism proposed by Dobberpuhl and Johnson [17]. According to their mechanism, the primary anodic response at 0.4 V is the result of oxidative desorption of ethylamine molecules that are adsorbed on the oxide-free surface in the potential region $E <$ ca. -0.1 V. A secondary contribution to the total anodic response in the region $E > 0.4$ V is the result of oxidation of ethylamine transported to the electrode surface during the process of AuO formation. A significant decrease is observed in the peak area for cathodic reduction of AuO (negative scan) in response to addition of ethylamine (compare curves b and a). This decrease is speculated to be the result of inhibition by adsorbed ethylamine of the process of oxide formation at $E > 0.2$ V. In other studies (data not shown), the anodic signal for ethylamine obtained during the positive scan was determined to be approximately a linear function of the scan rate with virtually no dependence on rotational velocity. These results also are in agreement with the mechanistic conclusions of Dobberpuhl and Johnson [17].

Residual voltammetric response at the $Au_{80}Ag_{20}$ electrode: Figure 3 contains representative *i-E* curves obtained by cyclic voltammetry as a

function of scan number at the freshly polished $Au_{80}Ag_{20}$ RDE in 0.10 M Na_2CO_3 in the absence of ethylamine. Anodic formation of oxide at Au sites on the alloy surface is concluded to occur at $E > 0.4$ V during the positive scan. This oxide is cathodically reduced during the negative scan in the region $0.3 > E > -0.2$ V. The smaller anodic and cathodic waves observed in the region $E > 0.7$ V are speculated to represent a quasi reversible redox couple involving Ag sites in the $Au_{80}Ag_{20}$ surface. It is apparent in Figure 3 that the area under the anodic wave assigned to this redox couple is significantly larger than that for the corresponding reduction wave (see curve a). It is speculated that this results from anodic discharge of H_2O during the positive scan with some evolution of O_2 occurring concomitantly with formation of the oxidized state of the Ag sites.

The voltammetric response from the redox couple at $E > 0.8$ V diminishes with increasing cycle number, approaching a reproducible response after 15 - 20 cycles. This decrease is indicative of a decrease in the density of Ag sites with repeated cycles of oxide formation and reduction. It also is apparent in Figure 3 that the anodic peak at 0.6 V (positive scan) decreases with increasing cycle number as does the peak at 1.0 V. This decrease at 0.6 V is speculated to indicate that the Ag sites are oxidized simultaneously with oxidation of Au sites, perhaps to AgO. Therefore, oxidation of Ag sites at $E > 0.8$ V (positive scan) is speculated to correspond

to conversion of Ag sites from their 2+ to the 3+ oxidation states.

XPS data for the $Au_{80}Ag_{20}$ surface: The $Au_{80}Ag_{20}$ surface was examined by XPS to determine if dissolution of Ag sites occurs during repeated cyclic potential scans in 0.10 M Na_2CO_3 without ethylamine. The freshly polished $Au_{80}Ag_{20}$ electrode was treated for a 1-h period using the triangular waveform applied in Figure 3. The XPS data for this surface indicated a surface composition of 79.7% Au and 20.3% Ag. These results are in good agreement with the bulk composition of the $Au_{80}Ag_{20}$ alloy. The $Au_{80}Ag_{20}$ electrode again was polished and its potential cycled for a 1-h period in 0.10 M Na_2CO_3 containing 5.0 mM ethylamine. The surface composition following this exposure was calculated from XPS data to be 79.8% Au and 20.2%. These data do not indicate a significant decrease in Ag concentration at the $Au_{80}Ag_{20}$ surface within the sampling depth of XPS, typically estimated to be 5 - 25 D for metals [18]. Nevertheless, we persist in the speculation that the density of Ag sites is diminished by the repeated formation and reduction of surface oxide at the electrochemically active surface, perhaps as a soluble Ag(I) species. Alternately, an atom-atom exchange between Ag, Au and O atoms might result in a decrease in the density of Ag sites at the electrochemically active surface.

It was not possible, using the x-ray photoelectron spectrometer available for this work, to determined the oxidation state of Ag sites in the

alloy electrode as a function of applied potential.

Ethylamine response at the $Au_{80}Ag_{20}$ electrode: Figure 4 contains representative *i-E* curves obtained by cyclic voltammetry as a function of ethylamine concentration at the $Au_{80}Ag_{20}$ RDE in 0.10 M Na_2CO_3. The residual response (curve a, dashed line) corresponds to the pretreated RDE at which the peaks at $E > 0.7$ V associated with the Ag sites have decreased to their reproducible size. An anodic response for ethylamine is observed during the positive scan (curves b - f) in the region $0.2 < E < 0.7$ V concomitantly with the anodic wave corresponding to formation of AuO. This ethylamine response (0.2 - 0.7 V) is speculated to correspond to that response mechanism described above for the Au RDE. Of greater significance to this study is the large anodic response observed at $E > 0.7$ V. The peak-shaped wave ($E_{peak} = 0.9$ V) observed during the positive scan is developed over the same potential region as the anodic peak assigned to oxidation of Ag sites from their 2+ to the 3+ oxidation states (see Fig. 3). This correspondence is speculated to be evidence that the anodic response mechanism for ethylamine at $E > 0.7$ V is catalytically associated with the 3+ oxidation state of the Ag sites. Furthermore, following scan reversal at 1.10 V, an anodic response for ethylamine persists ($1.0 > E > 0.8$ V) until the Ag sites are converted from their 3+ to the 2+ oxidation states ($E < 0.8$ V). This response is speculated to be characteristic of a mechanism involving

electron-transfer mediation by the Ag sites in their 3+ oxidation state. However, based on data presented below, it is apparent that preadsorption of ethylamine at the oxide-free sites (E < 0.0 V) is an important component of the response mechanism.

The voltammetric response was obtained as a function of cycle number at the freshly polished $Au_{80}Ag_{20}$ RDE in 0.10 M Na_2CO_3 containing 10 mM ethylamine. Of greatest significance was the gradual attenuation of the anodic response in the region E > 0.7 V for both the positive and negative scans until a stable response was obtained after 15 - 20 cycles. To illustrate, Figure 5 contains the *i-E* curves obtained for scan 1 (curve a) and scan 20 (curve b). Whereas the peak observed during the positive scan decreased by ca. 30%, the peak observed during the negative scan decreased by ca. 75%. This attenuation of ethylamine response is consistent with the speculation above that the density of Ag sites in this alloy electrode is decreased with increasing scan number.

Variations of scan limits: The voltammetric scan limits were altered to determine the effects on the anodic response of ethylamine at the pretreated $Au_{80}Ag_{20}$ RDE. Figure 6 contains representative *i-E* curves as a function of 0.10-V incremental increases in the negative scan limit. The ethylamine response (E > 0.7 V) remains virtually unchanged for the decrease in negative scan limit from -0.60 V to 0.00 V (curves a - e). However, further

increase in the negative scan limit (curves f and g) causes a significant decrease in ethylamine response for both the positive and negative scans. The lowest ethylamine response shown (curve g) corresponds to a negative scan limit of 0.2 V for which there is no evidence of cathodic reduction of surface oxide from the alloy electrode. This observation is consistent with the speculation that oxidative desorption of ethylamine that is preadsorbed at the oxide-free surface (E < 0.0 V) is an important component of the voltammetric response during the positive scan at both the Au sites (0.2 < E < 0.8 V) and Ag sites (E > 0.8 V).

Figure 7 contains *i-E* curves obtained at the pretreated $Au_{80}Ag_{20}$ RDE as a function of increased values for the positive scan limit. The anodic peak at 0.95 V (positive scan) is decreased approximately 20% for the increase in positive limit from 1.0 V (curve a) to 1.2 V (curve c). In comparison, the signal at 0.85 V (negative scan) decreases approximately 90% for this same change in positive limit. Examination of the cathodic peak (negative scan) corresponding to oxide reduction in the region 0.2 - !0.1 V reveals that the amount of oxide formed during the positive scan increases substantially as the positive limit is increased. Therefore, it is apparent that the large attenuation of the ethylamine response obtained during the negative scan is a direct consequence of the formation of an increased amount of surface oxide as the positive scan limit is increased.

Variations of rotational velocity and scan rate: The voltammetric response of ethylamine was obtained as a function of rotational velocity and scan rate for the purpose of distinguishing between transport-controlled and surface-controlled oxidation processes. Figure 8 contains *i-E* curves obtained by cyclic voltammetry as a function of increasing rotational velocity at the pretreated $Au_{80}Ag_{20}$ RDE in 0.10 M Na_2CO_3 containing 5.0 mM ethylamine. During the positive scan, the anodic peak at ca. 0.5 V is constant and the peak at ca. 0.9 V shows a very slight decrease for increases in rotational velocity from 15.1 rad s^{-1} (curve b) to 82.1 rad s^{-1} (curve f). These observations are indicative of surface-controlled mechanisms for ethylamine oxidation at both the Au sites (0.5 V) and Ag sites (0.9 V). Both anodic waves (positive scan) also were determined to be approximately linear functions of scan rate (data not shown) which is further evidence of surface-controlled response mechanisms. More specifically, a significant contribution to these peaks can be attributed to the oxidative desorption of ethylamine that is preadsorbed at the oxide-free sites in the region $E < 0.0$ V.

During the negative scan shown in Figure 8, the anodic response at 0.9 V is observed to decrease substantially (ca. 40%) with increasing rotational velocity as represented by curves b to f. This so-called *inverse Levich response* was confirmed by hydrodynamic chronoamperometric

curves (*i-t*) obtained at the preanodized electrode following a potential step from !1.3 to 0.90 V (data not shown). This inverse Levich response is speculated to indicate a coupled electrochemical process of the *ece* type.

Effect of added NaOH: Choice of 0.10 M Na_2CO_3 (pH 11.2) as the supporting electrolyte in these studies was based on results of a previous study of the pH dependence of the anodic response of ethylamine at preanodized Ag_5Pb_{95} electrodes [1,2]. It was concluded for that electrode that the anodic response mechanism involves adsorption of the amine moiety at Ag sites via non-bonded electrons on the N atom. Attenuation of the anodic signal for pH < ca. 10 was explained on the basis of protonation of the amine moiety. Attenuation of the ethylamine signal for pH > 11 was attributed to competitive adsorption by OH^- for the Ag sites.

Figure 9 contains *i-E* curves that demonstrating the effect of increased OH^- concentration on the voltammetric response of ethylamine at the $Au_{80}Ag_{20}$ RDE in 0.10 M Na_2CO_3. Curves a and b correspond to the response obtained in the absence and presence, respectively, of 5 mM ethylamine without added NaOH. Curves c and d correspond to *i-E* curves obtained following addition of 10 and 20 mM NaOH, respectively. A negative shift (ca. 60 mV per pH unit) is observed in the potential for the onset of ethylamine oxidation at the Au sites (positive scan). This shift corresponds to a similar shift in the potential for onset of Au oxide formation as a function of added

NaOH (data not shown). A comparable shift occurs in the potential of the cathodic peak for reduction of the surface oxide (negative scan). Because the positive scan limit remains constant in this study, the quantity of surface oxide formed during the positive scan increases at pH is increased. Therefore, the peak area for the cathodic reduction of surface oxide increases with increasing pH.

The anodic response for ethylamine observed during the positive scan in the region ca. $0.8 < E < 0.9$ V is observed to decrease substantially for the NaOH concentration is increased from 10 mM (curve c) to 20 mM (curve d). This attenuation is consistent with speculation that competitive adsorption by OH^- blocks adsorption of the ethylamine at the oxide-free Ag sites. Attenuation of ethylamine response at ca. 0.8 V during the negative scan as a consequence of added NaOH is attributed both to competitive adsorption by OH^- and the increased surface coverage by oxide formed during the positive scan.

Other voltammetric data: Ammonia and acetaldehyde are predicted to be the product of hydrolysis of the imine generated by the two-electron oxidation of ethylamine according to the mechanism of Hampson et al. as represented by reactions (1) to (3) [12]. Voltammetric data (not shown) obtained in the present study for the pretreated $Au_{80}Ag_{20}$ RDE revealed that addition of 10 mM NH_3 resulted in a significant increase in the anodic signal

(positive scan) in the potential region characteristic of the formation of AuO ($0.3 < E < -0.8$ V). Furthermore, a large anodic signal was obtained (positive scan) in the potential region for further oxidation of Ag sites ($E > 0.8$ V). No anodic response was obtained for acetaldehyde at the $Au_{80}Ag_{20}$ RDE in the potential region of interest ($E > 0.8$ V).

Conclusions

(i) Comparison of voltammetric data obtained at the Ag RDE (Fig. 1) and $Au_{80}Ag_{20}$ RDE (Fig. 3) are consistent with the conclusion that Ag sites are stabilized by neighboring Au sites in the alloy electrode. Therefore, the anodic response of ethylamine at Ag sites in the $Au_{80}Ag_{20}$ RDE occurs by a mechanism that is unique from the mechanism at the Ag RDE.

(ii) The quasi-reversible voltammetric peaks observed at $E > 0.8$ V for the $Au_{80}Ag_{20}$ RDE in the absence of ethylamine (Fig. 3) are concluded to correspond to a redox transition involving Ag sites in this alloy electrode. This redox transition is speculated to involve the 3+-2+ states for the Ag sites; however, this designation of oxidation states has not yet been confirmed by high resolution XPS data.

(iii) The observation of an anodic response for ethylamine at E >0.8V during both the positive and negative scans (Fig. 4) is concluded to be indicative of a response mechanism involving electron-transfer mediation by the Ag sites in their 3+ oxidation state. However, this designation does not eliminate the probability of a strong contribution to the total anodic response during the positive scan from oxidative of ethylamine that has been preadsorbed at the oxide-free electrode surface (E < 0.0 V). This designation of preadsorption of ethylamine at Ag sites in the $Au_{80}Ag_{20}$ electrode is consistent with the conclusion by Ge and Johnson [1,2] for ethylamine response at preanodized $Pb_{95}Ag_5$ electrodes in alkaline media.

(iv) The anodic response for ethylamine observed at ca. 0.9 V during the negative scan is decreased substantially as a consequence of increases in positive scan limit (Fig. 7). This observation is indicates that the oxide film formed during the preceding positive scan interferes with the mechanism of response at the Ag sites during the negative scan. We speculate that that the Ag sites become masked by the more extensive oxide generated at neighboring Au sites during positive scans to increased positive values of potential.

(v) The anodic response for ethylamine at $E > 0.7$ V is observed to decrease with increases in rotational velocity (Fig. 8). This so-called *inverse Levich response* is concluded to be consistent with an *ece* mechanism of the type proposed by Hampson et al. [12] and described above by reactions (1) - (3). More specifically, we conclude that reaction (1) occurs with a small heterogeneous rate constant so that the corresponding current response is virtually independent of the rate of convective-diffusional mass transport. The ammonia and, probably, the imine, but not acetaldehyde, are electroactive in this potential region at the $Au_{80}Ag_{20}$ electrode. Therefore, if either the imine or the ammonia generated in reaction (2) is not strongly adsorbed at the electrode surface, they can be lost from the diffusion layer of the rotated electrode by convective-diffusional mass transport. This loss of the imine and/or ammonia is consistent with the observation of the observed effect of rotational velocity on the anodic response.

(vi) Whereas the most rapid attenuation of ethylamine response at Ag sites in the $Au_{80}Ag_{20}$ electrode occurs during the first several cyclic scans in voltammetry (Fig. 5), the response is never observed to arrive at a constant value. The same is true for the

amperometric signal obtained at 0.9 V. Therefore, is must be concluded that the $Au_{80}Ag_{20}$ electrode is not suitable for anodic detection of alkyl amines in alkaline media. Nevertheless, this electrode has served as an interesting case study of the role of alloying agents in the design of electrochemical sensors.

Future efforts will continue the search for alloys of Ag that exhibit the following important properties: (i) stabilization of the Ag component against anodic dissolution in the presence of ligands that form strong coordination bonds with Ag(I), and (ii) stable electrocatalytic activity for the anodic detection of amines with a constant sensitivity.

Acknowledgment

The authors acknowledge financial support from National Science Foundation, Grant CHE-9634544. The authors are grateful to L.L. Jones and J.T. Wheelock, Ames Laboratory Materials Preparation Center at Iowa State University, for preparation of electrode materials and to M. Campo for helpful discussions.

References:

(1) Ge, J.; Johnson, D. C. *J. Electrochem. Soc.* **1995,** *142*, 1525-31.

(2) Ge, J.; Johnson, D. C. *J. Electrochem. Soc.* **1996,** *143*, 2543-2548.

(3) Johll, M. E.; Johnson, D. C. *Electroanalysis* **1999,** *in press.*

(4) Yeo, I. H.; Johnson, D. C. *J. Electrochem. Soc.* **1987,** *134*, 1973-7.

(5) Feng, J.; Johnson, D. C. *J. Electrochem. Soc.* **1990,** *137*, 507-10.

(6) Pamplin, K. L.; Johnson, D. C. *J. Electrochem. Soc.* **1996,** *143*, 2119-2125.

(7) Popović, N. Đ.; Cox, J. A.; Johnson, D. C. *J. Electroanal. Chem.* **1998,** *455*, 153-160.

(8) Dobberpuhl, D. A.; Johnson, D. C. *Anal. Chem.* **1995,** *67*, 1254-8.

(9) Dobberpuhl, D. A.; Johnson, D. C. *Electroanalysis* **1996,** *8*, 726-731.

(10) Jackson, W. A.; LaCourse, W. R.; Dobberpuhl, D. A.; Johnson, D. C. *Electroanalysis (N. Y.)* **1991,** *3*, 607-16.

(11) Dobberpuhl, D. A.; Hoekstra, J. C.; Johnson, D. C. *Anal. Chim. Acta* **1996,** *322*, 55-62.

(12) Hampson, N. A.; Lee, J. B.; Morley, J. R.; Scanlon, B. *Canadian Journal of Chemistry* **1969,** *47*, 3729-36.

(13) Hui, B.S.; Huber, C.O. *Anal. Chim. Acta* **1991,** 243, 279-285.

(14) Marioli, J. M.; Luo, P. F.; Kuwana, T. *Anal. Chim. Acta* **1993,** *282*, 571-80.

(15) Jin, J. Y.; Miwa, T. *Bunseki Kagaku* **1998,** *47*, 665-672.

(16) Morita, M.; Niwa, O.; Tou, S.; Watanabe, N. *J. Chromatogr., A* **1999,** *837*, 17-24.

(17) Dobberpuhl, D.A.; Johnson, D.C. *Electroanalysis*, **1996,** 8, 726-731.

(18) Settle, F. (Ed.), *Handbook of Intrumental Techniques for Analytical Chemistry*, 1st ed., Prentice Hall PTR: Upper Saddle River, NJ, **1997**, 811.

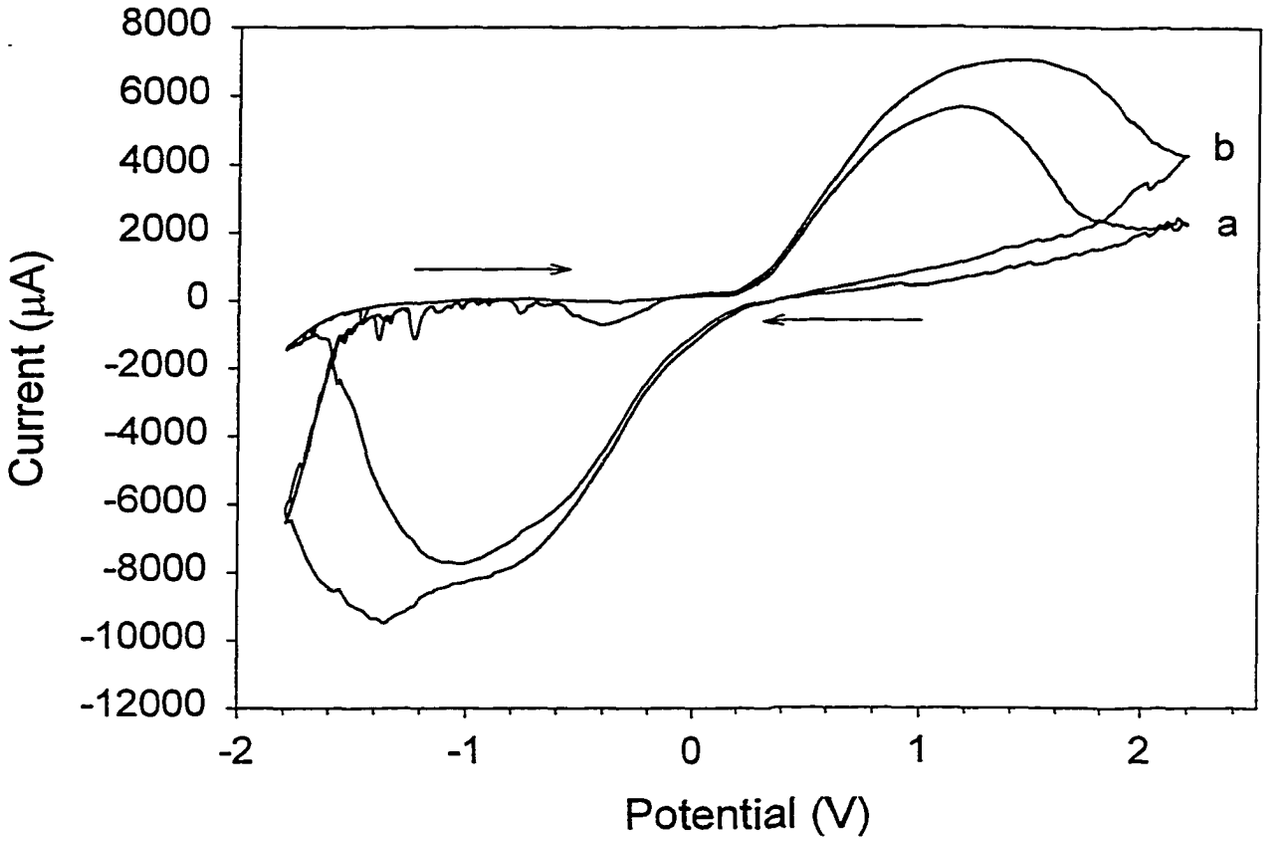

Figure 1. Voltammetric response for ethylamine at a Ag RDE in 0.10 M Na_2CO_3. Scan rate: 100 mV s^{-1}. Rotational velocity: 10.5 rad s^{-1}. Ethylamine concentration (mM): (a) 0, (b) 2.

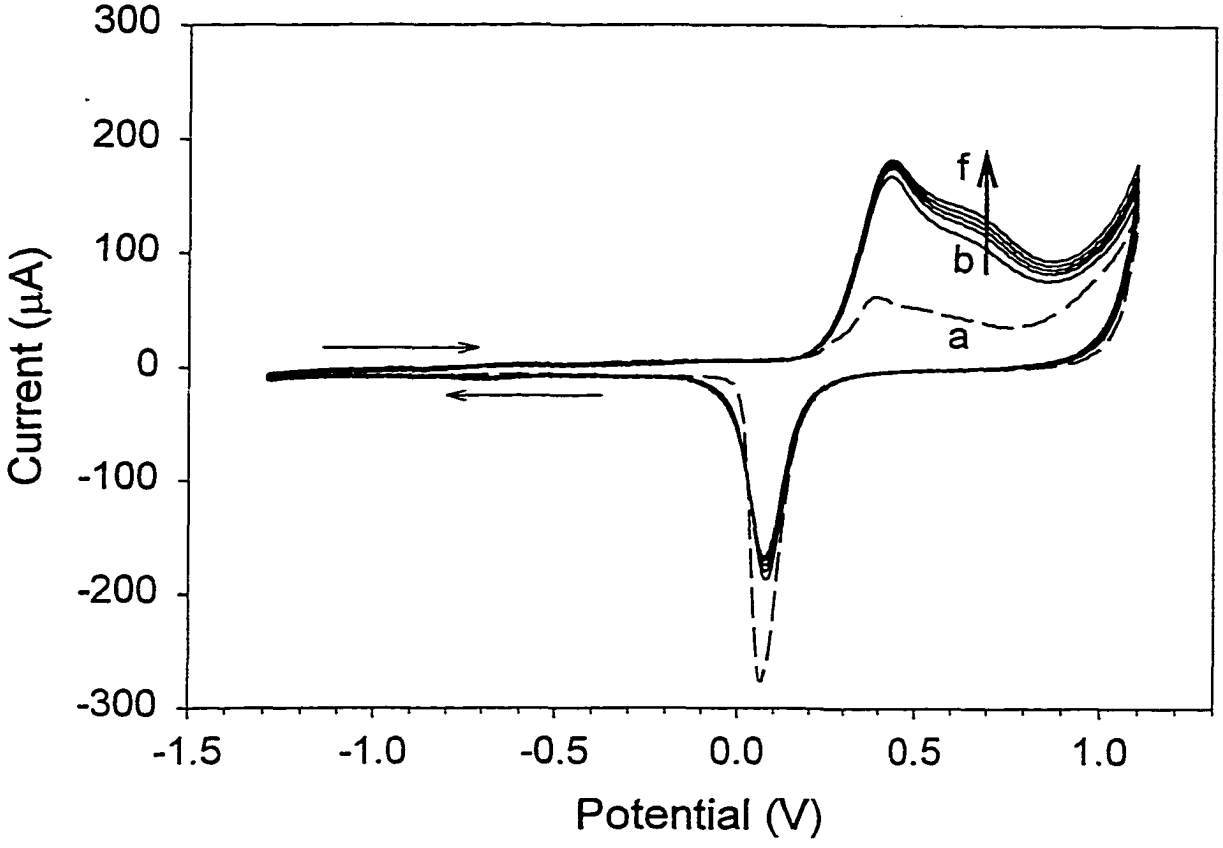

Figure 2. Voltammetric response at a Au RDE in 0.10 M Na_2CO_3 as a function of ethylamine concentration. Scan rate: 100 mV s^{-1}. Rotational velocity: 10.5 rad s^{-1}. Ethylamine concentration (mM): (a) 0, (b) 2, (c) 4, (d) 6, (e) 8, (f) 10.

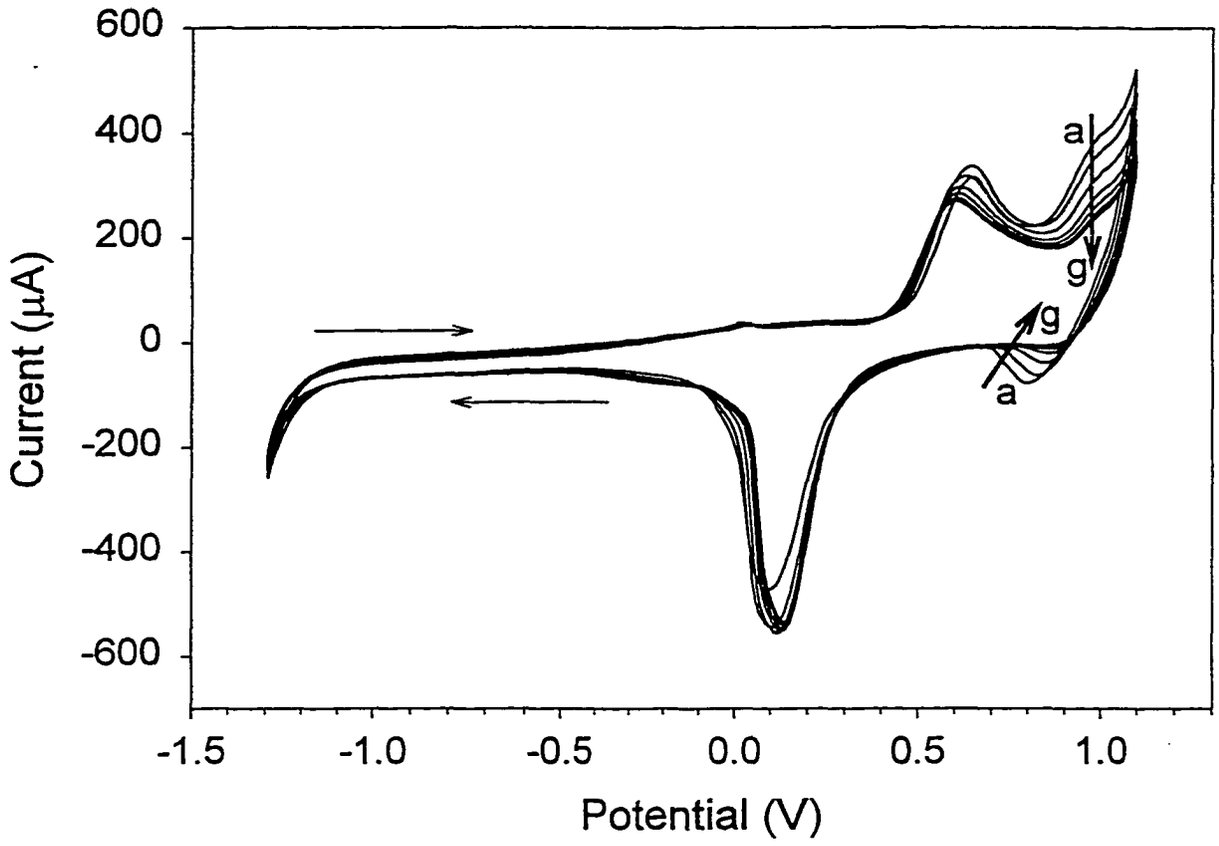

Figure 3. Residual voltammetric response for a $Au_{80}Ag_{20}$ RDE in 0.10 M Na_2CO_3 as a function of scan number. Scan rate: 100 mV s^{-1}. Rotational velocity: 10.5 rad s^{-1}. Scan number: (a) 1, (b) 5, (c) 10, (d) 15, (e) 20, (f) 25, (g) 30.

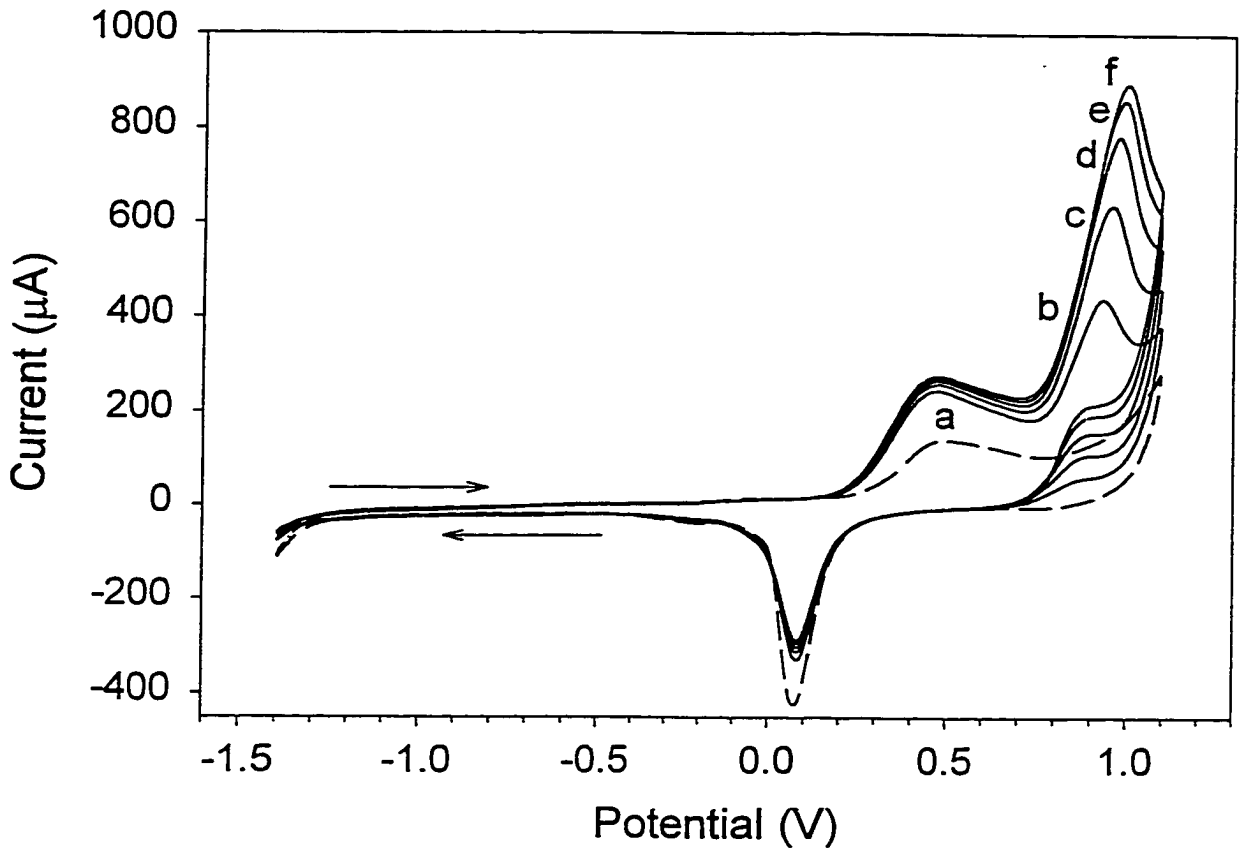

Figure 4. Voltammetric response at a $Au_{80}Ag_{20}$ RDE in 0.10 M Na_2CO_3 as a function of ethylamine concentration. Scan rate: 100 mV s^{-1}. Rotational velocity: 10.5 rad s^{-1}. Ethylamine concentration (mM): (a) 0, (b) 2, (c) 4, (d) 6, (e) 8, (f) 10.

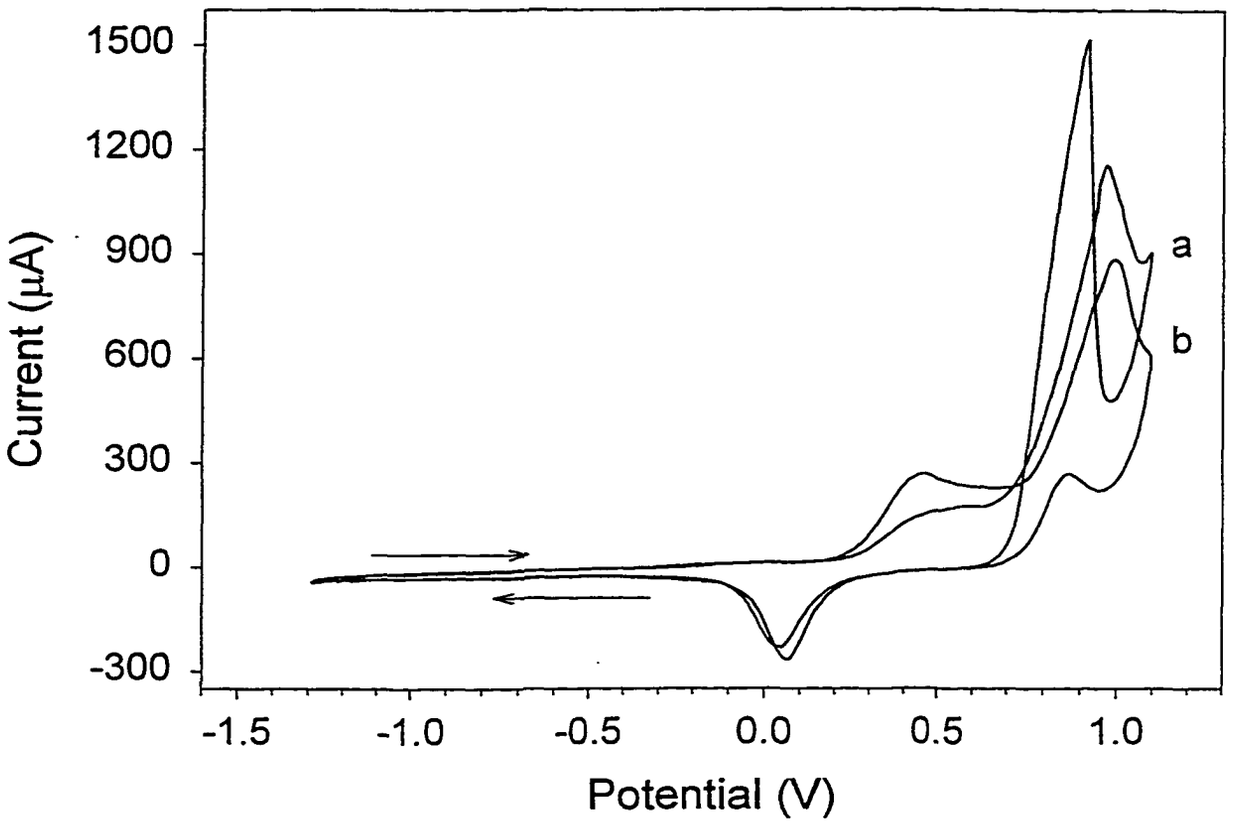

Figure 5. Voltammetric response for 10 mM ethylamine the freshly polished $Au_{80}Ag_{20}$ RDE in 0.10 M Na_2CO_3 as a function of scan number. Scan rate: 100 mV s^{-1}. Rotational velocity: 10.5 rad s^{-1}. Scan number: (a) 1, (b) 20.

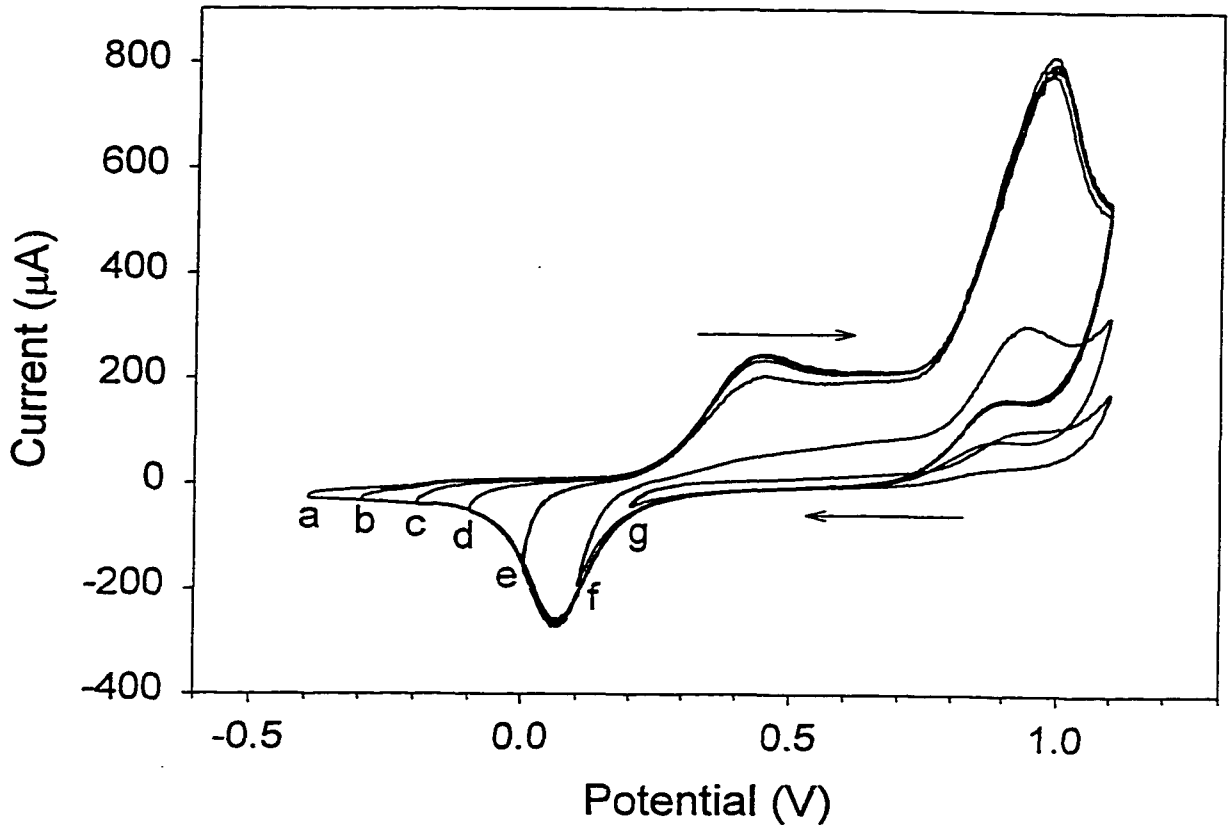

Figure 6. Voltammetric response for ethylamine at a $Au_{80}Ag_{20}$ RDE in 0.10 M Na_2CO_3 as a function of negative scan limit. Scan rate: 100 mV s^{-1}. Rotational velocity: 10.5 rad s^{-1}. Ethylamine concentration: 10 mM. Negative scan limit (V): (a) -0.4, (b) -0.3, (c) -0.2, (d) -0.1, (e) 0.0, (f) 0.1,(g) 0.2.

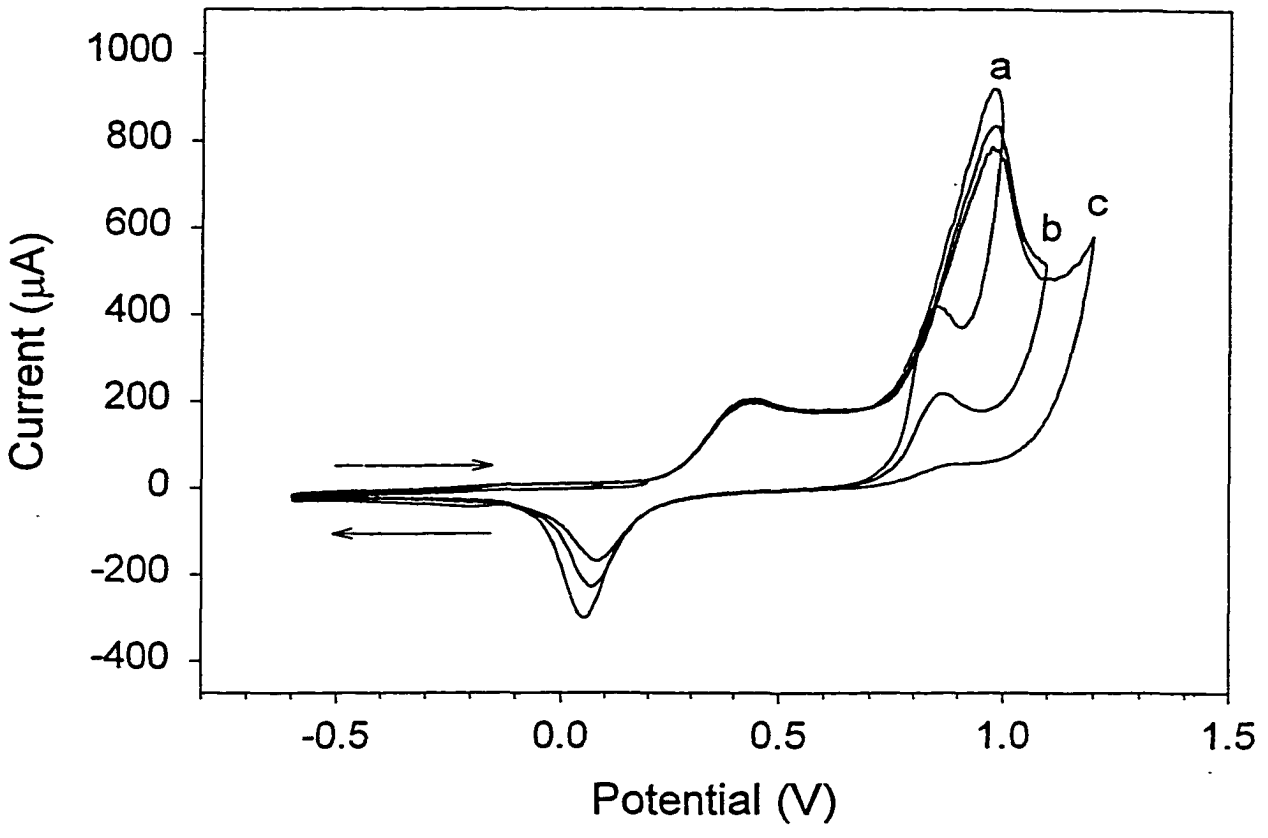

Figure 7. Voltammetric response at a $Au_{80}Ag_{20}$ RDE for ethylamine in 0.10 M Na_2CO_3 as a function of positive scan limit. Scan rate:100 mV s^{-1}. Rotational velocity: 10.5 rad s^{-1}. Ethylamine concentration: 10 mM. Positive scan limit (V): (a) 1.0, (b) 1.1, (c) 1.2.

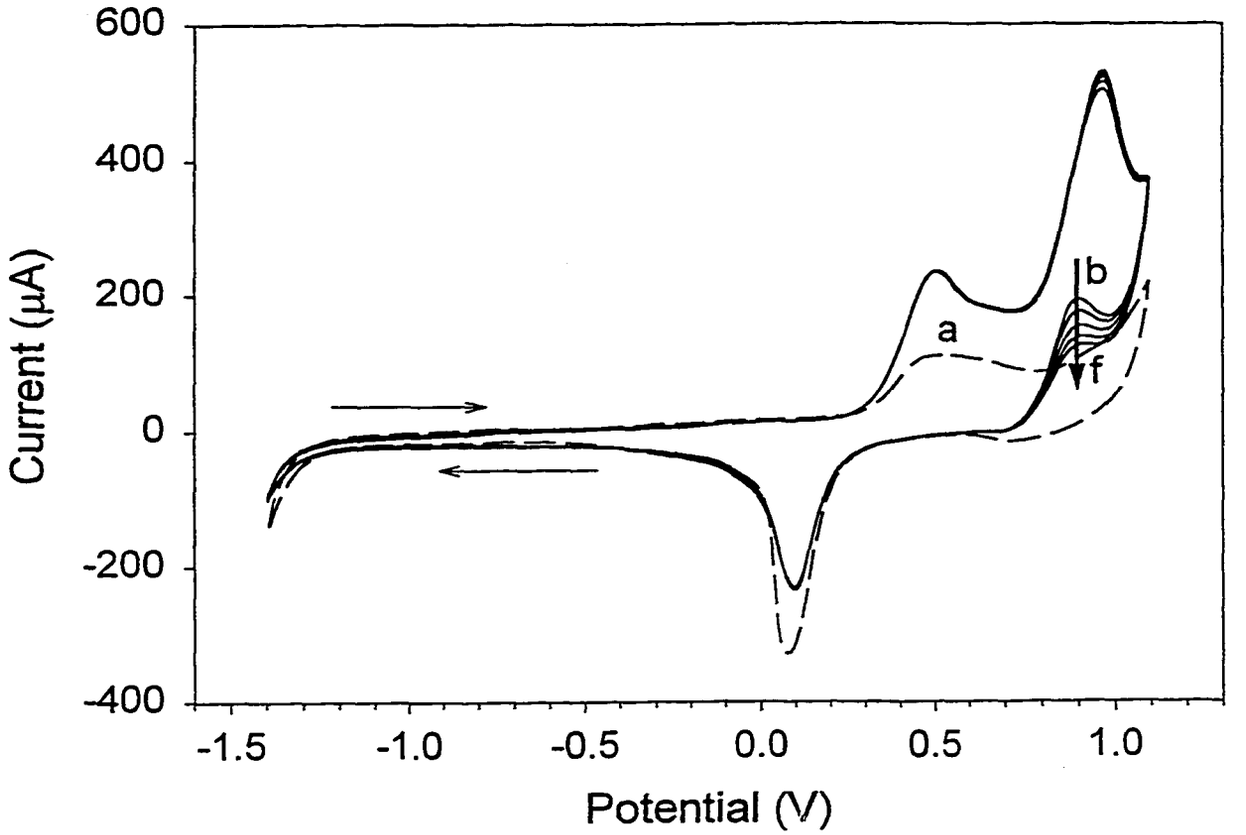

Figure 8. Voltammetric response for ethylamine at a $Au_{80}Ag_{20}$ RDE in 0.10 M Na_2CO_3 as a function of rotational velocity. Scan rate: 100 mV s^{-1}. Ethylamine concentration: 5 mM. Rotational velocity (rad s^{-1}): (a) residual, (b) 15.1, (c) 26.8, (d) 41.9, (e) 60.3, (f) 82.1.

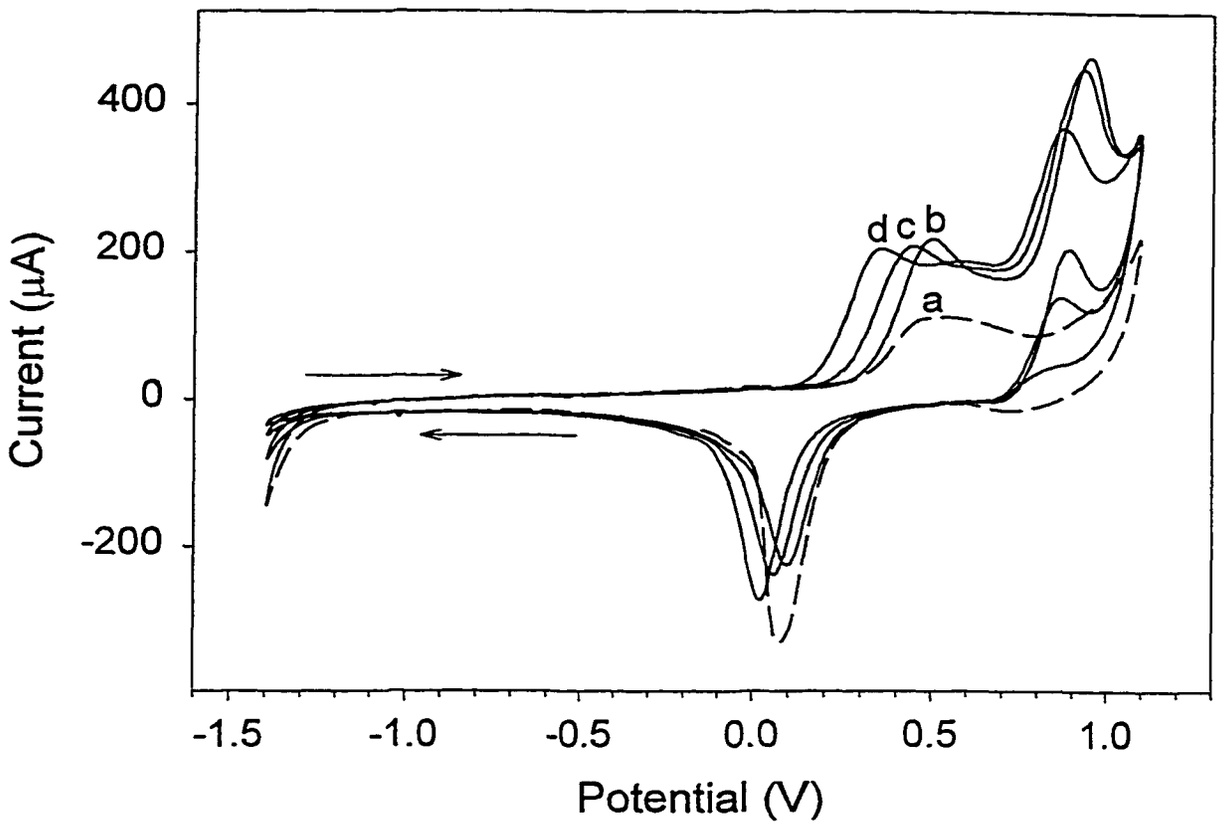

Figure 9. Voltammetric response for ethylamine at a $Au_{80}Ag_{20}$ RDE in 0.10 M Na_2CO_3 as a function of added sodium hydroxide. Scan: 100 mV s^{-1}. Rotational velocity 10.5 rad s^{-1}. Ethylamine concentration (mM): (a) 0, (b-d) 5. Concentration of added NaOH (mM): (a,b) 0, (c) 10, (d) 20.

CHAPTER 6. GENERAL CONCLUSIONS

General Conclusions

The goal of this research was to investigate the interactions of analyte molecules with the electrode surface and determine what factors can influence the rate of heterogeneous electrocatalysis.

The investigation into activated pulsed amperometric detection demonstrated that the oxidation of cysteine on platinum can be catalyzed by the presence of adsorbed hydroxyl radicals generated on the surface of the electrode by an anodic activation step.

The investigation of preanodized Au and Au-Ag alloy electrodes showed that the anodic oxygen-transfer oxidation of disulfides occurs on oxide covered noble metal electrodes. The Ag in the alloy promotes hydroxyl radical formation which catalyzes the anodic oxygen-transfer reaction.

The investigation of highly roughened preanodized Au electrodes demonstrated that an increased density of surface active sites for hydroxyl radical formation and analyte adsorption catalyzed the complete oxidation of the disulfide moiety.

The final investigation of Au-Ag alloy electrodes for the oxidation of ethylamine showed that the role of the Ag was as a redox couple for the mediation of an electron-transfer oxidation.

Recommendations for Future Research

Electrochemical sensor development is dependent on the discovery of new electrode materials. Binary (and ternary) metal alloys are an excellent source for new materials with electrocatalytic properties. The knowledge gained in the fundamental studies of electrode-analyte interactions will aid in the design of appropriate alloy electrodes for target analytes.

APPENDIX. LabVIEW PROGRAMS

Chronoamperometry Front Panel:

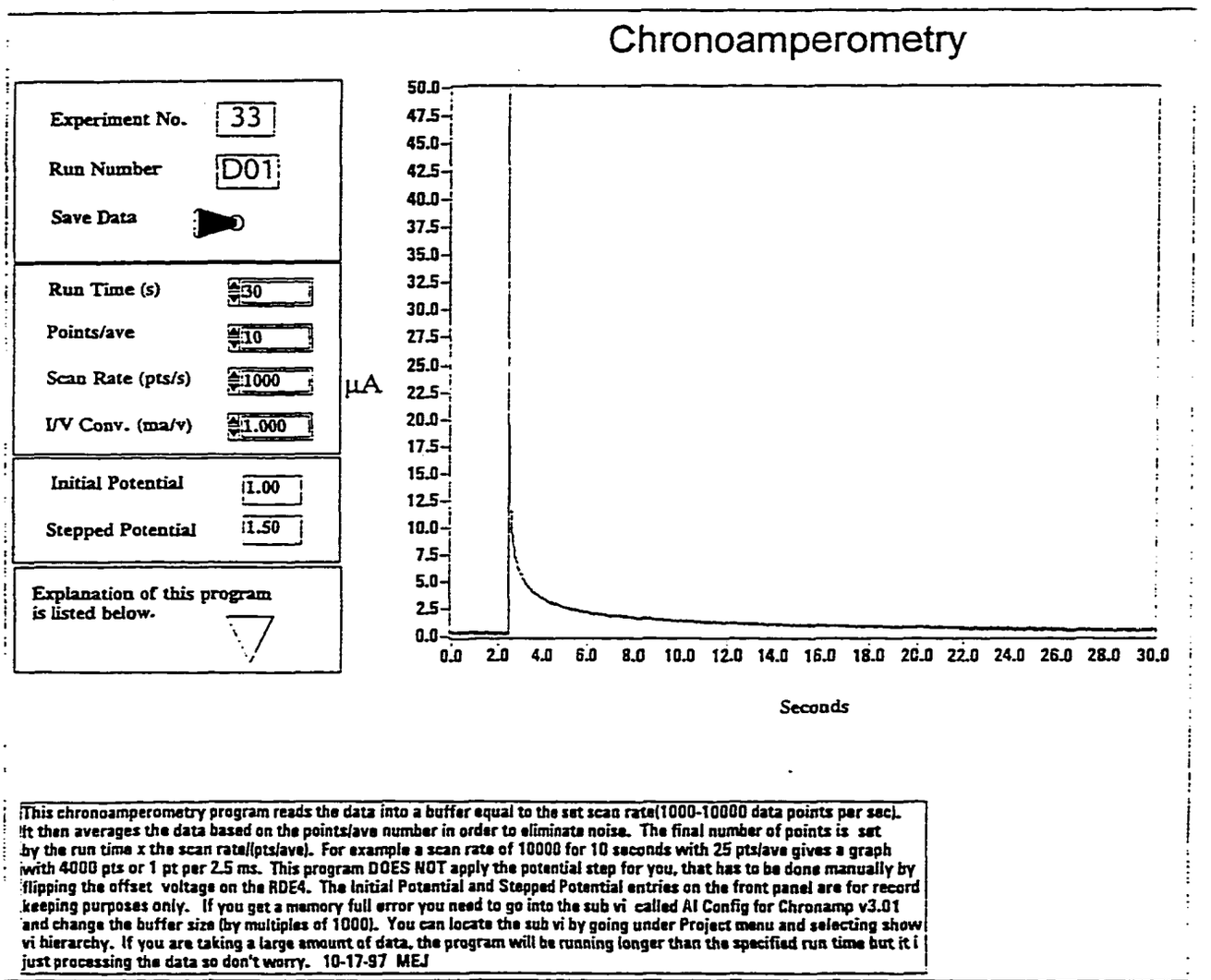

Chronoamperometry Block Diagram:

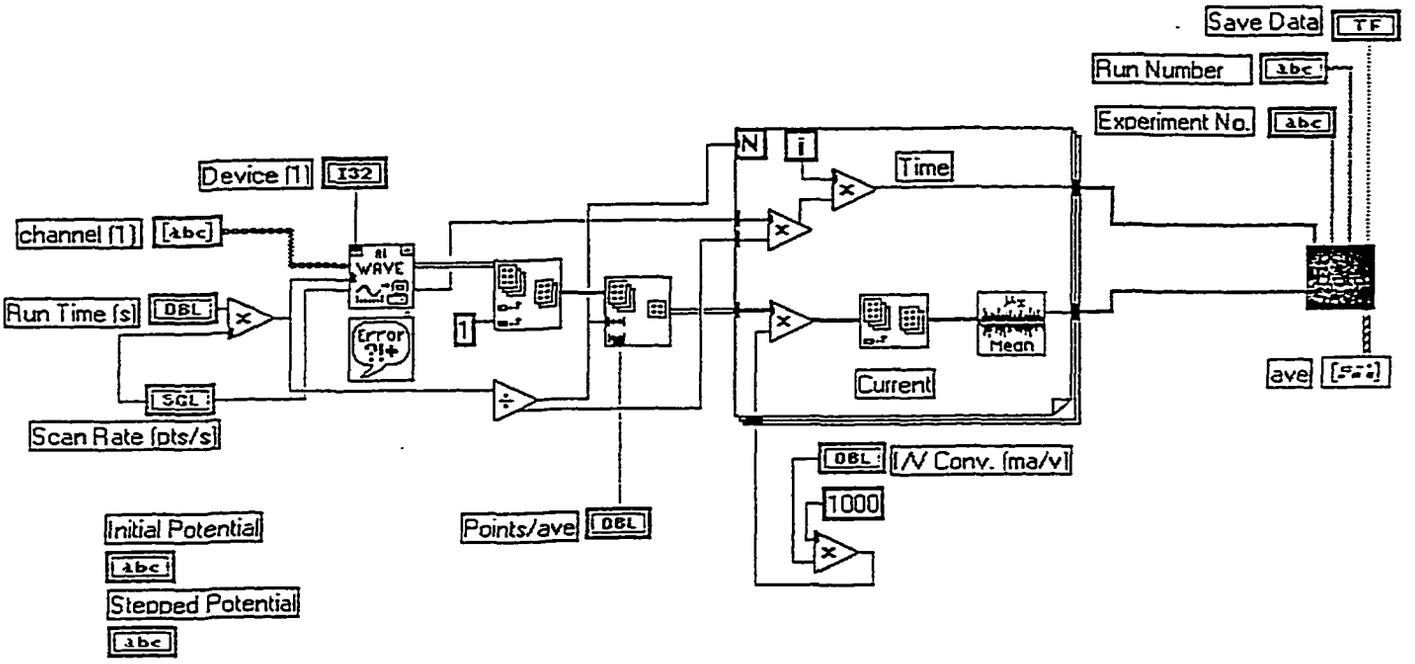

Chronoamperometry VI Hierarchy: